Asteroid Transfer and Capture into a Heliocentric Orbit in the Vicinity of the Earth-Moon System

Thesis Report

Viktor Jordanov

December 2, 2020

Technische Universiteit Delft

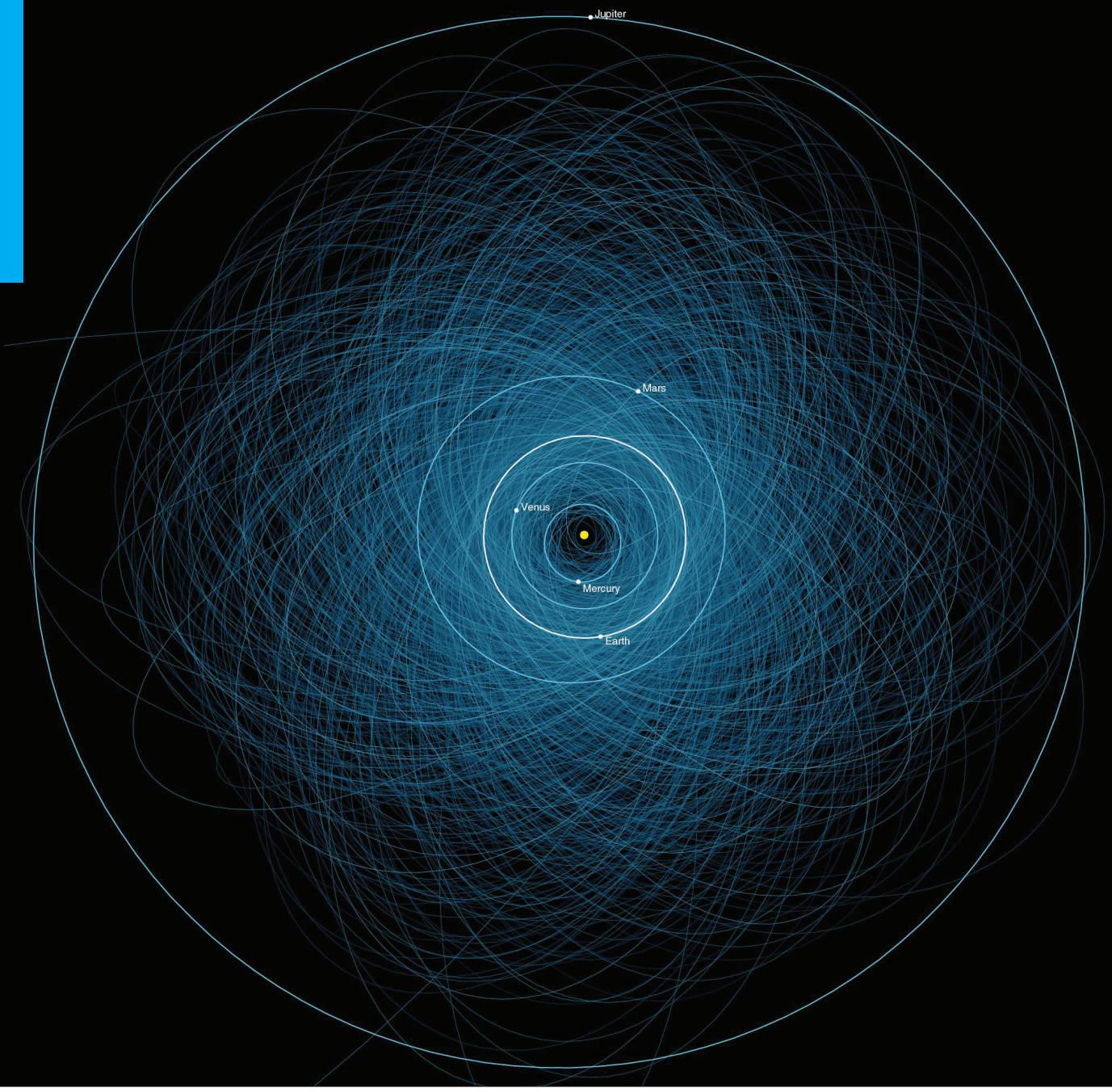

TU Delft Delft University of Technology

Challenge the future

Asteroid Transfer and Capture into a Heliocentric Orbit in the Vicinity of the Earth-Moon System

Thesis Report

by

Viktor Jordanov

4390105

December 2, 2020

in partial fulfillment of the requirements for the degree of

Master of Science
in Aerospace Engineering

at Delft University of Technology
to be defended publicly on Wednesday December 16, 2020 at 14:00.

Supervisor:	Ir. R. Noomen	TU Delft
Thesis committee:	Prof. dr. ir. P.N.A.M. Visser	TU Delft, Chair
	Ir. R. Noomen	TU Delft, Supervisor
	Dr. S. Speretta	TU Delft

Cover image: https://www.jpl.nasa.gov/spaceimages/details.php?id=pia17041

TU Delft Delft University of Technology

Preface

In front of you lies my thesis on the transfer of a near-Earth asteroid and capture into a suitable final heliocentric orbit in close proximity to the Earth. After effectively working on this project for ten months - even though the timeline is stretched out due to an internship in Montpellier in between - the end of my student time has arrived. A student time to which I look back with great joy and appreciation, full of unforgettable memories made. Now that the conclusion to this chapter in my life has come, I would like to thank a few people.

First of all, I would like to thank my supervisor during this thesis project, Ron Noomen. Starting in my first year in Delft, he increased my already existing passion for space through his way of giving lectures. This continued into the master phase of my studies, both during the lectures and throughout all the pleasurable meetings - offline and online - that we had for this thesis project. The critical questions that he asked me and the valuable advice he provided me with, in moments of uncertainty on how to proceed, are really appreciated.
Next, I would like to express my appreciation to the Tudat support team, starting with Dominic Dirkx, who is always on standby to help any student with questions about Tudat. I would also like to thank Marie Chambe, for her help during the modification of the software and her advice on how to best approach this modification. Of course, I would also like to thank Elmar Puts, who more than once made my struggle with C++ more bearable.

Furthermore, I would like to thank my friends for making my student time that much better. Both during the bachelor and master, there was always this special group of people around me that made going to lectures, studying together and everything outside of that way more enjoyable. Even during the past months, where almost everything had to be done online, I could always count on these friends to see or call each other and spend some precious time together. Thank you to the people at the VSV, with whom I have organised and attended many activities and events throughout the years. I would also like to thank my teammates at Velo, who could always provide some good moments of distraction from my studies.
Finally, I would like to thank my parents and my sister, who are always there for me and support me with everything I do. I cannot express in words how much I appreciate that.

Viktor Jordanov
Delft, December 2, 2020

Summary

The idea of capturing an asteroid has gained more and more attention in recent years, sparked by rapid technological developments and the growing general interest into the subject, both by scientists and commercial parties. The focus of this thesis project will be on transferring an asteroid from its original orbit to a safe, stable and easily accessible location with respect to the Earth.

Various studies have been performed on capturing asteroids into orbits around the Earth or the Moon, or even in stable orbits around certain Lagrange libration points. In this thesis report however, an alternative is investigated: a target orbit around the Sun, where the asteroid will always stay in close proximity to the Earth. Various benefits for placing an asteroid in this alternative target orbit have been identified. First, the safety risks that exist when transferring a heavy object into the Earth-Moon system are not present with this alternative target orbit. Furthermore, the stability in the heliocentric orbit, as opposed to an orbit in the Earth-Moon system, can be guaranteed in a more robust way. Finally, no capture inside the Earth-Moon system needs to take place, meaning that the required ΔV may be smaller with this alternative target orbit.
The benefits and drawbacks of both high-thrust and low-thrust propulsion are discussed, after which it is decided to use a low-thrust engine for this mission. From the various types of asteroids that exist in our Solar System, it is decided to focus on small near-Earth asteroids, such that some clear constraints can be applied when selecting the asteroid for this study. Due to the nature of this mission, where a solid and dense object is transported through interplanetary space, the choice is made to only include perturbing forces from third bodies during the analysis of both the target orbit and the transfer trajectory.

The asteroid selection process is started by generating a set of asteroids after the aforementioned constraints have been applied. This set of asteroids is analysed by means of a Lambert targeter, which is an analytical way of quickly finding the required ΔV for a certain transfer trajectory. For this analysis, the assumption is made to transfer each asteroid from its original orbit to the location of the Earth, which will give a good enough starting point for the detailed analysis that will follow later. A suitable candidate asteroid (2006 RH120) emerges from this analysis, which not only has a small diameter, a characteristic that translates to a low total mass for the asteroid and is seen as beneficial, but also requires a small velocity impulse to be transferred according to this Lambert analysis.

The following step is to define the most suitable target orbit for the asteroid to be captured in. This is an important step in this study, since the main goal of the thesis is to assure the safety, stability and accessibility of the asteroid once it has reached its final orbit, as was defined in the research question. The starting point of this target orbit analysis, is to take the state of the Earth in Kepler elements and change one or two of these elements while the others remain the same. The asteroid in this new state is subsequently propagated for 100 years and its orbital behaviour during this time period is analysed extensively. From this, conclusions can be drawn on its safety and stability during the next 100 years. To assess its accessibility throughout the complete time period, another analysis is performed, again using the Lambert targeter, in which the ΔV required to transfer from the position of the Earth to the position of the asteroid is calculated as a function of time. This yields attractive intervals to have access to the asteroid.
In this way, all three aspects of importance can be assessed. As said, different Kepler elements have been changed to see which change provides suitable target orbits. It is found that adding at least 0.03 to the eccentricity of the Earth gives suitable target orbits in which all three of the previously mentioned goals are achieved. A sensitivity analysis is performed to investigate how much the other Kepler elements may differ for the target orbit to still be suitable, which resulted in margins of $500\,000\,\mathrm{km}$ for the semi-major axis and $1°$ for the inclination. The epoch at which it arrives and thus its true anomaly in the orbit is found to also be of importance, which e.g. can be corrected by changing the right ascension of the ascending node with a certain value.

Lastly, the actual design of the transfer trajectory from the initial orbit of asteroid 2006 RH120 to the suitable target orbit can be performed. An analytical analysis is performed first, to assess what the best combination of departure date and time of flight is for the transfer trajectory. Use is made of the hodographic method for this part, since it can determine the required ΔV and maximum thrust force in an efficient way. It shapes a trajectory in a fast way using mathematical expressions, but therefore cannot take real-life physical forces into account. Through an optimisation process, the best combination of the aforementioned departure date, time of flight and free coefficients for the mathematical expressions is found. This resulted in the most optimal trajectories being a departure on the 15th of September 2027, with a time of flight of 313 days. The corresponding ΔV and maximum thrust force as resulting from the hodographic method are around $1000\,\mathrm{m/s}$ and $1.75\,\mathrm{N}$ respectively.
The obtained shaped trajectory is then used as an initial guess for the subsequent numerical analysis using the Sims-Flanagan method. The version of this method as implemented in Tudat was modified to be able to take into account various perturbing forces, generally third-body accelerations. An optimisation followed to find the best thrust profile and the accompanying transfer trajectory, in terms of required ΔV and the minimisation of the mismatch halfway the trajectory. During this thesis project, no mismatch of zero was found, which meant that the trajectory will have an accumulating deviation from half of the time of flight and onward.

This is the only element of the thesis project that did not result in a complete success, since all the other elements achieved exactly what was expected for them. It is recommended to perform a follow-up study in which, through the combination of better tuning, more computation time and perhaps a more efficient algorithm, the mismatch is effectively reduced to zero.

Contents

Nomenclature

Abbreviations

AU	Astronomical Unit
J2000	Epoch in Julian days since 01-01-2000
JPL	Jet Propulsion Laboratory
KISS	Keck Institute of Space Studies
LEO	Low Earth Orbit
NEA	Near-Earth Asteroid
RK4	Runge-Kutta 4
SEP	Solar Electric Propulsion
TUDAT	TU Delft Astrodynamics Toolbox

Greek Symbols

Δ	Difference or change	-
ΔV	Change in velocity, or velocity impulse	m/s
$\Delta\theta$	Angle between two position vectors $\mathbf{r}_1$ and $\mathbf{r}_2$	rad
θ	Azimuth	rad
θ	True anomaly	rad
μ	Standard gravitational parameter	m^3/s^2
μ_{Sun}	Gravitational parameter of the Sun	1.327×10^{20} m^3/s^2
ν	True anomaly	rad
ρ	(Atmospheric) Density	kg/m^3
Ω	Right ascension of the ascending node	rad
ω	Argument of periapsis	rad

Latin Symbols

A	Effective cross-sectional area/reference area	m^2
a	Semi-major axis	m
a_0	Ratio of applied thrust force to mass	-
C	Integration constant/Jacobi's integral	m^2/s^2
c	Chord	m
c	Speed of light	299 792 458 m/s
C_D	Drag coefficient	-
E	Eccentric anomaly	rad
e	Eccentricity	-
F	Force	N
f	Force	N
G	Gravitational constant	$m^3/kg{\cdot}s^2$
g_0	Gravitational acceleration at sea level	m/s^2
I	Impulse	Ns
i	Inclination	rad
I_{sp}	Specific impulse	s
J	Zonal harmonics coefficient	-
k	Various coefficients	-
$\dot{m}$	Mass flow	kg/s
M	Mass	kg
M	Mean anomaly	rad
m	Mass	kg
M_0	Initial mass	kg
M_e	Final mass	kg

n	Number of bodies	-
n	Number of segments	-
P	Position	-
r	Position vector	m
R	Radius of the Earth	m
r	Distance	m
r	Radial distance	m
t	Time	s
t_f	Time of flight	s
U_{eq}	Equivalent exhaust velocity	m/s
V	Velocity	m/s
v	Velocity	m/s
V_j	Effective exhaust velocity	m/s
W	Energy flux/Power density	W/m^2
W_p	Propellant weight	N
x	Cartesian Coordinate	m
y	Cartesian Coordinate	m
z	Cartesian Coordinate	m
z	Height	m

Miscellaneous

Υ	First Point of Aries	-
$\mathscr{E}_k$	Specific kinetic energy	m^2/s^2
$\mathscr{E}_p$	Specific potential energy	m^2/s^2

1

Introduction

By looking at the sky, humanity has learned a great many things, not only about our Solar System and the entire galaxy, but also about the Earth itself. Of course, various new insights can be obtained by visually exploring space, but with the further increase in technological developments, it has become possible to gather information about objects in space by actually visiting them, and even by collecting material from those objects to analyse. In recent years, the interest in asteroids has increased significantly, not only because of the commercial aspects that have to do with the potential mining of valuable resources from asteroids, but also due to the scientific information that possibly is stored in asteroids [1]. There are various theories and hypotheses that consider life on Earth to be originating from outer space (lithopanspermia), brought here by celestial bodies such as asteroids and comets [2]. To continue expanding our understanding of life itself, its history and the Solar System in general, conducting in-situ research on asteroids is necessary and a goal for the future of spaceflight.

1.1. Problem Definition and Research Question

To be able to conduct this research on an asteroid, it needs to be located in a safe, stable and easily accessible location. To achieve this, this thesis will look at capturing an asteroid from a to be determined location in the Solar System, after which it is transferred to the convenient and safe location, in order for the later (scientific) missions to reach it in a relatively easy and cheap way, i.e. with less propellant required. This is in contrast to directly sending a manned mission to an asteroid in its original orbit, since such a mission would pose too many risks for the humans travelling for a long time in interplanetary space.

This leads to the problem at hand, and the associated research question for this thesis. The goal is to study the relevant orbital mechanics and design the return phase of an asteroid capture mission, including additional aspects of the mission, such as the stability of the final target orbit. This should be done in the most efficient way, which means that the propellant mass of the asteroid capture mission, which alternatively can be expressed as the total change in velocity (ΔV), has to be minimised, also taking into account the total duration of the mission, or the time of flight. This results in the following research question:

How can an asteroid located in the Solar System be transferred most efficiently, with respect to propellant mass and time of flight, from its original orbit to a safe, stable and easily accessible orbit, and what is this new orbit?

1.2. Structure

In part one of this thesis report, it is started by collecting and discussing the heritage on asteroid capture missions in Chapter 2, from which it will become clearer what already has been done and what new research can be performed. This is followed by Chapter 3, in which more elaboration is given upon the types of asteroids that exist in our Solar System and a choice is made which asteroid type will be used for this study. Next, the different available propulsion methods will be discussed briefly

in Chapter 4, where a choice will be made on which propulsion method will be used to transfer the asteroid. Finally, the general background on astrodynamics will be discussed elaborately in Chapter 5. Then, the analysis part of the thesis project is started by performing the asteroid selection in Chapter 6, where the most suitable asteroid for this capture mission is determined. In the following so-called stability analysis in Chapter 7, an extensive analysis is performed to find the most suitable final state for the asteroid once it has been captured. Subsequently, the actual transfer trajectory from the asteroid's initial orbit to its final orbit can be designed, which is done in Chapter 8. Lastly, the main conclusions that can be drawn with respect to the results from this thesis study will be discussed in Chapter 9, together with some recommendations for further studies.

I

Background

2

Heritage

In this first chapter of the background part, several proposed missions and research studies will be discussed, to be able to get a good overview of what has already been done in this field of study and where the possibilities for new research lie.
The general focus in this chapter will lie on the proposed method for transferring the asteroid to its final orbit and even more important, the proposed location for this final orbit. It is started by discussing two research studies in more detail, after which several other proposals are briefly summarised. These two are discussed more elaborately here, since they propose two of the more often encountered ideas for the asteroid's target orbit.

2.1. Geocentric

The main idea of the first paper that will be discussed here [3], is that a Near-Earth Asteroid (NEA) with favourable characteristics that make it easy and cheap (using a small amount of propellant) to transfer it to a 1:1 resonant orbit with the Earth, is captured and transferred to this resonant orbit. Here, it will 'meet' the Earth once each year, where it will make a flyby with the Moon, in a way that will reduce its velocity with respect to the Earth, but will not reduce its velocity with respect to the Sun, so that it stays in a resonant orbit with the Earth. In this way, after several of these flybys with the Moon, its velocity with respect to the Earth will have decreased significantly, such that it finally can be captured by the Earth and will stay in the sphere of influence of the Earth, orbiting the Earth at a specific distance. Using the dynamics of both a gravity assist manoeuvre and the Earth-Moon system in such a clever way, reduces the total necessary velocity impulse, also greatly reducing the propellant mass of the spacecraft. An example of how the asteroid will pass by the Moon in each consecutive year (being resonant with the Earth's heliocentric orbit), and will be captured by the Earth eventually, can be seen in Figure 2.1.

Furthermore, in Figure 2.2 it can be seen how the relative velocity of the asteroid with respect to the Earth at infinity changes after each gravity assist, until it reaches zero and is thus captured by the Earth.
After the asteroid is captured around the Earth, there are various follow-up steps that can be taken according to the paper [3]. One of these is to continue letting the asteroid to have flybys with the Moon, which is only possible in case the orbit of the asteroid crosses the orbit of the Moon around the Earth, and if it can be ensured that the asteroid will actually meet the Moon and pass it by closely. In other words, it needs to have entered an orbit which is resonant with the lunar orbit around the Earth. Under those circumstances, the deceleration of the asteroid can be continued, in such a way that the eccentricity of the orbit decreases.
Another option is to let it stay in this orbit without performing any further decelerating gravity assists, such that in the case a hazardous object is approaching the Earth, and there is a serious risk it will crash into the Earth, the captured asteroid can make use of a lunar flyby where it accelerates, to escape the sphere of influence of the Earth. With this option, it can be pointed towards this hazardous object, where it will deflect the hazardous object and in this way prevent a collision with the Earth.

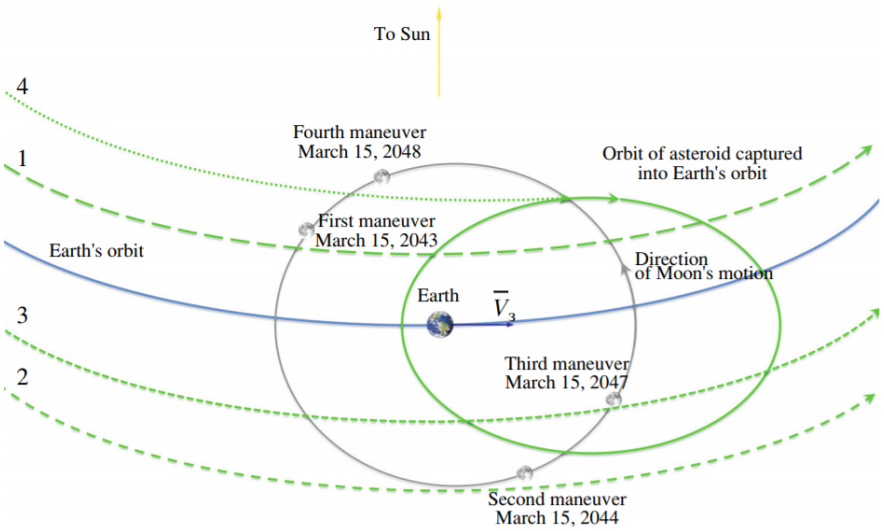

Figure 2.1: An illustration of how the asteroid can be captured in a geocentric orbit after multiple lunar gravity assists, as found by [3]. This simulation is made for the example asteroid 2014 QN266.

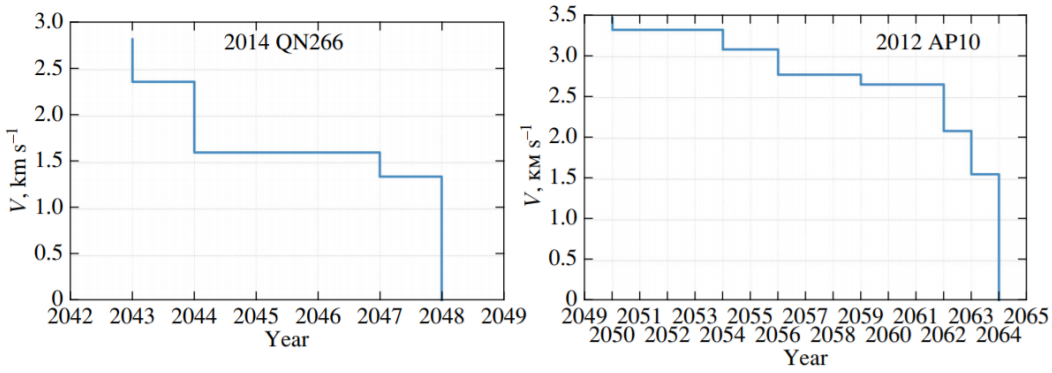

Figure 2.2: The change of relative velocity after each gravity assist, for two different example asteroids [3].

2.2. Selenocentric

This next paper is also used as a reference by the previous paper. A feasibility study [4] performed by the Keck Institute of Space Studies (KISS) discussed the possibility of locating, capturing and transferring a NEA with a diameter of approximately 7 m to a high lunar orbit. The mission is based on using a solar electric propulsion engine, which provides low thrust but with a high specific impulse. The profile of the mission according the Keck feasibility study is elaborated upon in the following paragraph, and can also be observed in Figure 2.3.

First, an Atlas V 551-class launch vehicle will place the spacecraft into a low Earth orbit (LEO), from which a 40 kW solar electric propulsion (SEP) system will transfer the spacecraft through a spiral orbit towards the altitude of the Moon. Once there, a gravity assist with the Moon will allow the spacecraft to escape from the sphere of influence of the Earth. Now in a heliocentric orbit, the SEP will transfer the spacecraft to the NEA. After it has arrived at the NEA, the spacecraft will analyse the size, shape and motion of the asteroid, such that it can be captured and (in case the asteroid was rotating too fast) de-tumbled, after which the SEP will be used to transfer the asteroid towards the Earth. When the spacecraft with the captured asteroid reaches the Earth-Moon system, another lunar gravity assist will be used, this time to be captured by the gravity of the Earth again and in this way continue its existence in the Earth-Moon system. Finally, after some time, the last manoeuvre can be performed and the asteroid can be captured in a stable high lunar orbit.

The philosophy behind this mission and final orbit around the Moon is that it is relatively easily accessible and reachable by (human) exploration missions, which can perform scientific experiments on

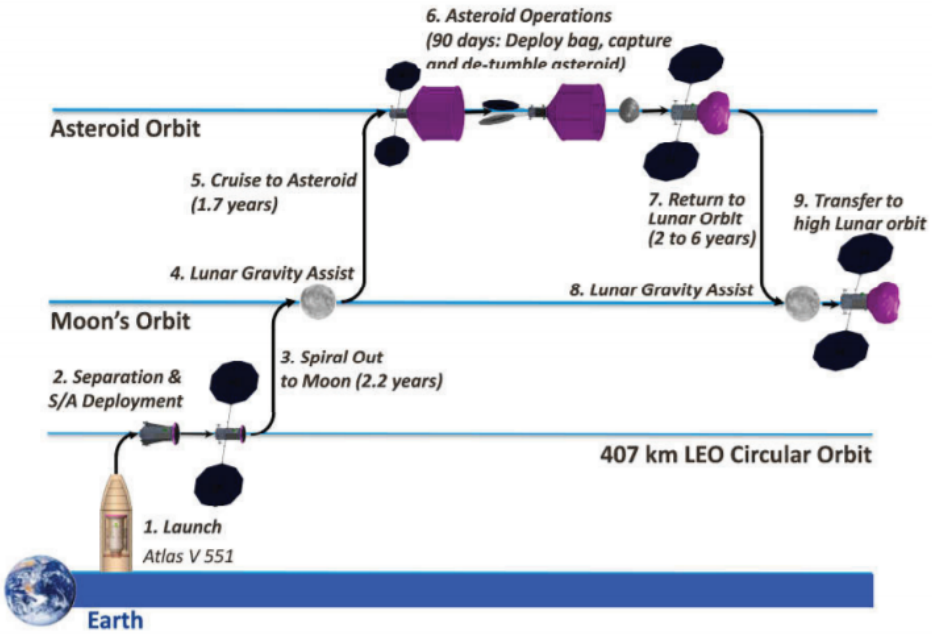

Figure 2.3: The proposed profile of the asteroid retrieval mission [4].

the asteroid, take samples back to the Earth and explore the future possibilities of using asteroids, potentially for the mining of valuable materials. Furthermore, once it is in a stable orbit, the asteroid is in a safe location with respect to the Earth, minimising the risk of a collision with the Earth itself.

Further investigations have been done on transferring the NEA to an orbit around the Sun-Earth L2 point, which would connect the interplanetary trajectories with a stable manifold. Using this, the L2 point should be approached asymptotically. This method was only examined, which means no further elaborate conclusions were drawn for this method.

Also, the option of not transferring a complete asteroid, but rather taking a rock/boulder from a larger asteroid has been discussed in [4]. In this way many more asteroids can be analysed as potential targets, since the larger NEA's are easier to find, meaning the database contains more of these. The taken boulder should still fall inside the mass constraints however. A disadvantage of this method, is that the process of removing a large mass from the surface of an asteroid is very complex, and can bring along multiple complications. Nevertheless, it is not completely written off, as more research can be performed on reducing the difficulty in technically achieving the asteroid capture, according the researchers in [4].

2.3. Alternative target orbits

In the aforementioned two studies, two main possibilities were considered in terms of final location for the asteroid, namely in an orbit around the Earth and in an orbit around the Moon. Mention was also made of placing the asteroid in an orbit around a libration point, in this case the Sun-Earth L2 point.

After these two studies that have been discussed extensively in the previous paragraphs, a few more studies will be discussed briefly. In these, some different perspectives will be discussed as well.

In [5] for example, the possibility of placing an asteroid in an orbit around the Earth-Moon L2 point is investigated, by using the stable manifold that is associated with the L2 point of the Earth-Moon system. Their method of direct capture uses a Lambert arc as the initial guess for the trajectory, after which the trajectory is finalised using a differential corrector.

In another paper [6], it is proposed to place an asteroid in an orbit around the Sun-Mars L1 or L2 point, where it could be beneficial for future Mars missions. In this case as well, use will be made of stable manifolds to reach the target orbit, according to the researchers.

2.4. Conclusions

With these various ideas and proposals summarised, a good idea is obtained on what kind of research has already been performed in this field of study. Not much research was found that discusses placing an asteroid in a heliocentric target orbit in close proximity to the Earth, where it will stay orbiting the Sun at a safe distance from the Earth, while being in a stable and easily reachable orbit with respect to the Earth. This is why it has been decided to focus on exactly this type of target orbit for this thesis project, such that a new area of research is expanded.

Placement of an asteroid in such a heliocentric orbit can have several benefits, one of them being that it does not need to be transferred into the Earth-Moon system with all its accompanying safety risks. Next to this safety benefit, the stability can also be guaranteed in a better way when it is not located in the Earth-Moon system. The required ΔV may be smaller in case gravity assists are used, due to the fact that it does not need to be captured in the Earth-Moon system. The accessibility however, will generally be worse for the heliocentric final orbit compared to an orbit in the Earth-Moon system. More on this will follow in Chapter 7, where an extensive analysis will be performed on the most suitable final location for the asteroid. Generally it can thus be concluded, that in terms of safety, stability and the required velocity impulse, this heliocentric final orbit may prove to be more beneficial than the already researched target orbits.

3

Asteroids

It is important to familiarise with asteroids, the various types that exist and their corresponding characteristics, to be able to design an asteroid capture mission. It is also necessary to assess their orbital parameters and physical properties, after which a preliminary choice can be made of which subset of asteroids is most appropriate for the study at hand. This will be discussed extensively in this chapter.

3.1. General information

After the formation of the Solar System and its large planets, many smaller objects were left in between these planets orbiting the Sun. These objects are seen as debris from the formation process, since they had not crashed into or merged with the planets increasing in size [1]. This debris ranges from very small particles of dust, which are not categorised as asteroids, up until larger multiple kilometre minor planets. In general, the term 'asteroids' is used for these objects which are larger than one metre in diameter.
The majority of these asteroids is located in between the orbits of Mars and Jupiter. This area is called the asteroid belt, for their overwhelming presence there. Furthermore, there are several other zones in the Solar System where significant numbers of asteroids are located. Two of these are the L4 and L5 Lagrangian points of the Sun-Jupiter system, which are stable points and therefore areas where objects can stay for long periods of time [7]. They are called Trojans and are divided into the Greek camp (L4) and the Trojan camp (L5) [8].
The Centaurs are asteroids (or comets) that have orbits in between the large gas planets. These bodies are often located in unstable orbits, which can either be transferred to orbits closer to the Sun, or be transferred outwards towards the Kuiper belt and the edge of the Solar System [9]. The Kuiper belt is another location in the Solar System where asteroids are abundant. The belt extends from the orbit of Neptune, at 30 Astronomical Units (AU) to around 50 AU [10]. These asteroids are located in both stable and unstable bands in this belt and could also contain considerable information about the origin of the Solar System.

Lastly, and most importantly for this study, are the near-Earth asteroids (NEA's), as already introduced in Chapter 2. These are the most attractive asteroids in our Solar System for this study, since they are the closest and most easily reachable objects as seen from the Earth [1]. This is because they can potentially pass close to the Earth, which means relatively little energy is required to change the orbital parameters of these asteroids to ensure a capture into the desired final orbit.

3.2. Near-Earth asteroids

The near-Earth asteroids are classified in four distinct groups. These are the Atiras, the Atens, the Apollos and the Amors [1]. The Atiras are asteroids that have a semi-major axis smaller than 1 AU, and an aphelion smaller than 0.983 AU, since the perihelion of the Earth is at 0.983 AU. This means that the Atiras are located completely on the interior of the Earth orbit at all times. Next are the Atens, which still have a semi-major axis smaller than 1 AU, but now have an aphelion larger than 0.983 AU.

This means that their orbit will pass the orbit of the Earth at some time in their orbital period, but will generally stay on the inside as seen from the Sun. The Apollos are similar to the Atens, in that they cross the orbit of the Earth somewhere throughout their orbital period, only now the semi-major axis is larger than 1 AU while the perihelion is smaller than 1.017 AU, which is the distance of the aphelion of the Earth to the Sun. This means that the larger part of their period is spent on the exterior of the Earth orbit. Finally, the Amors are asteroids that have a semi-major axis larger than 1 AU, and where the perihelion is also larger than 1.017 AU. This means that the Amors never cross the orbit of the Earth, similar to the Atiras, only now the orbit will always stay on the exterior of the Earth orbit. These four orbit types are illustrated in Figure 3.1.

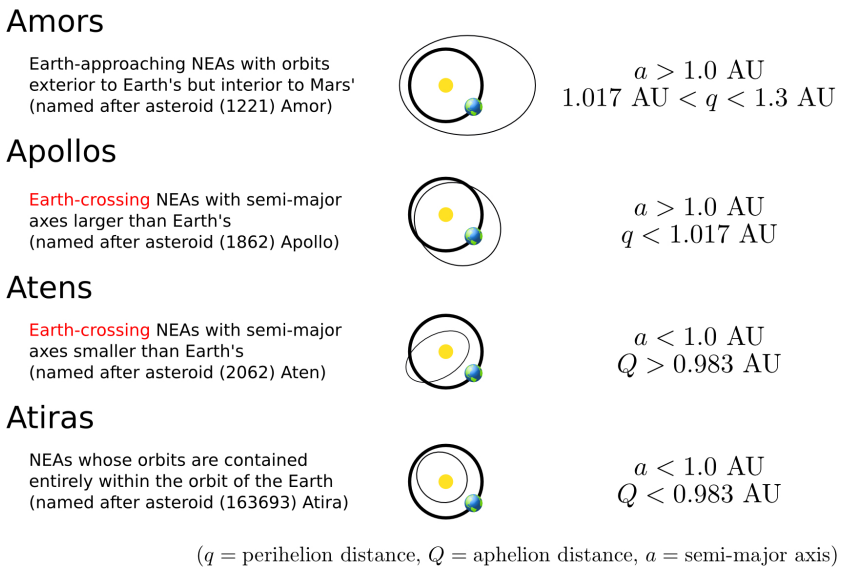

Figure 3.1: The orbits of the four types of near-Earth asteroids [11].

The distribution of the four types is not uniform at all, with a very high number of Apollos and Amors, a reasonable number of Atens and a very low number of Atiras. The most recent data at this moment is taken from the 'Minor Planet Center' by the International Astronomical Union [12], and can be seen in Table 3.1. The distribution is also illustrated in Figure 3.2, where it can also be seen how the semi-major axis and the eccentricity of the asteroids behave for the different orbit types. Note however that the illustration is older than the most up-to-date data from Table 3.1, which means the number of dots will not correspond perfectly. The general idea of the distribution is still conveyed very clearly however.

Table 3.1: The number of asteroids of each near-Earth orbit type [12].

NEA Type	# of asteroids
Atiras	45
Atens	1837
Apollos	12277
Amors	10206

3.3. Composition

In a selection of the most suitable asteroid for a capture and transfer, the composition of this asteroid clearly plays a role. To discuss the composition of asteroids, first the distinction between asteroids and comets needs to be made. This distinction is based on their composition; a comet can be defined as an object that shows certain activity, such as having a coma [1]. A coma is a layer of water gas and other volatile materials around the nucleus of the comet. This coma is caused by the fact that comets are mainly composed of dust and ice, which starts to evaporate when the comet approaches the Sun closely. Comets in general have very large orbital eccentricities, and thus spend a large part of their orbital period far away from the Sun, where the ice can stay in its solid form. The cometary activity can

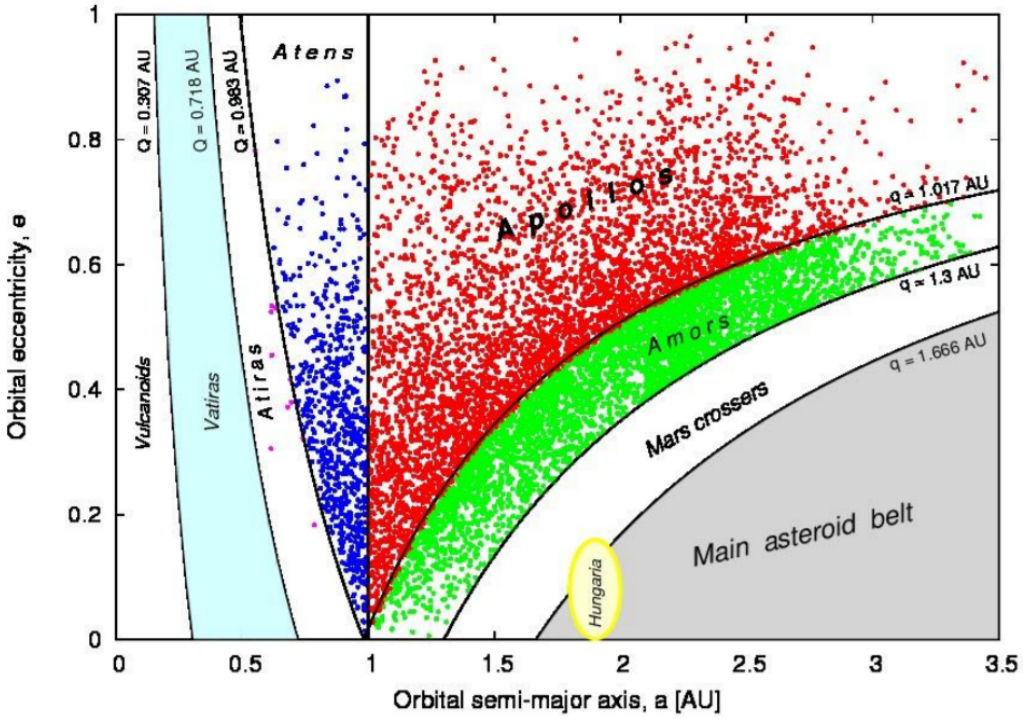

Figure 3.2: The distribution of the near-Earth asteroids, plotted for their semi-major axis and eccentricity [1]. *Q* indicates the maximum aphelion distance and *q* indicates the minimum perihelion distance.

then be observed in the proximity of the Sun, relatively close to the Earth and the other inner planets. Comets also have a low density in general, ranging from 500 until 1200 kg/m^3 [13], which is caused by the fact that they mainly consist of ice and dust, which is mixed together in a rather porous state.

Asteroids on the other hand are generally composed of various minerals in rock form. The materials in the asteroids are much more densely packed inside the rock, and since quite some asteroids also contain various metals like iron and nickel, the overall density of asteroids is much higher than the density of comets [14]. This is in the range of around 2000 kg/m^3 for carbonaceous chondrites up until around 7000 kg/m^3 for irons, with most rocky asteroids between 2000 and 3000 kg/m^3. To know the density of the asteroid is very important for an asteroid capture mission, since many aspects of the mission depend on its size and mass. Once the size of a target asteroid is known, using its expected density a total mass can be calculated, which is important to know in terms of the dynamics of the transfer trajectory.

3.4. Orbital characteristics

The orbital characteristics are the most important information when working on an asteroid capture mission. It is essential to know exactly where the asteroid is at what time, and what its spatial behaviour is. In Sections 3.1 and 3.2 it was already discussed what kind of asteroids are of interest for a capture mission, and broadly elaborated on what the orbits of these asteroids look like. The four types of NEA's, which could be used for an asteroid capture, are only defined based on their semi-major axis and their eccentricity, which when combined define the point of perihelion and aphelion. The inclination with respect to the planetary disc however is not defined in this characterisation, while it can make a very significant difference in the required velocity impulse to be applied to the asteroid, such that it can be transferred to its target orbit. From [3] it is understood however, that a larger angle between the ecliptic and the orbit of the asteroid does not immediately make the asteroid unsuitable, since this inclination difference can be corrected through multiple gravity assists with the Earth or the Moon. Although it is not immediately unsuitable, the larger angle is certainly more challenging and is thus seen as unfavourable.

A study [15] has shown that it is also possible to go to the main asteroid belt, where asteroids can be used for mining valuable resources, since there is much more material present in the main belt. The study concludes however, that for most of the best options in the asteroid belt, the manoeuvre to arrive there and rendezvous with an asteroid will require a velocity impulse between 7 and 8 km/s. This means, that to actually give these asteroids a push and transfer them to the proximity of the Earth will require such a large velocity impulse, that it is not seen as feasible with present-day available technology.

The required orbital characteristics will thus mainly be constrained by the semi-major axis of the asteroid around the Sun, and its eccentricity and inclination. The more favourable options will be asteroids which are already relatively close to the Earth, and preferably pass by the Earth in close proximity. These can then be pushed towards an orbit in which they eventually will be captured by the Earth-Moon system, with the least amount of propellant.

3.5. Conclusions

A few conclusions can be drawn in terms of what kind of asteroid will be preferred when designing an asteroid capture mission.

In terms of mass and size, it is beneficial to find an asteroid as small as possible, since such an asteroid will not have a large mass and therefore the transfer by means of an attached spacecraft will be more realistic and feasible. Generally, an assumption for the density of rocky asteroids can be made of approximately 2500 kg/m^3, which will also be used once an asteroid is selected.
Furthermore, the orbital characteristics as mentioned in Section 3.4 provide enough information to get a general idea of the favourable parameters. These are a semi-major axis which is close to 1 AU, an eccentricity close to zero and a low inclination with respect to the ecliptic, such that the velocity close to the Earth does not differ from the Earth's velocity too significantly.

The final choice of a single asteroid will not be made at this point in time, but once the mission design process is started in the asteroid selection chapter, which is Chapter 6.
During this selection process, use can be made of different databases, such as JPL's Small-Body Database Search Engine [16] and the Minor Planet Center [17].

4

Propulsion Methods

To be able to perform the asteroid capture mission using a spacecraft that will apply velocity impulses to the asteroid, a rocket engine will be necessary. There are two major concepts for propulsion using rocket engines, which can be useful for a mission like the asteroid capture. These are the high-thrust engine and the low-thrust engine. In this chapter both will be discussed briefly, along with their characteristics, advantages and disadvantages.

4.1. High-thrust propulsion

The traditional way of propelling objects in space, is by using thermal rocket engines [18]. These engines rely on a chemical reaction between a fuel and an oxidiser. The reaction causes the products to exit the nozzle of the engine with a very high velocity. This is the earlier-mentioned exhaust velocity, which can be seen as a measure of the engine's efficiency. This efficiency is defined as the specific impulse of the engine, or I_{sp}, which is in seconds. It shows how much impulse can be produced per unit of propellant weight, as is shown in Equation (4.1). Here, I is the impulse in N s and W_p is the weight of the propellant in N.

$$I_{sp} = \frac{I}{W_p} \tag{4.1}$$

This specific impulse can also be related to the exhaust velocity as can be seen in Equation (4.2). Here, U_{eq} stands for the equivalent exhaust velocity, which is the same as the effective exhaust velocity, and g_0 is the gravitational acceleration at sea level.

$$I_{sp} = \frac{U_{eq}}{g_0} \tag{4.2}$$

It is called equivalent, because the value varies with varying altitude. This means that the I_{sp} will also vary over the course of the launch. For a specific engine, often the sea-level value and the vacuum value for the I_{sp} are given. Since the engine will generally operate in a vacuum for the asteroid capture mission, from here on the I_{sp} of the engine will be considered in vacuum, except if otherwise stated.

The I_{sp} of high-thrust engines is roughly in the range of 170 until 450 s, highly dependent on the type of engine [18]. The two main types of high-thrust engines are liquid propellant engines and solid propellant engines. A third type is the hybrid engine, but it will not be discussed here. Solid propellant engines are generally less complex, but have a significantly lower I_{sp}, which ranges from 170 until almost 300 s, as can be seen in Figure 4.1. Liquid propellant engines on the other hand, are more complex to design and build, but can provide an I_{sp} of up to around 460 s. Another advantage of liquid propellant engines is that they can be made restartable, so that they can be used throughout multiple phases of a mission in space. Furthermore, liquid propellant engines can be made throttleable to reach a more desired thrust level.

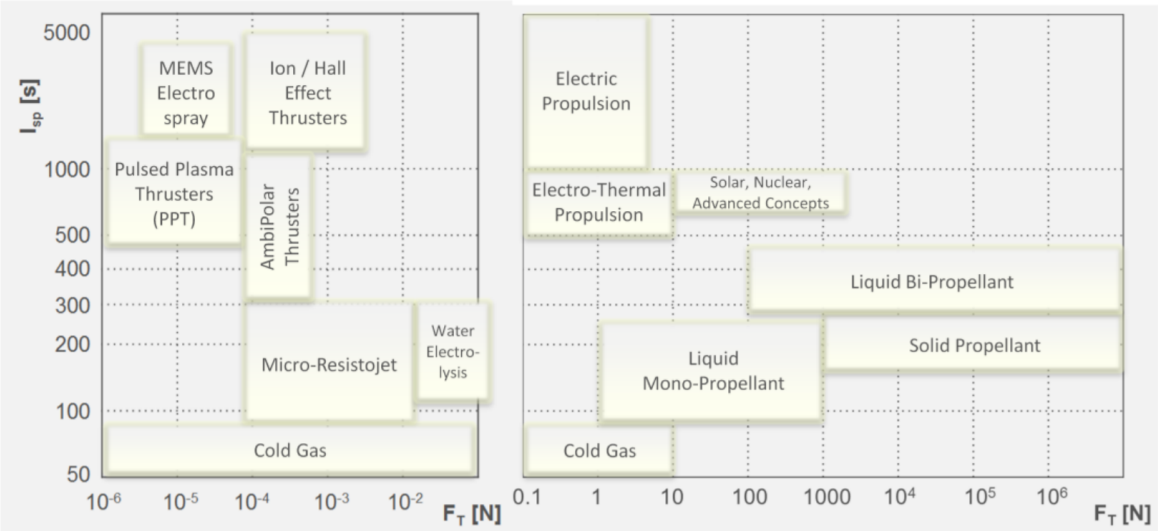

Figure 4.1: Various sources of thrust, plotted for their thrust and specific impulse [19].

4.2. Low-thrust propulsion

Next to the established high-thrust rocket engines, much research has been conducted in the last few decades on low-thrust rocket engines. These are characterised by a low thrust, but a significantly higher I_{sp}. There are various principles on which low-thrust engines can work, as can be seen in Figure 4.1, but in this section the focus will lie on ion propulsion systems, which encompass a few concepts of propulsion, of which the Hall effect thrusters are a famous example.

These Hall thrusters work on the principle of accelerating ions using an electrostatic field [20]. An electromagnetic field however exerts a strong force on the electrons and produces thrust for the engine in this way. The I_{sp} for these electric propulsion engines can be quite large, in the order of 2000 s. This means that a significantly lower amount of propellant is needed to achieve a certain ΔV with respect to high-thrust engines. The difficulty for electric propulsion engines however, next to the very low thrust level, is the large amount of energy that is required to power the electric thruster. This power needs to be generated somewhere on the spacecraft and is generally done using solar panels, with a few exceptions using a nuclear reactor. The large power requirement causes the solar panels to have a very large surface and potentially requires many batteries, which makes the complete system heavy and more complex. This can be seen as a large disadvantage of electric propulsion, since the mass it saves due to its higher efficiency in exhaust velocity is partially (or completely) cancelled by the mass increase due to larger power generating systems and more added complexity.

Ion thrusters are another type of low-thrust engines that will shortly be discussed here. They are based on an electrostatic field, which accelerates ions, but work on a different principle than the Hall thrusters [20]. Compared to the Hall thrusters, they are generally larger and heavier and also their thrust per power unit level is lower. However, they have shown a longer lifetime than the Hall thrusters, as well as a higher power efficiency, especially at high I_{sp} levels. These I_{sp} levels can reach above 5000 s, which indicates a high efficiency in terms of propellant use. Both the Hall thrusters and the ion thrusters are shown schematically in Figure 4.2.

The thrust level of ion propulsion systems are based on the amount of energy they receive from the power system. From multiple sources that have conducted research on asteroid retrieval missions [4] [21] [22], the assumption can be made that for a power level of around 40 kW, which is a reasonable value for a mission like this, a thrust level of around 2 N can be achieved, with the use of multiple thrusters and an efficiency of the thruster of around 70 %.
Furthermore, there have been several investigations on high-power solar electric propulsion (SEP) that reaches 300 kW power levels [23]. These are mainly conceptual studies so far, but could be realised

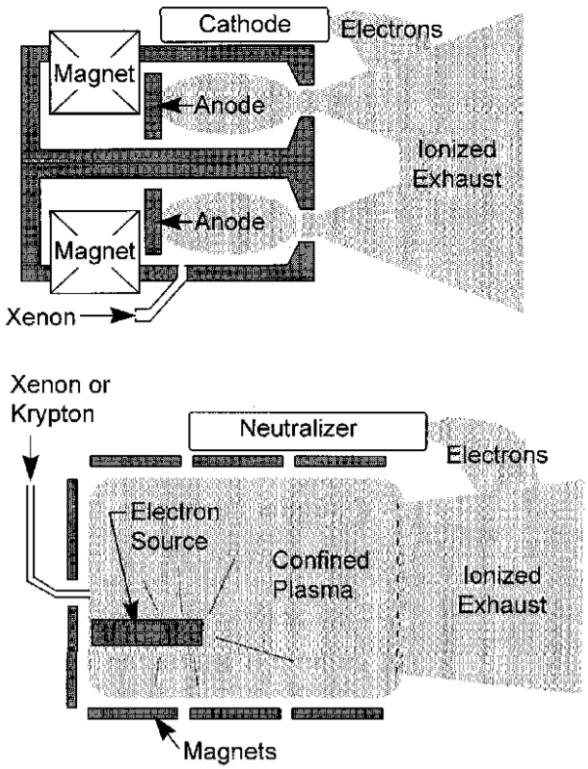

Figure 4.2: A schematic overview of the working principle of the Hall thruster (top) and the ion thruster (bottom) [20].

in the not-so-far future. Using such a propulsion system will provide a much higher thrust and thus a possible faster transfer, as well as be attractive for larger target asteroids. On the other hand, both the power system and the propulsion system will be large and thus heavy, and the amount of necessary propellant can become very high when aiming for larger target asteroids.

4.3. Conclusions

After discussing both fundamentally different methods for space propulsion, a conclusion can be drawn on which method will be used for a mission like the asteroid capture mission.

When looking at feasible designs in terms of the velocity impulse to be applied, and the consequent amount of propellant that needs to be brought on board of the spacecraft, opting for the low-thrust options seems like the better option. The high-thrust option does have advantages in that it can apply velocity impulses much faster, but this is not deemed absolutely necessary in a mission such as the asteroid capture mission.
The proposed search space for these low-thrust engines can be defined by their I_{sp} and thrust. As mentioned in this chapter, an I_{sp} between 2000 and 5000 s seems like a good range in which the analysis can be performed. Furthermore, with the mentioned thrust levels, including the conceptual studies for the near future, a thrust force up to 5 N is deemed feasible.

5

Astrodynamics

In this chapter, the basics of astrodynamics will be discussed, which are very important when designing a mission that revolves around transfer orbits and simulating trajectories of spacecraft and other celestial bodies. It is started with the most fundamental parts, namely the reference frames and coordinate systems that will be used, followed by a description of the two-body problem and perturbations that can be added. Next, low-thrust trajectories are discussed, which is then followed by an extensive description of stability in celestial context. All information in this chapter is taken from [24], except when stated otherwise.

5.1. Reference frames

It is started by defining the system with respect to which everything is described in space. This system is called a reference frame, and is based on an origin from which the location of other objects or points in space are defined. The reference frame uses axes or planes to define a certain direction or distance from the origin. In this section, various reference frames that will be used throughout this thesis project on capturing an asteroid will be shown.

5.1.1. Geocentric reference frame

The first type of reference frames that will be discussed is the geocentric reference frame, which as the name already says, is centred in the Earth. There are multiple variations of this reference frame, on which a brief elaboration will follow in this section. It should be noted that, although this reference frame will not be used extensively during this thesis project, due to the fact that most of it takes place in the heliocentric reference frame, this geocentric frame will still be discussed for completeness and since it is the primary reference frame from which all missions depart.

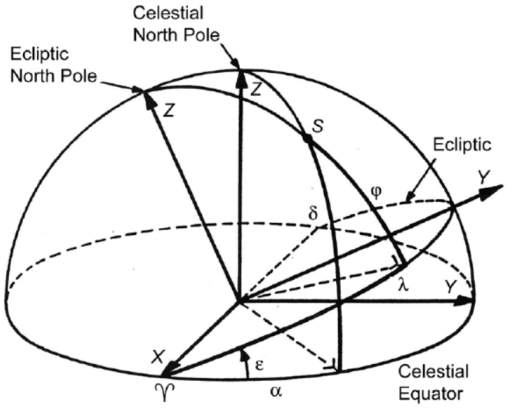

Figure 5.1: The non-rotating geocentric reference frames presented in one picture: the ecliptic and the equatorial variant [24].

The non-rotating frames are based on the fact that the stars in the sky stay in the same orientation with respect to each other and the Earth in the timeframe of interest for humanity. First, the *x*-axis is defined as pointing towards the First Point of Aries (♈), which can be assumed to be inertial with respect to the stars. From there on, the *y*-axis is at a 90° angle in the plane of interest, which can either be the equatorial plane or the ecliptic plane. This difference will differentiate the geocentric non-rotating equatorial reference frame from the geocentric non-rotating ecliptic reference frame. In the case of the equatorial reference frame, the *z*-axis is chosen to be directed towards the North Pole of the Earth, such that the right-handed system is completed. For the ecliptic reference frame however, the *y*-axis is located in the ecliptic plane, and the *z*-axis is thus directed perpendicular to this plane, in the Northern direction. The orientations of these planes can be seen in Figure 5.1. In this illustration, the angle ε is of importance. It is the obliquity of the ecliptic, which is the angle between the *z*-axes of the two reference frames, and has a mean value of 23°27′.

Next to the non-rotating geocentric reference frames, the rotating geocentric reference frame exists. This frame is set up in such a way, that it rotates along with the rotation of the Earth, and is thus defined in correspondence to the longitudes and latitudes on the surface of the Earth. The *x*-axis in this frame is located in the equatorial plane, where it crosses the Greenwich meridian, or longitude 0°. The *z*-axis is then pointed along the rotation axis of the Earth, in the direction of the North Pole of the Earth, just like in the equatorial non-rotating geocentric frame. The *y*-axis lies in the equatorial plane, 90° from both other axes, to complete the right-handed system. The rotating geocentric reference frame is useful for defining objects on or close to the surface of the Earth.

5.1.2. Heliocentric reference frame

The heliocentric reference frame is another reference frame commonly used in space applications, especially in the domain of interplanetary travel. The heliocentric reference frame is fairly similar to the non-rotating geocentric ecliptic reference frame, but has its origin in the centre of the Sun. The *x*-axis is again defined in the direction of the First Point of Aries ♈, which is exactly parallel to the direction of the *x*-axis in the geocentric reference frame. This is because the celestial sphere has an infinite radius, which means that the line from the Earth to ♈ is parallel to the line from the Sun to ♈. Furthermore, the *z*-axis is (similar to the geocentric ecliptic reference frame) located perpendicular to the ecliptic plane, in the Northern direction. The *y*-axis, finally, is located in the ecliptic at an angle of 90° from the *x*-axis, such that it completes the right-handed system.

This heliocentric reference frame will especially be useful when considering the motion of bodies in orbit around the Sun. The part of the asteroid capture mission in this thesis project will occur completely in interplanetary space and will thus make use of this reference frame extensively.

5.2. Coordinate systems

The reference frames discussed in Section 5.1 are very important to know where an object of interest is located with respect to the origin of the frame, but the way it is described in the given frame is dependent on the used coordinate system. The representation of coordinates of an object can differ greatly between coordinate systems, even though the object is located in the exact same location within a given reference frame. Useful coordinate systems for the asteroid capture mission will be discussed in this section.

5.2.1. Cartesian coordinates

The first coordinate system to be discussed is arguably the most common and well-known coordinate system: the Cartesian or rectangular coordinate system. This system consists of three axes, the *x*-, *y*- and *z*-axis, which all form a 90° angle with each other in a right-handed orientation. An object can thus have a distance from the origin in the *x*-direction, in the *y*-direction and in the *z*-direction, which respectively form the *x*-, *y*- and *z*-coordinates. The values for all three axes can take any possible real number, both positive and negative. In this way, each point in a three-dimensional space can be defined using the Cartesian coordinate system. A similar reasoning goes for the velocity representation.

5.2.2. Kepler elements

In astrodynamics and other space applications, Kepler elements are very often used to describe the orbit and position in which an object is located. These orbital elements are named after Johannes Kepler.

There are six Kepler elements, of which the first two describe the size and shape of the orbit. These are the semi-major axis a and the eccentricity e. Furthermore, the inclination i and the right ascension of the ascending node Ω determine the orientation of the orbital plane with respect to the reference frame. The argument of periapsis ω describes the way the conic section is oriented in the orbital plane. Finally, the true anomaly θ describes the angle at which the object is located in the orbit at a specific moment, with respect to the periapsis. A visualisation of the semi-major axis and eccentricity can be seen in Figure 5.2a, while the inclination, right ascension of the ascending node, argument of periapsis and true anomaly can be seen in Figure 5.2b.

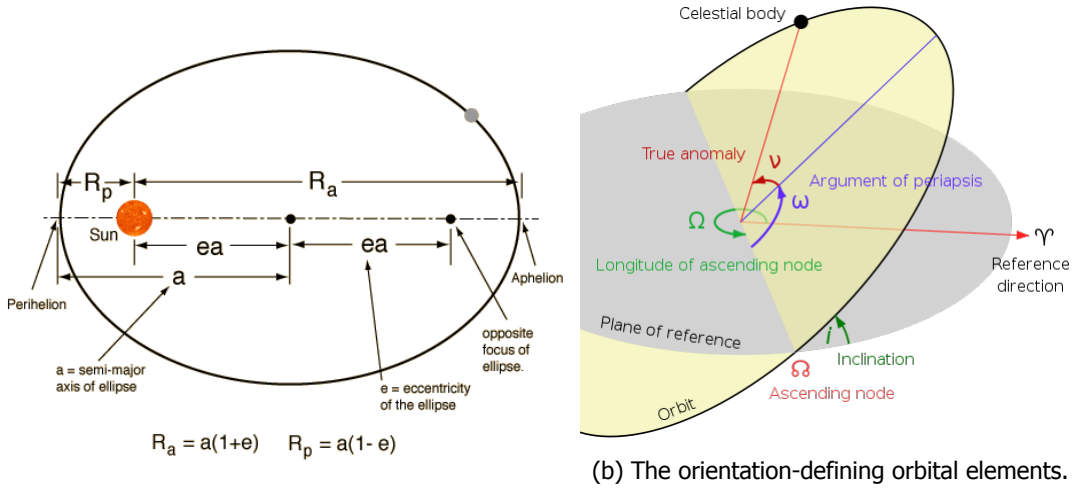

(a) The shape-defining orbital elements. In this example visual representation, the focus is the Sun.

(b) The orientation-defining orbital elements. Note that the true anomaly here is depicted using the Greek letter ν instead of θ.

Figure 5.2: The six Kepler elements [25].

5.3. Two-body problem

To be able to start the analysis of objects orbiting around other objects, first the most basic concept should be discussed. This is the two-body problem, which describes the motion of one object around a much larger object, without any other forces working on the smaller object, such as various perturbations or forced impulses. The mathematical formulation for this basic problem can be seen in Equation (5.1), where k is the larger body around which body i orbits. Their interaction is shown using the subscript ki, which means that the motion of i is defined relative to body k, located in the origin of a non-rotating (or inertial) reference frame. Lastly, the mass is defined by m, the distance by r and the universal gravitational constant by G.

$$\frac{d^2\mathbf{r}_{ki}}{dt^2} = -G\frac{m_k + m_i}{r_{ki}^3}\mathbf{r}_{ki} \tag{5.1}$$

Since the mass of the smaller body in almost all problems considered, including the asteroid capture mission, is much smaller than the mass of the larger body, or $m_k >> m_i$, Equation (5.1) can be simplified to Equation (5.2). In here, the term μ is equal to Gm_k and is called the standard gravitational parameter of the larger body. This assumption can only be made if the mass of the larger body is indeed much greater than the mass of the smaller body. It will also lead to the larger body experiencing no acceleration from the smaller body.

$$\frac{d^2\mathbf{r}}{dt^2} = -\frac{\mu}{r^3}\mathbf{r} \tag{5.2}$$

5.4. Perturbations

In Section 5.3, the motion around a larger body was described, without any perturbing forces working on the bodies. In real applications however, this could be a fairly inaccurate model, since various perturbations act on bodies in our Solar System at every moment in time, and to be able to model these perturbations better, they should first be analysed thoroughly and understood well. In this section, a few of the most important perturbations that can act on the spacecraft and/or asteroid during the mission will be discussed.

5.4.1. Thrust

The first and most dominant force on the spacecraft will be the thrust applied on the spacecraft by the rocket engine. This can be done either by a high-thrust chemical engine, or a low-thrust engine, both of which have been discussed in Chapter 4. The equation for the thrust force by any rocket engine that works on the principle of expelling mass to propel itself, can be seen in Equation (5.3), where $\dot{m}$ is the mass flow through the engine in kg/s and V_j is the effective exhaust velocity in m/s.

$$\mathbf{F} = \dot{m} V_j \tag{5.3}$$

With this equation, the force on the body can be calculated. Since the acceleration is dependent on the mass of the object on which the force acts, and this mass decreases over time due to it being expelled by the rocket, the acceleration is always a momentary value. To subsequently find the total impulse, which the engine has provided to the object over a certain period of time, an integration can be performed with the mass as a variable over time. This will result in the famously known 'Tsiolkovsky equation' or 'rocket equation', which can be seen in Equation (5.4). In this equation, ΔV is the total impulse or change in velocity in m/s, V_j is again the effective exhaust velocity in m/s, M_0 is the initial mass and M_e is the final mass, both in kg.

$$\Delta V = V_j \ln \frac{M_0}{M_e} \tag{5.4}$$

5.4.2. Third-body attraction

Since there are quite some large objects in our Solar System, such as the Sun, the planets and large moons, objects that move in space will experience small accelerations due to the gravitational force from other large objects in the Solar System. These accelerations are called third-body accelerations, and can make the object deviate quite significantly from its two-body problem orbit. The equation for the acceleration due to a third body can be seen in Equation (5.5), where the subscript d is for the third body that perturbs the main body, and the subscript s is for the main body.

$$\frac{d^2\mathbf{r}}{dt^2}_d = \mu_d \left(\frac{\mathbf{r}_{sd}}{r_{sd}^3} - \frac{\mathbf{r}_d}{r_d^3} \right) \tag{5.5}$$

For the asteroid capture, during various phases of the mission these forces need to be modelled accurately. The most important phase is when the asteroid has reached its final state around the Sun and needs to stay in proximity to the Earth-Moon system in a safe and stable manner. Furthermore, when travelling in a heliocentric orbit, en route to the final state of the capture mission, these forces can also play a role when designing the optimal trajectory.
The contribution of third-body attractions is significantly different at various locations in the Solar System. An illustration of this can be seen in Figure 5.3. It can be seen that it is very important at what distance from the Sun the object is located. It was established that during the largest part of the asteroid capture mission, especially the one inside the scope of this thesis project, the object of interest will be close to 1 AU from the Sun. With this in mind, it has been decided to take the Earth, the Moon, Venus, Jupiter and Mars into account as causing relevant third-body perturbations.

5.4.3. Gravity field perturbations

With a perfectly spherical celestial body, including a homogeneous mass distribution on the inside, the gravity field will also be homogeneous or spherically symmetric. In practice however, many bodies do not have these qualities and can thus cause perturbations.

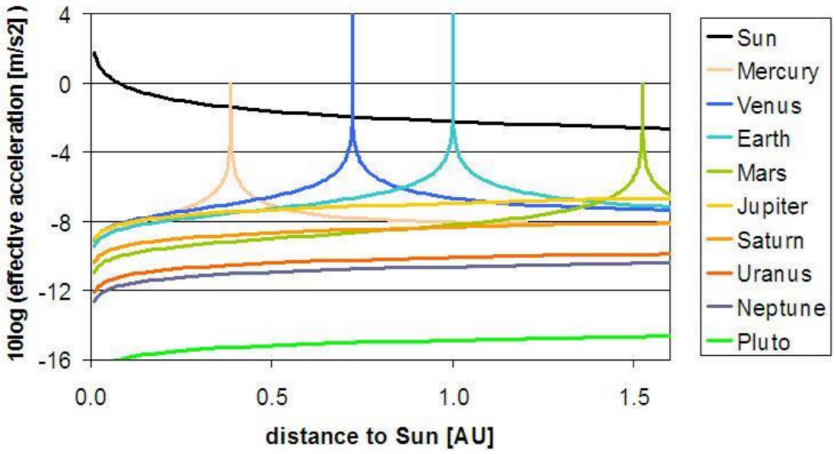

Figure 5.3: Third-body perturbations in the sphere of influence of the Sun [26].

The Earth for example, has a slightly flattened shape. This oblate shape, together with many smaller irregularities in both the shape and the mass distribution inside the Earth, cause the gravity field of the Earth to also have irregularities. The most prominent of these irregularities comes from the zonal harmonics coefficient J_2, which has to be taken into account in case the object of interest is orbiting the Earth. This coefficient has a numerical value of 1.083×10^{-3}. The acceleration caused by this perturbation can be seen in Equation (5.6), where r is the radius at which the acceleration is to be calculated, R is the radius of the Earth, μ is the gravitational parameter of the Earth, J_2 is the coefficient itself and z is defined as $r \cdot \sin\phi$.

$$\mathbf{f} = -\nabla\left[\frac{1}{2}\mu J_2 \frac{R^2}{r^3}\left(3\frac{z^2}{r^2} - 1\right)\right] \tag{5.6}$$

During the part of the asteroid capture mission on which is focused in this thesis project however, there will be no occurrence of geocentric orbits, which means that this perturbation will not be taken into account during further analyses in this thesis.

5.4.4. Solar radiation pressure

The momentum of the photons coming from the Sun, hitting an object in space, can cause a small acceleration on that object. To be able to model that acceleration, the energy flux at the desired location needs to be known. This energy flux from the Sun is inversely proportional to the square of the distance from the Sun, being around $1361\,\mathrm{W/m^2}$ at 1 AU. The relation for the acceleration on an object in space due to the solar radiation pressure, can be seen in Equation (5.7).

$$\mathbf{f} = -C_R \frac{WA}{Mc}\mathbf{e}_S \tag{5.7}$$

In this equation, W represents the energy flux or power density from the Sun at the location of the body, A represents the effective cross-sectional area of the object as seen from the Sun, M is the mass of the object on which the force acts, c is the speed of light and $\mathbf{e}_S$ is the unit vector from the body of interest to the Sun.
For the parts of the asteroid capture mission that are analysed during this thesis project, the solar radiation pressure will not play a significant role. This is due to the fact that the mass to cross-sectional area ratio for an asteroid is very high (caused by its solid shape and dense composition), meaning the acceleration caused by the Sun will be insignificant.

5.4.5. Aerodynamic drag

Finally, aerodynamic drag can be a quite significant perturbation when passing through an atmosphere. For the asteroid capture mission however, this perturbation will not play a role in general, since the mission will mostly occur far away from the Earth, in deep space. There are moments throughout the entire mission, in which drag could play an important role, but these do not occur in the phases on

which this thesis project has its focus. For completeness however, the relation for the aerodynamic drag can be seen in Equation (5.8).

$$\mathbf{f} = -C_D \frac{1}{2} \rho \frac{A}{M} |\mathbf{v}| \mathbf{v} \tag{5.8}$$

In this equation, C_D is the drag-coefficient, ρ is the atmospheric density, A is the reference surface area, M is the mass of the object and $\mathbf{v}$ is the velocity vector, relative to velocity of the atmosphere around it.

5.5. Low-thrust trajectories

As already mentioned before, the focus of this thesis project will lie on the design of the transfer trajectory from the initial position of the asteroid to its final state in a heliocentric orbit somewhere in the proximity of the Earth. The spacecraft performing this transfer will make use of low-thrust engines, which means that some theoretical background on low-thrust trajectories will have to be known and be discussed in this section. It should be noted that the examples as discussed in this section use a geocentric trajectory, but naturally low-thrust trajectories can also be applied to heliocentric transfers.

Since for low-thrust engines, contrary to the high-thrust engines, the applied ΔV can not be seen as an instantaneous velocity impulse, but rather a slow and continuous build-up of velocity, quite different mechanics are at work in the process. Initially, a differentiation can be made between applying the thrust in the tangential direction, or in the radial direction [24]. Applying the thrust in the radial direction however, will only be useful if the ratio between the thrust and the mass of the object is high enough, providing a sufficiently high acceleration. If this is not the case, the object will not be able to escape the main body it is orbiting around. An illustration of this can be seen in Figure 5.4. Here, a_0 is that ratio of the applied thrust force and the mass (times the Earth's gravitational acceleration in this case). If that ratio becomes larger, which means the acceleration on the object is larger, it can be seen that the object will escape. This process will happen faster with higher accelerations, as can also be seen in the illustration. For the asteroid capture mission however, this will not be useful, since the mass of the object will be too large and thus the acceleration will be (too) low.

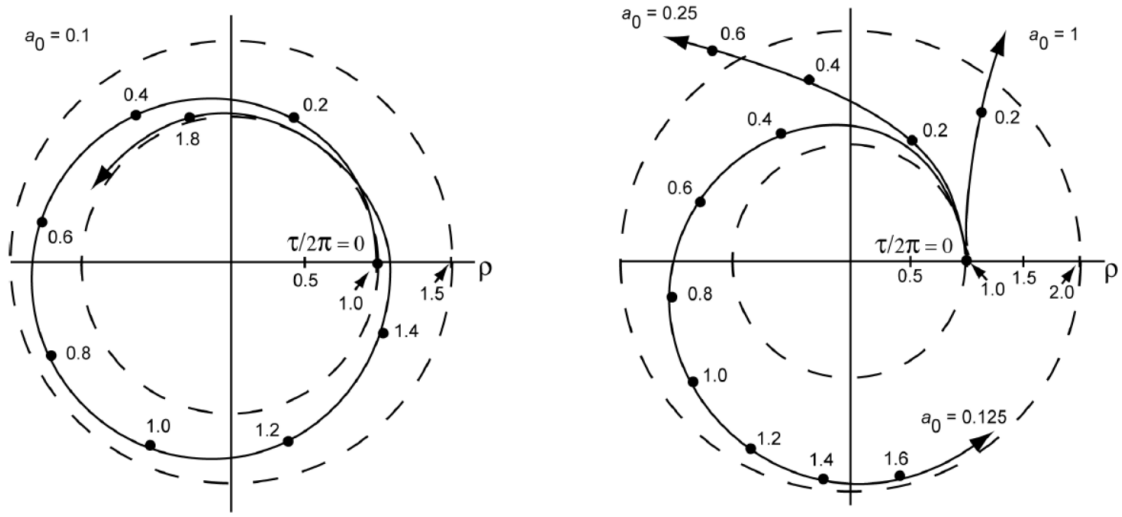

Figure 5.4: Two illustrations of the trajectories following radial thrust being applied to the spacecraft. Various accelerations show different behaviour of the trajectory of the object [24].

The other option is applying the thrust force in the tangential direction. In this case, something interesting and contradicting can occur when starting from a low orbit around e.g. the Earth. In case the above mentioned a_0 is low enough, which generally is the case for larger spacecraft and will certainly be the case for the asteroid capture mission, the acceleration initially will be so low that it can be seen as a small perturbation. Although a velocity impulse is being applied in the direction of

motion (tangential), the object's velocity will not increase. The applied acceleration is so low, that a very dense spiral motion outward will be initiated. Unlike the case with a high-thrust velocity impulse, the velocity will not be increased to a value higher than the local circular velocity, but instead the orbital altitude will very slowly be increased and the velocity will stay approximately equal to the local circular velocity. This local circular velocity decreases with increasing altitude however, which means that the velocity of the object also decreases, even though a thrust force in the forward tangential direction is being applied. The energy of the spacecraft does increase with time, as a result of the continuous propulsion.
After multiple revolutions, of which the number depends on various factors, such as the velocity of the object and the gravitational attraction of the main body, a point will be reached where the object is outward enough with respect to the main body. At this point, the local circular velocity will be so low, that the acceleration of the spacecraft will actually start increasing its velocity again, after which the outward spiral motion will become significant and the object will soon escape the main body. This is paired with a change of the flight path angle γ, which will not be close to zero anymore like in the first phase of the outward spiral, but will rapidly change and approach $90°$, indicating an escape in the radial direction as seen from the main body. It should be noted, that for spacecraft where the propellant mass makes a large part of the total mass of the object, the speed of this process is highly dependent on the efficiency of the engine, or its I_{sp}. Again contrary to what one would intuitively expect, with a higher exhaust velocity and thus I_{sp}, the process will take longer. This is caused by the fact that propellant will be used up in a slower fashion, meaning that the spacecraft will retain a larger mass for a longer amount of time. This means that the acceleration of the object will increase significantly slower than if the I_{sp} would be much lower. This should be taken into account when designing low-thrust trajectories and time plays an important role.

The motion of a low-thrust trajectory with tangential thrust, as described above, can be analysed in a convenient way using an analytic shape-based method. Here, the kinematics of the (outward) spiral are modelled by a suitable mathematical description, of which various implementations exist. As an example, the outward spiral can be seen as an exponential sinusoid from the main body [27]. By setting up a relation for this exponential sinusoid, the computation of these low-thrust trajectories can be simplified significantly and a more efficient way of designing missions can be used. The relation for this method, expressed in polar coordinates, can be seen in Equation (5.9). In this relation, k_0, k_1, k_2 and ϕ are coefficients which define the shape of the spiral. Furthermore, θ and r are the polar coordinates.

$$r = k_0 exp[k_1 \sin(k_2\theta + \phi)] \tag{5.9}$$

Using this shape-based method, and by 'playing' with the coefficients, all kinds of spiral low-thrust trajectories can be expressed. A visualisation of changing e.g. the factor k_2 is shown in Figure 5.5. In a search space that is basically infinitely large, using these exponential sinusoids can make identifying suitable trajectories for low-thrust missions easier.

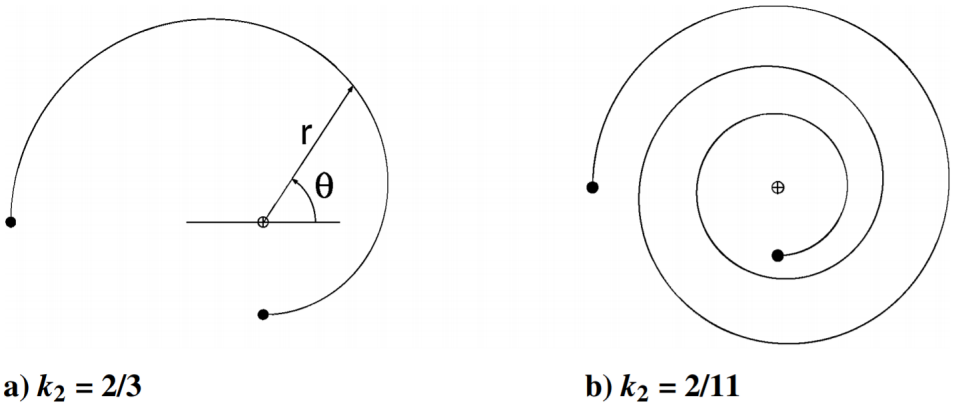

Figure 5.5: An example of changing one of the coefficients in this shape-based approach [27].

In [28], it is proposed to combine these shape-based methods with a genetic algorithm, to be able to efficiently find solutions for the given problem. The example is an asteroid rendezvous mission, which is quite close to the asteroid capture mission, since the performed actions in both missions will partially overlap each other. Generally, the unknowns for these kind of problems are variables such as the launch date and the number of revolutions, which can thus be found using a genetic algorithm that does not need a priori information. They conclude that combining these methods can provide a feasible solution for the problem, taking into account modern-day technology levels.
Finally, the hodographic method and Sims-Flanagan's method for low-thrust trajectories are also useful and convenient ways of analysing various types of low-thrust trajectories. These methods and their theoretical background will be discussed extensively in Sections 8.2.1 and 8.3.1 respectively.

5.6. Stability

In this section, the physics of stability in space will be discussed. This subject is based on the balance (or imbalance) of multiple forces working on a certain body. It is important to analyse the stability of the orbit of the body of interest, which in this mission will be the asteroid. This is especially essential for the final orbit in which the asteroid will be located, since a key requirement for the mission is to deliver the asteroid to a safe and stable orbit, where it will not pose any danger to the Earth or other protected bodies. For completeness, it is started by discussing the 'n-body' system, after which the orbital stability of objects will be discussed.

5.6.1. N-body system

To start the analysis of stability in a certain space, which in the case of this mission will be our own Solar System, multiple bodies in this space will need to be considered. This 'n-body' system, where *n* is the number of bodies, can be defined in a certain reference frame and thus from a certain origin, as already discussed in Section 5.1.

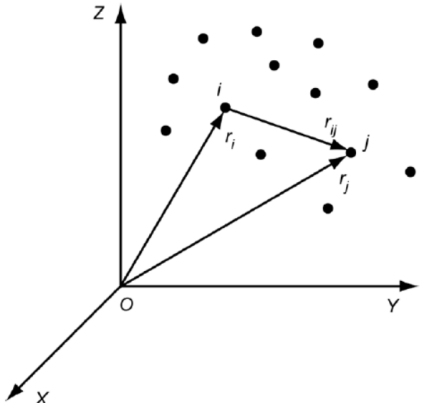

Figure 5.6: An illustration of a multiple-body or n-body system in a Cartesian coordinate system.

A visualisation of such an n-body system is shown in Figure 5.6. In this system, the present masses are assumed to be point masses. The body i has a mass of m_i and a distance from the origin r_i. It is experiencing gravitational attraction from all other bodies j, to which it has distance r_{ij}.
In this way, each body is affected by a gravitational force from all other bodies, whether it is a strong force or a weak force. This is dependent on the mass of the other bodies and the distance to the body of interest. A general relation for body i can be written as done in Equation (5.10), where it can be seen how the mass and distance are related to the attraction. In this equation, j starts at 1 and goes to *n*, but excludes $j = i$.

$$\frac{d^2\mathbf{r}_i}{dt^2} = \sum_{j \neq i} G \frac{m_j}{r_{ij}^3} \mathbf{r}_{ij} \tag{5.10}$$

This problem can be solved analytically for $n = 2$, but a numerical analysis is necessary for larger numbers of *n*.

For closed systems of *n* bodies, which means that there are no external forces working on the bodies, the laws of conservation apply. This means that total linear and angular momentum of the system are conserved, as well as the total energy of the system. Furthermore, the barycentre (or centre of mass) of the whole system will stand still or move in a linear way with respect to the inertial reference frame. The angular momentum vector will have one specific direction and magnitude, and the plane perpendicular to this vector is called the 'invariable plane of Laplace'.
This plane is defined using the fact that the bodies are point masses, which in reality is not the case. The fact that the bodies also have a rotation around their own axes, takes away from the angular momentum they have around the origin of the reference frame and thus changes the orientation of the invariable plane slightly. In our Solar System however, these changes are small and the invariable plane stays fairly constant with respect to the ecliptic of the Earth around the Sun at $1°35'$.

The total specific energy of a closed systems can be expressed with the integration constant *C*. This constant can be related to the two different forms of specific energy, potential and kinetic energy, as can be seen in Equation (5.11).

$$\mathscr{E}_k + \mathscr{E}_p = C \tag{5.11}$$

This means that these two forms of specific energy are always balanced in such a way, that the total of both stays constant for a closed system of bodies. The value of the potential energy is always negative, whereas the value of the kinetic energy is always positive. The sum of these two, the previously mentioned integration constant *C*, can give some valuable information about the stability of the bodies inside the system. If the value of *C* is equal to or larger than zero, then the system is always unstable. This means, that after a period of time, one or more of the bodies will escape the system by moving away from the origin of the system. On the other hand, when the value is less than zero, the system will generally be stable, although it is not always the case: the potential and kinetic energies can have specific values which make *C* less than zero but still cause an unstable system.
A stable system is thus a system where no escapes occur and where the bodies will stay enclosed in a certain three-dimensional space. Furthermore, the bodies inside this system should not collide with each other, which means a certain minimum distance between all bodies should exist at all times.

5.6.2. Orbital stability

In the previous section, the n-body problem and the corresponding forces have been discussed. More general stability in 'normal' Kepler orbits around bodies is vital for the asteroid capture mission, not only as a possible final orbit for the mission, but also in intermediate stages of the mission when the spacecraft or spacecraft and asteroid are orbiting for longer periods of time in a certain orbit.

A small body that is orbiting a larger body in a two-body system will have an elliptical orbit. This elliptical orbit will not change significantly without large external forces, and therefore this body will have orbital stability. This means that the orbital parameters will stay (almost) equal over longer periods of time. When adding small perturbing forces, as mentioned in Section 5.4, the orbital parameters will start to change and this can become quite significant over time. With a slightly smaller or larger semi-major axis e.g., the true anomaly will change and can become exactly opposite of what it would be without the perturbation, while the other orbital parameters could still be close to their original value. This means that although the orbit looks quite stable, large changes are occurring in at least one of its orbital parameters. Therefore, a distinction needs to be made between 'orbital stability' as coined by Poincaré, which would still consider the above-described change of true anomaly as stable, and the 'isochronous (or dynamical) stability' as proposed by Lyapunov, which would consider the described change as unstable.

It is also important to perform an extensive analysis on the duration that a certain orbital stability can be maintained. If the asteroid is located somewhere in the Earth-Moon system, orbiting either of the two bodies, how long will it be able to stay in that specific orbit without any added velocity impulses? The perturbing forces will act on the object and will cause its orbital parameters to differ over time, but it is crucial to know how significant this will be for various orbits. It is known that for certain orbits, such as very low Earth orbits, the perturbing forces can be so large that the orbital parameters change drastically in a short period of time, which makes the orbit very unstable, as already discussed

in Section 5.4.5. It is thus essential for the asteroid capture mission to find an orbit that will experience very little perturbations, in order for the asteroid to stay in its orbit for long periods of time without added velocity impulses.

To assess this, use can be made of numerical integration models that will simulate longer periods of time (in the order of multiple decades), as will be done in Chapter 7. In these models, the expected significant perturbing forces will be included, in order to make the analysis sufficiently realistic and accurate. Attention should be payed to accumulating integration errors, especially in case a risk of encountering singularities exists. An example of this, could be the close passage (at periapsis) to the main body in a highly eccentric orbit. A solution to this can be the use of regularisation, which is to perform transformations on variables. Transforming both the dependent and independent variables could optimise the form for numerical integration for the equations of motion. In this way, the accumulation of numerical errors can be limited.

5.7. Conclusions

A brief conclusion will follow on this chapter in which some background is provided on the topic of astrodynamics. Since the goal of this thesis project is to transfer an asteroid to an orbit around the Sun in close proximity to the Earth, the reference frame that will be used throughout the thesis is the heliocentric reference frame. Furthermore, numerical integrations will generally be performed using Cartesian coordinates, but some definitions of orbits can be given in Kepler elements.
It has been discussed which perturbing forces are expected to play a significant role during this thesis project, and these will therefore be used throughout the analysis. These perturbing forces are gravitational accelerations caused by bodies in our Solar System, such as Venus, the Earth, the Moon, Mars and Jupiter. Some possibilities of quickly analysing low-thrust trajectories have been discussed, with a further elaboration upon some techniques still to come in Section 8.2.1.
Finally, the stability of the asteroid orbit, especially once it has reached its final state around the Sun in the proximity of the Earth, has been discussed. Various forces should be taken into account and these should be balanced in such a way that the final orbit of the asteroid will remain stable for the decades to come. As already mentioned, the complete Chapter 7 will focus on this very important aspect of the mission.

II

Analysis

6

Asteroid Selection

In this chapter, a preliminary analysis will be performed on a set of NEA's, to assess whether each of them is a suitable candidate for the asteroid capture mission. It is started by explaining the reasoning behind this analysis in Section 6.1, which is followed by a description of the approach towards this analysis in Section 6.2. The used method will be elaborated upon, with explanations on how it will be implemented in the software. This is followed by results of the analysis in Section 6.3, with various figures to visualise how 'optimal' each candidate is and to show how certain parameters affect the final results. The chapter ends with the conclusions on the subject and a final best candidate, which will be used throughout the remainder of the thesis.

6.1. Reasoning

To design the asteroid capture mission and end up with the best and most optimal results, it is very important to analyse which asteroids are most suitable for such a mission. This means that a preliminary analysis is to be performed, which roughly assesses how large the velocity impulse to be applied on the asteroid should be.
The reasoning for this preliminary analysis, is based on the fact that the final analyses for the asteroid capture mission can possibly be very extensive and require long computation times. This is due to the expected low-thrust trajectories and the possibility of multiple revolutions (and thus long propagation times), as well as the possible variety in the thrust profile compared to high-thrust trajectories. Next to this, the optimisation of all these trajectories is also expected to require large numbers of computations. Performing these extensive analyses on a large number of asteroids is therefore not seen as an efficient method of approaching the asteroid capture mission, especially given the limited duration of time in which the thesis is to be performed.

Following the conclusion drawn above, it is decided to perform the previously mentioned preliminary analysis on a batch of asteroids that already has been filtered through certain constraints. From this batch, ideally at least a few asteroids will come out as potential targets for the asteroid capture mission, looking at the various constraints that have already been identified in Chapter 3. It will then be possible to continue the extensive analysis on the single 'best' asteroid, instead of doing this for tens, hundreds or even thousands of asteroids.

6.2. Method and program

An easy and convenient method to analyse multiple transfer trajectories in a relatively quick manner, is by using a Lambert targeter. A Lambert targeter is an algorithm that tries to find a minimum-ΔV trajectory for an object, when a departure and arrival position (or position vector from the Sun) are given, together with a time of flight for the object between the departure and arrival position. The original algorithm assumes instantaneous velocity impulses [29], from which it follows that a high-thrust propulsion system is used in the assumption. This means that the output of the Lambert targeter will be a high-thrust transfer trajectory with the smallest velocity impulse that is required to reach its target

destination. However, during the past few decades many researchers have found other methods of solving Lambert's problem, also using trajectories suitable for low-thrust spacecraft [30]. Both will be discussed briefly below.

First, a summarised mathematical explanation on Gooding's method of the high-thrust Lambert targeter will be given in this section. It is started by stating that only three elements are required to define the time to transverse an elliptical arc [24]. These are the sum of the previously mentioned position vectors ($\mathbf{r}_1$ and $\mathbf{r}_2$) from the focus point (which in this case is the Sun), the length of the chord (c) between the departure and arrival position and the semi-major axis (a) of the ellipse. A visualisation of the geometry that is used for the Lambert targeter can be seen in Figure 6.1.

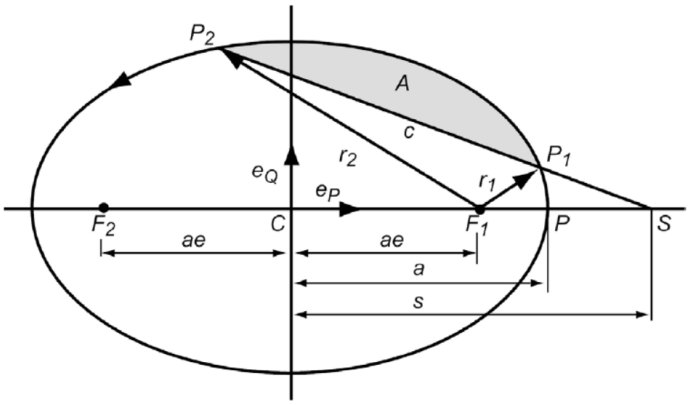

Figure 6.1: The geometry that is used for Lambert's problem [24].

Using the above described points of departure and arrival (P_1 and P_2), an eccentric anomaly can be defined for each of these points, being E_1 and E_2 respectively. The time of flight from P_1 to P_2 can then be formulated as seen in Equation (6.1).

$$t_f = \sqrt{\frac{a^3}{\mu}} \left[E_2 - E_1 - e\left(\sin E_2 - \sin E_1\right)\right] \tag{6.1}$$

As defined in [29], the parameter x has been set up, which will be used in a process of iteration until conversion. The formulation for the parameter x can be seen in Equation (6.2), with s being equal to half of the sum of r_1, r_2 and c.

$$x^2 = 1 - \frac{s}{2a} \tag{6.2}$$

After various mathematical manipulations and introduction of new parameters, a value for x can be obtained. A few of these new parameters can be seen in Equations (6.3) to (6.6), in which $\Delta\theta$ is the angle between $\mathbf{r}_1$ and $\mathbf{r}_2$.

$$q = \frac{\sqrt{r_1 r_2}}{s} \cos(\Delta\theta/2) \tag{6.3}$$

$$E_{lam} = x^2 - 1 = E_{lam}(x) \tag{6.4}$$

$$y = \sqrt{|E_{lam}|} = y(x) \tag{6.5}$$

$$z = \sqrt{1 - q^2 + q^2 x^2} = z(x) \tag{6.6}$$

These parameters can then be used in the normalised version of Equation (6.1), which can be seen in Equation (6.7). The value for x can thus be obtained through this equation after several iterations.

$$F(x) = T - \frac{2(x - qz(x) - d(x)/y(x))}{E_{lam}(x)} = 0 \tag{6.7}$$

With this value of x, which also contains the semi-major axis of the transfer orbit, both the departure and arrival velocity vectors can be computed, with which the total required velocity impulse (ΔV) can be determined.

Next to the above-described method, various other methods have been found to solve the low-thrust version of Lambert's problem [30]. One of these is Izzo's method, which uses exponential sinusoids to model the (multi-revolution) trajectories from the point of departure to the point of arrival [31][32]. In this way, the same problem can be solved for a low-thrust spacecraft. The principle is the same, only with a different mathematical approach to achieve a different (computationally faster [32]) method.

The idea for this first analysis, is thus to perform a Lambert targeter analysis on each of the asteroids in the batch. For this assessment, it is assumed that the asteroid will simply be transferred to the exact location of the Earth, with respect to the Sun. This means that no additional velocity impulse will be given to the asteroid once it has reached the exact location of the Earth, either for it to be captured in a certain orbit around the Earth or in an orbit around the Sun in close proximity to the Earth. This shows the (low) level of detail that is used for the preliminary asteroid selection, in order for it to be performed in a fast and efficient manner.

Tudat (TU Delft Astrodynamics Toolbox) will be used for the creation of software with respect to the transfer trajectories. This means that built-in functions and libraries can be used when writing a new program, which will thus be done extensively.
The very first step in the process is to generate a list of asteroids that will be analysed through the software that will be written. This list is generated using the 'JPL Small-Body Database Search Engine', which is a tool created by JPL to find small bodies and their corresponding orbital and physical parameters [16]. A useful feature of this search engine is the ability to apply constraints on a multitude of parameters, before the list is generated. In this way, a selection can be made of asteroids that comply with certain wishes of the designer. In the case of the asteroid capture mission, after trying different combinations of constraints on various parameters, it was decided that a list will be generated of all NEA's (Atiras, Atens, Apollos and Amors) with a maximum diameter of $100\,\mathrm{m}$, without any additional constraint on orbital parameters. With this constraint, a reasonable set of 52 asteroids was formed, from which the orbital parameters (and the corresponding epoch), the object diameter and the full name of each asteroid were listed in a table.
During the process of analysis, a few studies were found in which favourable asteroids were proposed and discussed. One of these studies proposed two specific asteroids as potential targets, which had a combination of favourable orbital parameters and a small diameter [33]. After further reading [34] [35], it was decided to add these two asteroids to the list of 52. Fortunately, both were present in the JPL database, which made inclusion in the table convenient. It was found that the reason why these two asteroids were not included in the first 52 asteroids, was the absence of a specified size of both asteroids in the database: they were not taken into account, when a constraint on size was placed. With the inclusion of these two asteroids, the final list contained 54 asteroids.

To give an overview of the category to which these 54 asteroids belong, and a general idea of their spread in terms of semi-major axis and eccentricity, these two parameters have been plotted in yellow circles with black edges over the image of the complete distribution of asteroids in this spectrum that could be seen in Figure 3.2, taken from [1]. This visualisation can be seen in Figure 6.2. The layout of the generated table can be seen in Figure 6.3, where the first few rows are shown. Note that this table does not show any units of the parameters, nor does it have a nice and professional layout. It is merely shown to indicate the way in which the search engine outputs the requested parameters.
As established previously, the asteroid selection can be done by using the position of the asteroid at a certain moment in time, together with the position of the Earth at another moment in time. This means that these positions need to be loaded into the software in some way, or they need to be extracted from an existing system in Tudat, like the SPICE kernels. The most efficient way of being able to use a position at any time in the future, is by using ephemeris data. For planetary bodies in our Solar System, like the Earth, this ephemeris data can indeed be extracted through Tudat. For various smaller asteroids however, this problem needs to be approached in a slightly different way. With the orbital parameters (Kepler elements) of the asteroids in the generated list, combined with the epoch of these parameters,

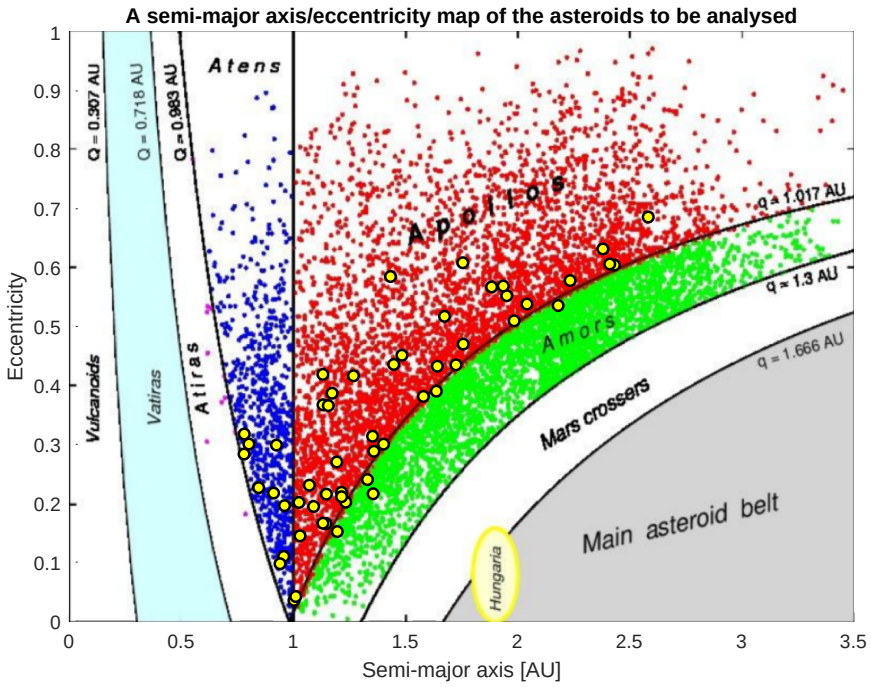

Figure 6.2: The 54 asteroids that will be analysed, plotted for their semi-major axis and eccentricity over the image of a general distribution of NEA's from [1].

a	e	i	om	w	ma	epoch_mjd	diameter	full_name
0.910899342	0.217273846	2.101256124	159.3676612	119.4810799	93.88877846	58600	0.096	450237 (2002 XY38)
1.130933313	0.418805011	8.70873619	73.39828973	232.8209901	202.8392136	56497	0.099	506590 (2005 XB1)
1.192939035	0.269988356	7.176856497	154.7342042	265.2735457	70.16450042	58600	0.083	518810 (2010 CF19)
1.232902162	0.201841404	1.481034424	84.3663179	209.3671431	71.54311122	58600	0.03	(1998 KY26)
0.923729452	0.298742132	3.692301757	202.6487061	253.9036781	133.8041622	58600	0.028	(2002 JR100)
1.267198334	0.416373233	5.992314749	279.6471644	278.2067304	318.2050241	55209	0.05	(2010 AE30)
1.755128191	0.608291133	2.03041901	21.57932165	183.7844012	331.9440076	58600	0.089	(2010 AG40)
1.935703598	0.568798289	9.566358829	120.9820451	60.58714095	142.0655113	58600	0.08	(2010 BC)
1.14658599	0.215396174	27.2767126	141.4573425	77.87373481	306.5665418	55240	0.084	(2010 CK1)
1.070409329	0.230633971	6.181261746	327.4915035	73.84394537	185.1368728	58600	0.034	(2010 CO44)

Figure 6.3: The first few rows of the table as generated by [16], used in the asteroid selection program.

ephemeris data can be created in Tudat. This function proves to be very useful, since the resulting ephemerides can be used in the Lambert targeter function. Both Gooding's and Izzo's methods are implemented in Tudat and for this preliminary analysis it was decided to use Izzo's algorithm, due to it being identified as the algorithm with the best ratio between robustness, speed and accuracy [30].

A grid search is created subsequently, which performs the Lambert targeter algorithm for different departure dates and different times of flight. This means that these two variables will need to be set up with bounds, which the grid search algorithm can use throughout its computations. The bounds for the departure date were set on 1 January 2023 and 1 January 2030, to span a timeframe that is large enough and in this way mitigate significant time-related fluctuations. Next to this, the bounds for the time of flight have also been set up to span a large search space, from 100 to 1000 days. After establishing these bounds, the number of steps in each direction has been defined. This is based on a simple trade-off between accuracy and computation time. It was eventually found that 500 steps in each direction of the search space will provide a sufficient coverage of the complete search space, while not causing the program to run for very extensive periods of time. This results in steps of approximately 5.1 days in departure date, and steps of 1.8 days in time of flight.

6.3. Results

The program will thus perform the Lambert targeter function for each of these 250 000 combinations and output the required ΔV for each point. The lowest ΔV and thus most optimal solution is saved in a list, with the corresponding departure date and time of flight. This complete process is placed inside a loop in the program, and is thus repeated for all 54 asteroids.
The result of this, which was also the final goal of this program, is a list with all asteroids and the ΔV for the most optimal multi-revolution trajectory from their position between 2023 and 2030 to the position of the Earth, between 100 and 1000 days later. This list is subsequently sorted based on the ΔV, such that a clear tabulated overview is present wherefrom it can be seen which asteroid is the most appropriate and thus best asteroid to continue analysing for the asteroid capture mission. The first few rows of this sorted list can be seen in Figure 6.4.

ΔV (m/s)	Departure day (Years CE)	Time of flight (days)	Diameter (km)	Object name
880.2394057	2025.132265	644.6893788	0.0025	'(2006 RH120)'
1428.69763	2023.322645	971.1422846	0.0035	'(2009 BD)'
2888.813009	2029.242485	628.4569138	0.032	'(2010 HA)'
3319.672014	2023.476954	871.9438878	0.0025	'(2012 XB112)'
3359.627861	2023.57515	347.0941884	0.03	'(1998 KY26)'
3487.523498	2026.549098	193.7875752	0.013	'(2010 KV7)'
4445.069521	2030	130.6613226	0.096	'450237 (2002 XY38)'
4867.932104	2023.757515	534.6693387	0.008	'(2010 GH7)'
5061.375498	2028.288577	976.5531062	0.064	'(2010 HX107)'
5236.375502	2024.360721	776.3527054	0.018	'(2010 FT)'

Figure 6.4: The first few rows of the list of asteroids, sorted based on the required ΔV, including their departure date, time of flight and diameter.

As already concluded in Chapter 3, the captured asteroid should not be too heavy, since the capture mission will become increasingly less feasible with increasing mass. It was established that a density range between 2000 and 3000 kg/m^3 can be expected, meaning that the mass will be dependent on the size using a set assumption for this density. It is therefore beneficial to have a smaller-diameter asteroid, for the mission to be feasible. This means that this strict criterion should also be assessed when selecting the most optimal asteroid. To make this process easier and clearer, scatterplots that contain all 54 asteroids have been created, plotted for their most optimal ΔV value on the *x*-axis, and their diameter on the *y*-axis. Furthermore, to show how some of the Kepler elements influence the 'ease of capturing' a certain asteroid (and thus the required velocity impulse), each asteroid has been given a colour on the three different scatterplots, depending on either their semi-major axis, eccentricity or inclination. These three plots can be seen in Figures 6.5 to 6.7 respectively.

First of all, an observation can be made with respect to the position of all asteroids on these plots. It can be seen that the asteroid with the (tied) smallest diameter, also has the lowest required velocity impulse to transfer it from its location to the location of the Earth by means of a Lambert targeter transfer orbit. This can be seen as an incredibly positive and convenient result, since a small diameter (and thus probably low mass) will result in a lower amount of required propellant for a certain velocity impulse and a lower required velocity impulse will consequently also reduce the required propellant mass, thus increasing the feasibility of the mission. The reason for this convenient correlation between their smaller diameter and the suitability for the asteroid capture mission (which is dependent on the orbit they are located in at the moment) could possibly be explained by the fact that smaller asteroids can be observed more easily once they are in closer proximity to the Earth.
This means that this asteroid, which is identified as "2006 RH120", is the perfect candidate for the asteroid capture mission. Next to this asteroid, there are two other asteroids that have a small diameter (one being the other asteroid with an approximate diameter of 2.5 m and the other being an asteroid with an approximate diameter of 3.5 m), and have reasonably low required velocity impulses (in this preliminary high-level Lambert targeter analysis), of approximately 3.32 km/s and 1.43 km/s respectively. These two asteroids, which are identified as "2012 XB112" and "2009 BD" respectively, will also be potential candidates for the asteroid capture mission, but follow "2006 RH120" by quite a distance in terms of being the most optimal candidate.

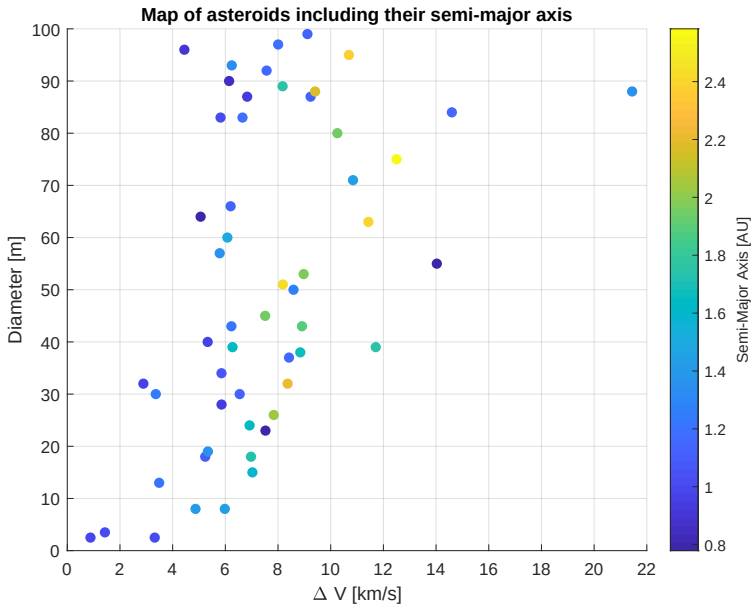

Figure 6.5: A scatterplot of the diameter against the minimally required velocity impulse of the asteroids that were analysed through the program described above. A colour scheme is added to show the semi-major axis of each asteroid.

On the first scatterplot, which is depicted in Figure 6.5, a colour has been added to the asteroids, depending on their semi-major axis around the Sun in Astronomical Units. It can be observed, that in general asteroids that require larger velocity impulses to be transferred to the Earth, have semi-major axes further away from 1 AU, with a few exceptions that will be discussed later in this section. This is quite logical when observing the laws of physics and the mathematical expressions for transfer trajectories like these: when two orbits have larger differences between their semi-major axes, the objects in these orbits will be located further away from each other in general, which will require a larger velocity impulse.

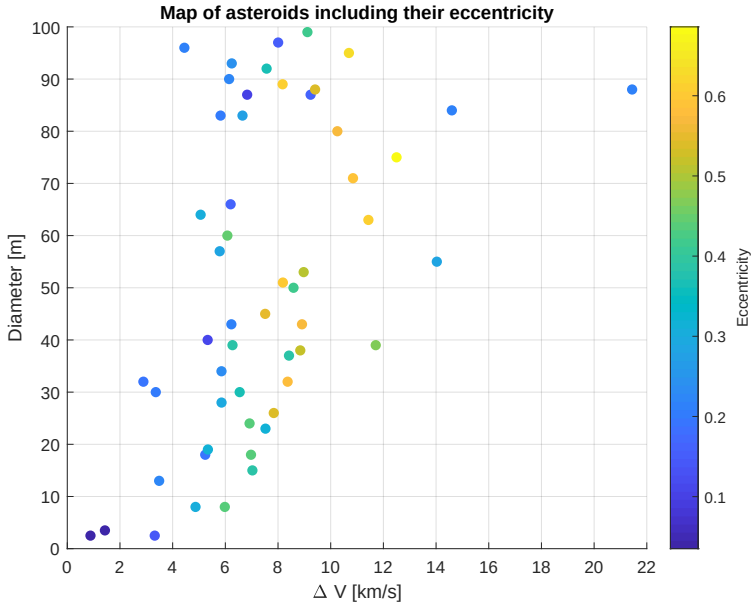

Figure 6.6: A scatterplot of the diameter against the minimally required velocity impulse of the asteroids that were analysed through the program described above. A colour scheme is added to show the eccentricity of each asteroid.

The second scatterplot, which is depicted in Figure 6.6, is somewhat connected to the first scatterplot. It is connected, due to the fact that a large deviation from a semi-major axis of 1 AU, will mean that the asteroid will most probably also have a larger eccentricity, for it to remain a 'near-Earth asteroid', which comes relatively close to the orbit of the Earth now and again. This can also be seen in Figure 6.2, where all asteroids with a large semi-major axis have a larger eccentricity. Because of this, a large number of the asteroids analysed with the program and shown in these scatterplots, share a reasonably similar colour in Figures 6.5 and 6.6. There are exceptions to this however, with asteroids that do not specifically have a large semi-major axis, but still have quite a significant eccentricity. These asteroids will therefore require a larger total velocity impulse to be transferred to the position of the Earth, and thus be located in the middle or more towards the right-hand side of the figure.

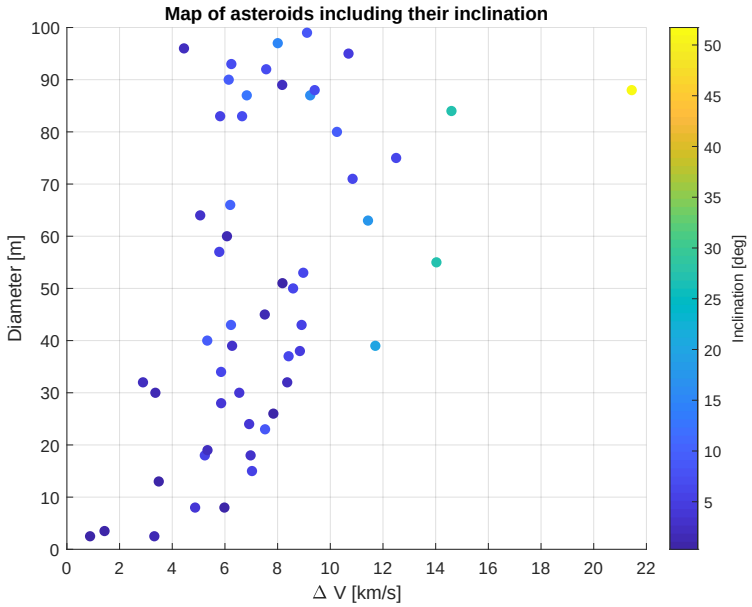

Figure 6.7: A scatterplot of the diameter against the minimally required velocity impulse of the asteroids that were analysed through the program described above. A colour scheme is added to show the inclination of each asteroid.

There is also another factor that can be examined during this analysis, which brings us to the third scatterplot that is depicted in Figure 6.7. In this scatterplot, the colour of the asteroids represents the inclination of the specific asteroid orbit with respect to the ecliptic plane. A clear correlation can be seen between the inclination of the asteroid and the required velocity impulse. This also follows the known laws of astrodynamics, in which (large) plane changes require large velocity impulses.

6.3.1. Verification and Validation

For this first preliminary analysis of which asteroid will be the most suitable candidate for the asteroid capture mission, the verification and validation part will be discussed briefly in this paragraph. First of all, use has been made of already existing functions in Tudat, which have been extensively tested, verified and validated, both internally and externally. With this given, it can be assumed that using these functions in a straightforward manner (without applying any modifications to them) will provide correct results.

Furthermore, throughout the implementation of the given problem for the asteroid selection, intermediate results were constantly checked whether they have the correct value, and in this way verified that the appropriate computations were performed. Examples of this are states (of the asteroids or the Earth) at certain epochs at which the correct value is known.
Next to this, since this analysis is purely based on mathematical computations (through the Lambert problem) and thus no perturbing forces have been added to the analysis, an important factor of mistakes or inaccuracies has been evaded. As will be seen in Section 8.3.4, where perturbations will be added to the analysis, verification and validation will be more elaborate to ensure the high quality of the results.

Finally, the three scatterplots that have been created in Figures 6.5 to 6.7 serve as a good check to see whether the results make sense from an astrodynamical point of view. This is a very important aspect of the design process for engineers, namely to perform such a 'sanity check' and see whether the obtained results make sense taking into account all the knowledge the designer has on the field of mathematics, physics etc. Asteroids with certain orbital elements that differ significantly from those of the Earth require much more ΔV to be transferred to the position of the Earth. This is also the conclusion that was drawn when analysing the three scatterplots, which reinforces this sanity check.

6.4. Conclusions

Based on the obtained results from the written program and analysis, a conclusion can be drawn. The main candidates have already been mentioned in Section 6.3, but the final decision will be summarised here. For clarity, an extra figure has been created of the lower-left corner of the previous three scatterplots, with the added names of the three potential candidates. This can be seen in Figure 6.9. From this final plot, it becomes clear that asteroid "2006 RH120" is the best candidate, looking at both the required total velocity impulse and the diameter of the asteroid. It is a clear winner and will thus be used from now on as the main asteroid capture candidate. It is followed at a distance by asteroid "2009 BD" and "2012 XB112", which will still be treated as potential candidates, but more as a back-up. This means that the following steps of this thesis can be taken with a well-suited asteroid to be captured. In addition to the provided image in Figure 6.9, the orbital elements of the three discussed asteroids are shown in Figure 6.8.

a [AU]	e	i [deg]	Ω [deg]	ω [deg]	M [deg]	Epoch [days]	Diameter [km]	Full name
1.001861501	0.035128561	1.08773103	292.7942227	226.7806661	307.8249579	54105	0.0025	(2006 RH120)
1.009762523	0.041631181	0.384479452	58.12755333	109.8709552	349.7265315	55256	0.0035	(2009 BD)
1.028875864	0.1446215	1.321926423	76.87102687	88.83578948	333.1476506	58600	0.0025	(2012 XB112)

Figure 6.8: The orbital elements of the three candidate asteroids.

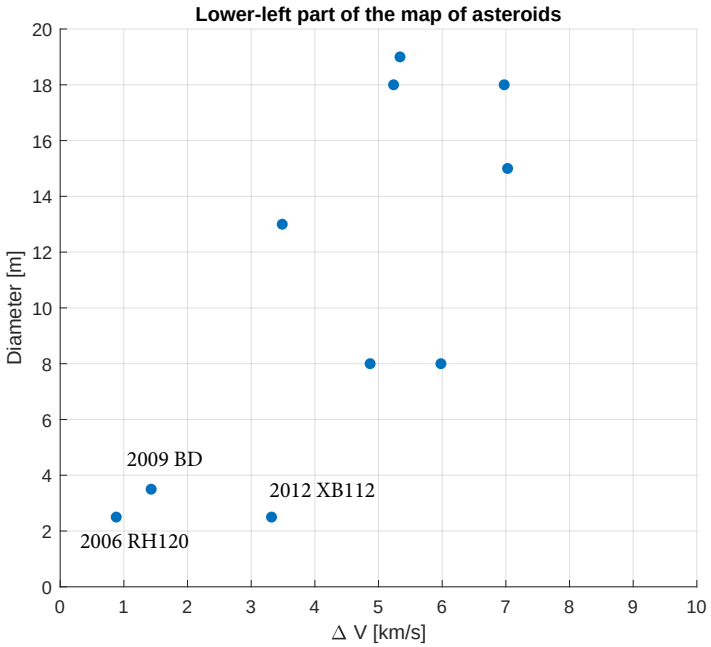

Figure 6.9: A zoomed-in version of the lower-left part of the map of asteroids, including the names of the three candidate asteroids.

7

Stability Analysis

The next step in the process of the design of the asteroid capture mission, is the assessment of the final orbit of the asteroid, after it has been captured. This is a crucial aspect of the mission, since the asteroid has to remain in this final orbit for a long period of time. In addition to this, it is desired for the asteroid to be in a conveniently reachable location from the Earth, such that the scientific missions in prospect can efficiently reach the asteroid.

It was already decided in Chapter 2 that the target orbit for the asteroid in this thesis project will be a heliocentric orbit in close proximity to the Earth. In this chapter however, it will be investigated where exactly around the Earth is the most suitable location for the asteroid to be transferred to.
It is started in Section 7.1 by going through some definitions from the research question and translating these into real values, so that the analysis has something concrete to hold onto. The so-called 'stability analysis' that will be performed in this chapter, will follow a certain approach, which will be discussed in Section 7.2, including the software setup. This is followed by the results of all of the various analyses in Section 7.3, which includes a sensitivity analysis and a brief section about the verification of the software. The chapter ends with the conclusions and a summary of the findings.

7.1. Definitions

As already mentioned in the description of the research question of this thesis report, which can be read in Section 1.1, a very important aspect of the design of an asteroid capture mission is the location of the final orbit. The objectives for this final orbit have been summarised in a concise but complete manner in the research question, namely that it should be a safe, stable and easily accessible orbit. Safe, in terms of the risk that it may collide with another celestial body, mainly the Earth, causing a variety of problems in our Solar System or to humanity. Stable, with respect to the body it is orbiting and the other bodies it approaches closely during its orbit. And finally, easily accessible for future scientific missions, in terms of the required velocity impulse to be applied (or ΔV) to reach the asteroid at any given moment in time.

In order for the analysis to be performed with a meaningful outcome, explicit (numerical) definitions need to be formulated for these objectives. In this way, it will not only be clear what the analysis should work towards throughout the writing of the program, but also which outcomes are desired and should be looked out for and which outcomes can quickly be discarded.
As a start, the safety of the final orbit can be defined with a minimum distance the asteroid needs to keep at all times with respect to other bodies, most importantly the Earth. A good reference value that can be used for this, is the Hill sphere of a body, which indicates where the zero-velocity surfaces, or surfaces of Hill are located for that body [24]. For the Earth, this is approximately at a distance of 1.5×10^6 km [36]. This means that if the asteroid at any point in time during the complete simulation has a distance to the Earth of less than 1.5×10^6 km, this set of initial conditions is seen as infeasible.
For stability, it is desired that the orbit of the asteroid does not change significantly with respect to the orbits of the bodies around it, such as the Earth and the Moon. This means that it is not desirable if

the asteroid starts drifting away from the Earth-Moon system, even if its orbit around the Sun remains relatively equal to the visible eye, or with approximately the same shape- and plane-defining Kepler elements. It is thus possible to translate this requirement to a numerical value of the maximum distance the asteroid should have with respect to the Earth, at any point in time during the complete simulation. This distance can then be defined in various ways, which all have a degree of arbitrariness. Keeping the occurrence of 'drift-away' in mind, in which the asteroid could move away from the Earth to a position as far as approximately 2 AU from the Earth (on the other side of the Sun but in a similar orbit), it is decided to take a fraction of the distance to this limiting drift-away point. The distance along a circular orbit to this point can be found by multiplying the radius of the orbit (1 AU) with π, which results in about 4.7×10^8 km. By saying that the asteroid should not drift-away more than $10\,\%$ of this distance (which equals to $18°$ along the orbit), the resulting maximum distance of 4.7×10^7 km is achieved.
Finally, for the accessibility of the asteroid other criteria than the minimum or maximum distance to the Earth will be used. For the accessibility, it will be analysed what the required ΔV will be for a transfer trajectory from the Earth to the location of the asteroid, at any point in time throughout the complete simulation. This is done to ensure a constant availability of possible transfer trajectories from the Earth to the asteroid over long periods of time, in contrast to only having a few small time slots in which missions could be performed, which for example is the case if the asteroid starts drifting away from the Earth-Moon system. The goal here, is thus to minimise the required ΔV and ensure a constant availability of possible transfer trajectories throughout the complete simulation period.

7.2. Approach

This stability analysis thus contains many different aspects that have to be taken into account, so that the most optimal final orbit (in terms of the three previously mentioned criteria) can be found. In order to proceed in a structured way, it has been decided to start analysing the stability of the asteroid in a very close proximity to the Earth.

7.2.1. Method and software setup

To achieve this, the software is written to first simply propagate the Earth and the Moon for a certain period of time, including accelerations of various bodies. These bodies are the Sun, Venus, Mars and Jupiter. Furthermore, the central gravity of the Moon is an acceleration for the Earth and vice versa. For this propagation, use was made of certain ephemeris files from the SPICE kernels [37] available in Tudat, combined in such a way that the propagation can be performed for a time period of 100 years, which is an appropriate time frame to analyse the stability of a body. This time period for a propagation of 100 years has been chosen after a trade-off, looking at the balance between effectively showing the long-term stability of an object in space relevant for space exploration missions and the computational time for the propagation. The simulation will thus run from the year 2030 to 2130, which is seen as a realistic time frame for the analysis.

The next step after this initial propagation of the two known bodies, is to add a fictional 'asteroid' to the propagation. This asteroid has been given a certain mass, based on the diameter of the most optimal asteroid, found in Chapter 6. This diameter is 2.5 m, which gives a mass of $20\,453$ kg, assuming a perfect sphere and the in Chapter 3 established density of $2500\,\text{kg/m}^3$. To achieve the aforementioned close proximity to the Earth(-Moon system), it has been decided to take the state of the Earth at the starting time of the simulation in Kepler elements, change one or two of its elements slightly and use this newly obtained state as the initial state for the fictional asteroid in the 100 years propagation. In this way, it can be analysed what the long-term behaviour is of an arbitrary body with a certain initial state, in close proximity to the Earth. It should be noted, that what is called 'initial state' in this section and chapter, to specify the starting point of the 100 years propagation and thus stability analysis, is actually the 'final state' of the asteroid as it will be defined in Chapter 8 after the transfer trajectory from its real orbit.

The program was then written in such a way, that it can loop through multiple values of whichever Kepler element is desired to be changed, with the step size and number of steps fully customisable. This first loop was subsequently placed inside a second loop, which can loop through a second Kepler element. In this way, a 2D search space can be analysed, in which two different Kepler elements are slightly changed with respect to the elements of the Earth. It should be noted that adding more than

two Kepler elements in this analysis would lead to a too large number of computations. This means that a 2D grid is created, in which each point represents an initial state of the asteroid with the exact same Kepler elements as the Earth at the start of the simulation period, with the actual values of the *x*- and *y*-coordinates of that grid point as an exception. Each of these initial states is thus propagated for 100 years, so that it can be analysed how the stability of each of these points behaves throughout this time period. For ease of future reference, each one of these 100-year propagations with a slightly changed initial state with respect to the Earth will be called a 'simulation point'.
The process of assessing the two Kepler elements to be used, was started by changing the right ascension of the ascending node (Ω), to see the effect of moving the initial location of the asteroid in a reasonably similar orbit as Earth's orbit (due to the inclination and eccentricity being very low), thus moving it ahead or behind of the Earth in its orbit. As the second Kepler element, tests were performed using the semi-major axis (a), eccentricity (e) and inclination (i) of the Earth as elements that could be slightly changed. Due to the fact that the orbit of the Earth has a very small eccentricity and inclination, changing the argument of the periapsis (ω) was established to not give any significant difference with respect to changing the right ascension of the ascending node, thus not providing any new information. The results of how the stability of the asteroid turned out to be in certain orbits, by changing either of the three aforementioned Kepler elements, will extensively be discussed in Section 7.3.

With the main part for the analysis of the stability completed, the elements of the code that analyse the measure of accessibility can be added. In a similar fashion to the method used in Chapter 6 for the asteroid selection, which is chosen as a fast and not particularly detailed but very effective approach, a Lambert targeter is used to analyse the measure of accessibility of the asteroid after a certain period of time. In Section 7.1 it was already established that this measure will be based on the required ΔV for a transfer trajectory from the Earth to the state of the asteroid at any point in time. It should be noted, that this means that no parking orbits around the Earth or similar situations are considered, but purely a transfer from the exact state of the Earth to the exact state of the asteroid. This is not the most realistic approach, but still gives a very good idea which solution is the most optimal.

A grid search is thus created, which analyses a multitude of combinations of departure date and time of flight for a Lambert targeter from the position of the Earth at the departure date to the position of the asteroid at the departure date plus the time of flight. The boundaries for the departure date of this grid search have been set up in such a way, that they start five years after the starting time of the simulation, to prevent outliers and other undesired output that can occur at the very beginning of the analysis, and they end at the end of the simulation period minus the maximum duration for the time of flight. The outliers that can occur, are especially of importance if the asteroid drifts away from its location around the Earth. The Lambert targeter would still show a relatively low 'best ΔV' if the boundary of the grid search was at the beginning of the complete simulation time, which is not desirable since the required ΔV would be very high during the remaining time of the simulation.
For the time of flight, boundaries have been set up from 100 days up to 500 days. This is done, because the Lambert targeter that has been used for this analysis is again Izzo's multi-revolution (low-thrust) Lambert targeter (as was done for the asteroid assessment), due to the fact that it proved to be the most robust algorithm during this application. With this in mind, a range from 100 to 500 days was deemed to be a sufficiently large search space in terms of time of flight. Due to the use of the multi-revolution algorithm for this analysis however, some realism is lost when considering that this transfer from the Earth to the asteroid could very well be a manned mission, in which case the time of flight should be minimised as much as possible. This loss of realism is not very significant for the goal of this analysis however, since the Lambert targeter is purely used to assess how accessible the asteroid is from the Earth, in which the actual ΔV values are not as important as the general idea that can be obtained from this analysis on how 'expensive' in terms of propellant such a mission could turn out to be.

With the maximum time of flight known, which is thus set at 500 days, the boundaries for the departure date can also be defined. These are thus from 1 January 2035 to 18 August 2128 (500 days before the end of the simulation period). With the accessibility analysis part added, the software is complete and the analyses can be performed.

7.2.2. Output description

Next to the approach of writing the software, a careful consideration had to be made what exactly should come out as output of the program. Attention should be payed to which parameters, variables or results are of importance in the analysis and consequently in what form or layout they should be outputted. The description hereof will be given in the following paragraph.

Following the same order in which the software has been set up, first the propagation of the bodies will be inspected. From the way the program was written, it has been decided to output the state (in Cartesian elements) of each body at each integration step. This can easily be done in Tudat and the states that are being saved can be used in a convenient way to analyse the positions of the bodies (with respect to each other) and visualise their general motion in space. This information is very important for the analysis of safety and stability for each simulation point, which will be done extensively in Section 7.3. Furthermore, these states at each integration step can be used to find the states in between steps, by means of an interpolator, which then can be used in other functions, such as a Lambert targeter. This process of saving and outputting the Cartesian states of each body at each integration step is done for all simulation points.

The next piece of information that is being outputted, is the minimum required ΔV per simulation point. This is a result from the Lambert targeter function, from which the lowest of all ΔV's is extracted and placed in a vector, together with its corresponding departure date, time of flight and initial state in Kepler elements. Using these vectors for each simulation point, a matrix with valuable information in terms of the measure of accessibility is created that can be used during the analysis of the results. Next to outputting only the lowest ΔV for each simulation point, a vector that contains the best required ΔV for each departure date is created. Using this vector, an analysis can be performed on the consistency of the required ΔV's throughout the simulation time, thus showing both the stability of the orbit and the measure of its accessibility.

Furthermore, it was decided to output the Cartesian states at the end of the simulation period of 100 years and transform these states in Kepler elements for both the asteroid and the Earth. With these two states, a comparison can be made between the behaviour of both bodies and where both orbits are located after the complete propagation, showing whether the elements have changed significantly or only slightly. This analysis can again be seen in Section 7.3.

Finally, a so-called info-matrix has been outputted, which contains information on the boundaries of the grid search and the number of changes in both Kepler elements for that analysis. This information is used in the analysis and visualisation of the results, by making it possible for this visualisation-code to be written in a more modular manner.
With this collection of various types of output, a complete analysis can be made in order to assess which final state is the best and most suitable state for the asteroid to be transferred towards.

7.3. Results

As already stated in Section 7.2.1, it is started by analysing what the effect is of slightly changing different Kepler elements alongside the change in the right ascension of the ascending node. This means that a broad and general analysis will be done for the three aforementioned Kepler elements, namely the semi-major axis (a), the eccentricity (e) and the inclination (i).

7.3.1. Change in semi-major axis

The first Kepler element to be changed alongside the right ascension of the ascending node, is the semi-major axis. After some initial tests with various changes of both Kepler elements, it was decided to change the semi-major axis in steps of half a million kilometres, or 5×10^8 m. This is done with five steps, which means that the steps can be summarised in the following way: -1×10^9 m, -0.5×10^9 m, 0 m, 0.5×10^9 m and 1×10^9 m, which represent the difference with respect to the state of the Earth at the start of the simulation period.
For the right ascension of the ascending node, again after multiple initial tests, it was decided to use steps of $2°$ between each simulation point. For this parameter however, six steps were used instead of five, since the exact same right ascension of the ascending node as the Earth would give problems and

errors during the computation and thus with six steps still a symmetric analysis could be performed. These problems and errors are caused by the fact that starting a propagation of two bodies at the exact same location or very close to each other (which would be the case if a simulation point is closer than 1° to the Earth), leads to unwanted phenomena such as gravity assists or other significant perturbations, which immediately change the orbit of the asteroid in such a way that its solution becomes unusable. In the same way as for the change in semi-major axis, the steps for right ascension of the ascending node can thus be summarised as follows: −5°, −3°, −1°, 1°, 3° and 5°, again representing the difference with respect to the state of the Earth at the start of the simulation period.

This means that for this analysis, 30 simulation points exist and will be analysed for a period of 100 years. To have a clear overview of all 30 simulation points in one figure, with multiple elements of information, from which various conclusions in terms of safety, stability and the measure of accessibility can be drawn, Figure 7.1 is created. The 30 simulation points can be seen as white dots with a black edge, with the difference in semi-major axis and right ascension of the ascending node with respect to Earth's elements at the simulation start on the *x*-axis and *y*-axis respectively. Around each of these 30 simulation points, four rectangles have been drawn which each represent another important piece of information. Each of these sets of four rectangles have been bounded by thick red lines, for increased reading comfort. The colours of the rectangles show the normalised value of a certain result. These values are normalised, such that they can be represented by one single colour scheme, with its corresponding colour bar at the right hand sight of the figure.

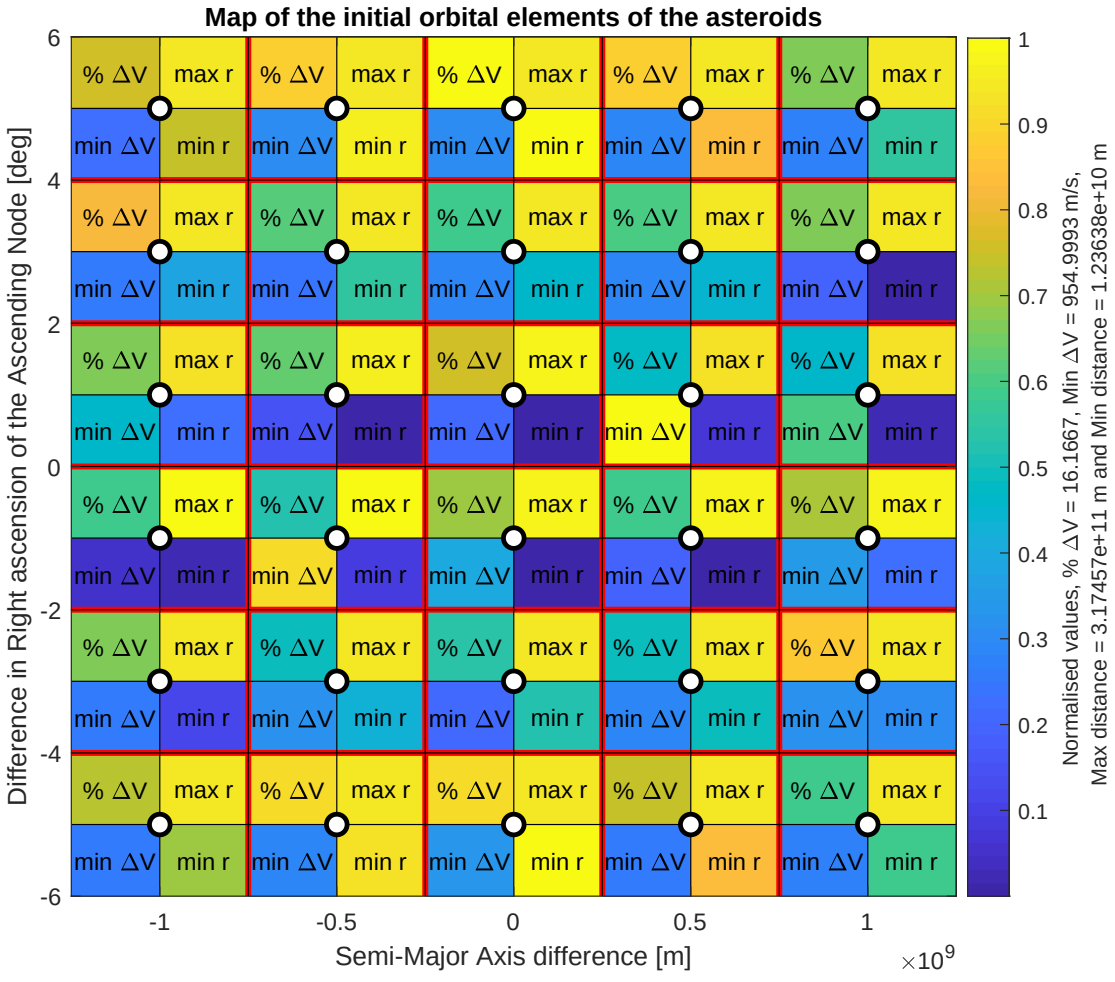

Figure 7.1: The main stability analysis map for a change in semi-major axis and right ascension of the ascending node.

Starting with the right column of each block (of four), the upper right rectangle indicates the maximum distance between the asteroid and the Earth at any point in time over the complete simulation period,

marked by 'max r'. Since 1 AU is approximately equal to 1.496×10^{11} m, a value of 3.175×10^{11} m as a maximum distance indicates that the asteroid is at the other side of the Sun at that point in time, meaning that the asteroid has drifted away from the Earth and is not in a stable position with respect to the Earth. A yellow colour of this upper right rectangle indicates this occurrence, whereas a blue colour indicates that the maximum distance between both bodies stays relatively low and thus no drift-away occurs.
The lower right rectangle on the other hand, indicates the minimum distance between the asteroid and the Earth at any point in time over the complete simulation period, marked by 'min r'. The highest value of this result is around 1.236×10^{10} m, which means that a yellow colour indicates a 'closest approach' distance of around 12 million kilometres, which is regarded as safe. As described in Section 7.1, this closest approach distance should stay above 1.5 million kilometres at all times, which means that the dark blue rectangles are considered unsafe.

In the left column of each block, the upper left rectangle shows a percentage. This percentage is linked to the in Section 7.2.2 mentioned vector that contains the lowest ΔV for each departure date. The value in this rectangle represents the percentage of ΔV's that are below a certain threshold value. This percentage thus shows how many of the departure dates per simulation point have an acceptable value, with respect to all departure dates. The threshold value is set at 2000 m/s, which after some analyses proved to be a good value to be able to draw conclusions. For this rectangle, 100 % means that throughout the complete simulation period, the required ΔV is relatively low and thus the measure of accessibility but also the stability of the orbit can be assured. With a low percentage, there will be large parts of the simulation period in which a (much) higher ΔV is required, which does not fulfil the desire of a constantly reachable asteroid from the Earth. As can be seen, the highest percentage in this analysis is 16.2 % , which means that all points in this analysis have an equal or lower percentage of accessibility. A visualisation of two examples of the fluctuation in ΔV over the simulated period will be shown and discussed later in this section, i.e. in Figures 7.5 and 7.11.
Finally, the lower left rectangle of each block shows the absolute value of the lowest ΔV for all departure dates throughout the complete simulation period. Through this rectangle, it becomes clear for each simulation point what the expected required ΔV is in the most optimal case, through the analysis of the Lambert targeter. A bluer rectangle in this case thus means a more optimal 'best solution' throughout the simulation period. It should be noted however, that just because the overall lowest ΔV is lower for one simulation point with respect to another, it does not mean that the initial conditions of that simulation point will provide an overall better result, looking at the three different criteria.

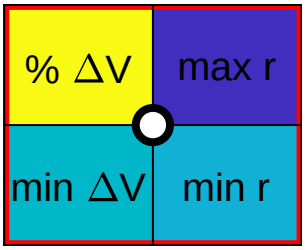

Figure 7.2: An example simulation point, indicating a suitable final target state.

To give an example of how the four rectangles around a simulation point should look preferably, the visualisation in Figure 7.2 is created. In here, a simulation point that adheres to all three elements of importance (safety, stability and accessibility) is shown. It should be noted that the normalised value for the maximum distance is equal to around 3.175×10^{11} m, indicating the complete drift-away, while the normalised value for the minimum distance is again around 12 million kilometres, the normalised value for the percentage is equal to 100 % and the normalised value for the velocity impulse is around 1980 m/s.
It can be seen how the 'maximum distance' rectangle is dark blue, indicating no drift-away has occurred. Furthermore, the 'minimum distance' rectangle is somewhere between 0.4 and 0.5 of the normalised value, indicating it always remains at a safe distance from the Earth. Finally, the percentage rectangle is yellow, indicating accessibility throughout the complete simulation period, while the minimum required velocity impulse is also quite low.

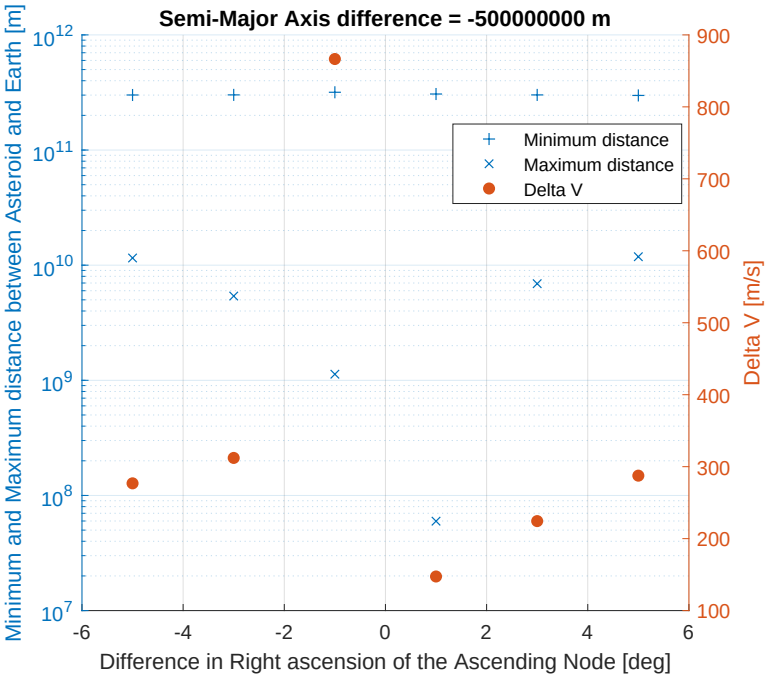

Figure 7.3: The minimum and maximum distance between the asteroid and the Earth and a minimum required ΔV for an initial difference in semi-major axis of -5×10^8 m.

Since it can be seen in Figure 7.1 that there is no single simulation point where the rectangle indicating the maximum distance is not yellow, it can be concluded that any asteroid placed in an orbit with the initial state corresponding to the simulation points, will drift away from the Earth and is therefore not placed in a desirable location. Next to this, from the maximum percentage of around $16\,\%$, the same conclusion can be drawn, namely that for each simulation point the asteroid drifts away from the Earth and during large parts of the simulation time the required ΔV to reach the asteroid from the Earth is deemed too high.
Despite this fact, various other analyses and visualisations can be made with the data that has been outputted by the program, to show the behaviour of some of the simulation points. In Figure 7.3 for example, the six simulation points corresponding to a difference in semi-major axis of -5×10^8 m can be seen, with their minimum and maximum distance to the Earth at any point in time in crosses and plus signs respectively, while the minimum required ΔV is indicated in red circles. From this figure, the actual values for each of the six simulation points can clearly be seen, such as the maximum distance for all points being around 3×10^{11} m, indicating the drift-away to the other side of the Sun.

For each of the simulation points, the complete simulation period is visualised as well, such that the behaviour of each asteroid can be analysed. As an example, this is done for a random simulation point (since none of the 30 points has been identified to be suitable), to show its behaviour of drifting away. The absolute distance between the asteroid and the Earth can be seen in Figure 7.4a, while the difference in the three position coordinates in the Cartesian system, the *x*- *y*- and *z*-axis, can be seen in Figure 7.4b. From these two visualisations, it can be seen how the asteroid drifts away from the Earth to the other side of the Sun at its maximum distance from the Earth of around 3×10^{11} m. Also, the period of this drift-away (which will differ for different initial conditions) and the moments in time it reaches its minimum and maximum distance with respect to the Earth can be seen.

Finally, the last visualisation that can be made and contains very interesting information, is the required ΔV for each departure date throughout the complete simulation time, which can be seen in Figure 7.5. As can be seen, the plot approximately follows the behaviour of Figure 7.4a, which can be expected, since a larger velocity impulse is required with the Lambert targeter algorithm, to transfer a body to a location significantly further away.

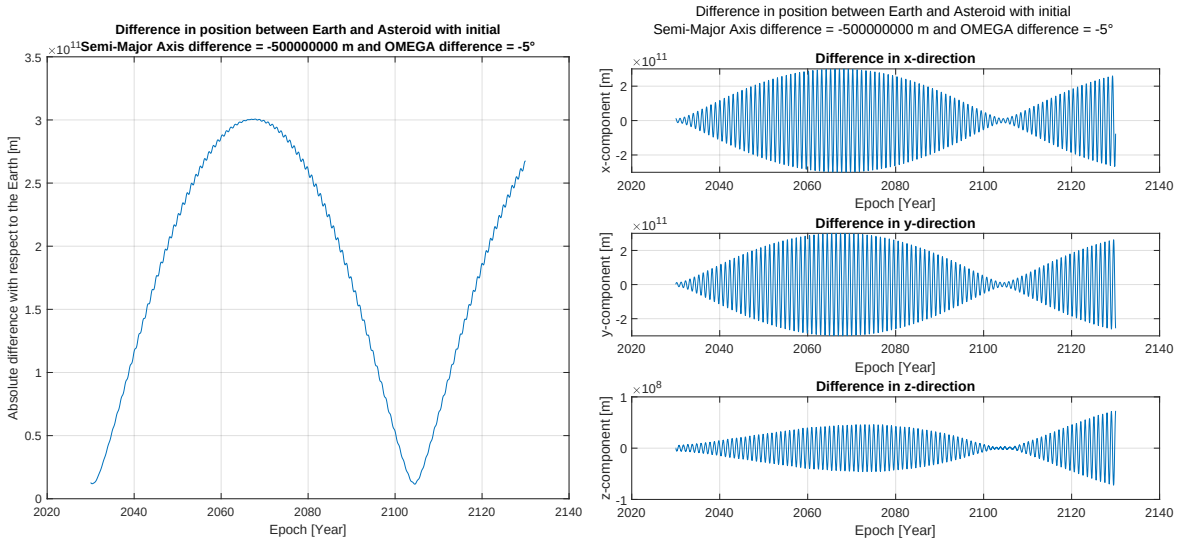

(a) The total distance between the asteroid and the Earth.

(b) The distance between the asteroid and the Earth in three directions.

Figure 7.4: The behaviour of the asteroid for a certain random set of initial Kepler elements.

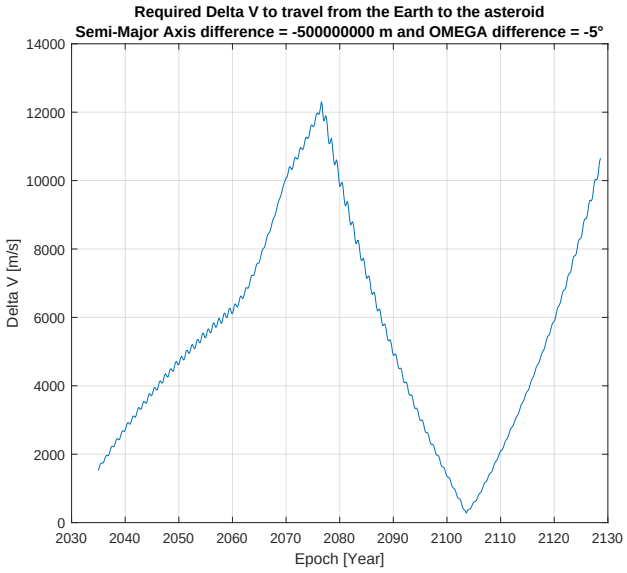

Figure 7.5: The required ΔV for a transfer from the Earth to the asteroid using the Lambert targeter at every starting date throughout the complete 100-year simulation for a change in semi-major axis.

7.3.2. Change in inclination

The next Kepler element in the analysis is the inclination. The same approach will be used as for the semi-major axis in Section 7.3.1. For the inclination, after several tests with various changes, it was decided to change the inclination in steps of $0.0025°$. This was done in five steps, which were all added to the initial value of the inclination (of the Earth), to prevent negative inclinations. This thus resulted in inclination differences with respect to the inclination of the Earth at the simulation start of: $0°$, $0.0025°$,$0.005°$, $0.0075°$, $0.01°$. Furthermore, the right ascension of the ascending node was changed in the same way as for the semi-major axis, in six steps of $2°$.

With this information, a similar visualisation can be made as the visualisation in Figure 7.1, only now for the change in inclination. This can be seen in Figure 7.6.

Similarly to the analysis on the change of the semi-major axis, it can be seen that a change in the

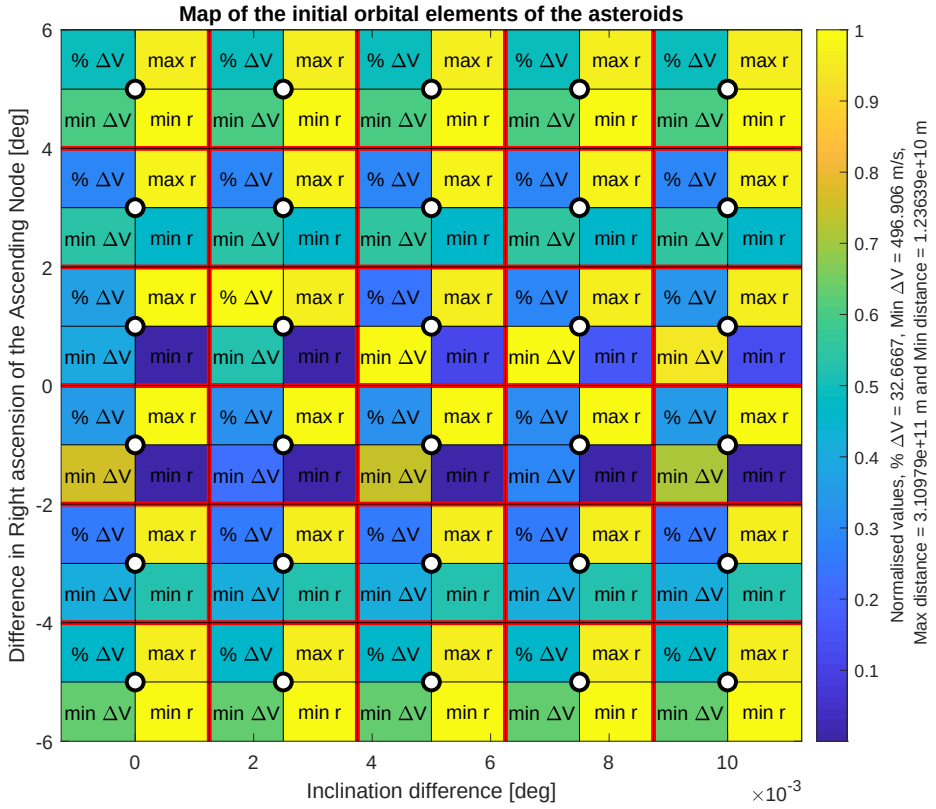

Figure 7.6: The main stability analysis map for a change in Inclination and right ascension of the ascending node.

inclination does not provide a suitable result: all simulation points have a yellow 'maximum distance' rectangle (with a value around the 3.1×10^{11} m), which is a clear indication of a drift-away, as was already discussed in Section 7.3.1. Next to this, when looking at the indicator for accessibility (the percentage of ΔV's) it can be seen that the maximum number for this is $32.7\,\%$ and occurs only once, with all other simulation points having even lower values than this. This fact also shows that the change in inclination does not provide any suitable results.

Furthermore, it can be observed that the left column in this analysis, is the same as the middle column in the analysis with the semi-major axis, as can clearly be seen when looking at the squares for minimum and maximum distance (the other squares have different colours due to the different value with which they are normalised). This makes sense when it is realised that both columns indicate no change with respect to the first Kepler element and exactly the same change in terms of the second Kepler element, or the right ascension of the ascending node.

7.3.3. Change in eccentricity

The final Kepler element that will be changed, is the eccentricity. In a way similar to the previous two elements, the analysis is started with a relatively broad analysis in terms of step size. The eccentricity of the Earth at the starting epoch is taken, to which steps of 0.02 have been added. This step size is chosen, to ensure the proximity to the Earth. This has been done for five steps, which means the additions to the original eccentricity are: 0.0, 0.02, 0.04, 0.06 and 0.08.

The stability analysis map for this first analysis can be seen in Figure 7.7. A few noteworthy observations can be made immediately. The first and perhaps most important one, is that not all 'maximum distance' rectangles are yellow: two simulation points in the third and the complete fourth and fifth column have blue rectangles, which is a first indication that a drift-away does not occur. Furthermore, the percentages (of suitable ΔV's) for these simulation points in the third and fourth column are yellow and with a normalised value of $100\,\%$ thus very high, which is another indication of a potentially suitable simulation point. The highest 'minimum distance' for each of these simulation points is not dark blue, indicating a potential safe minimum distance to the Earth. A final observation that can be made, is the

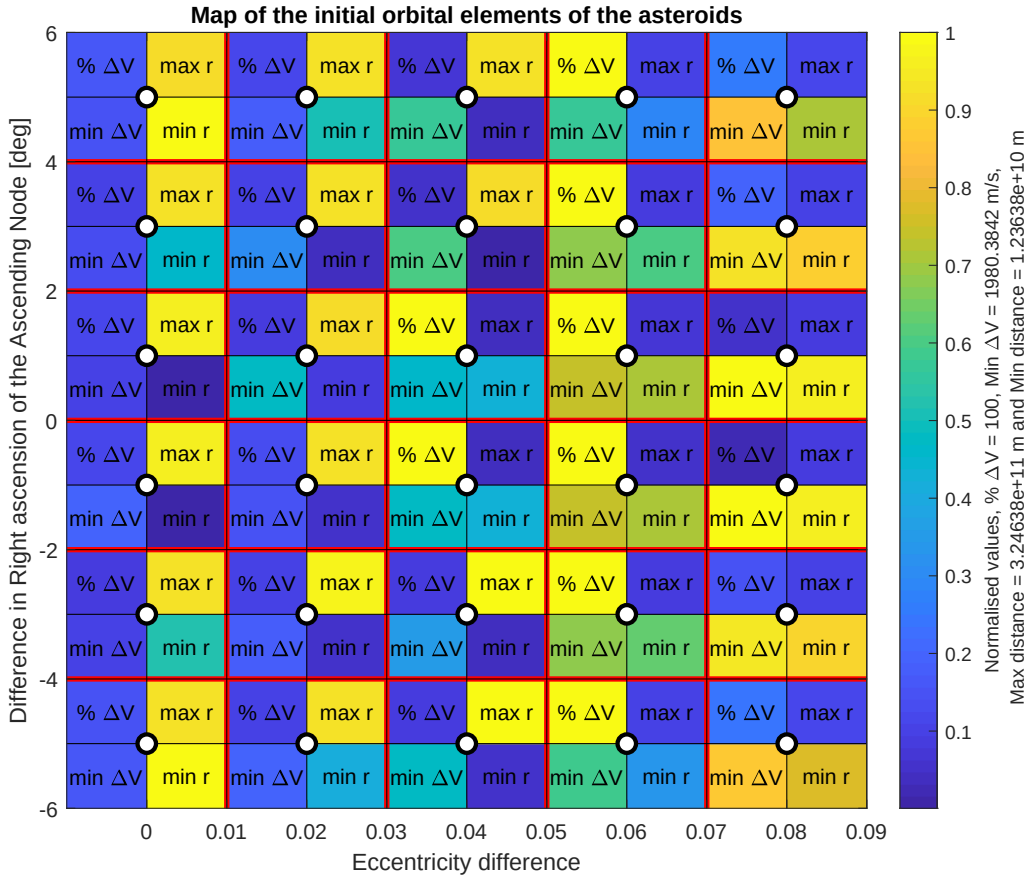

Figure 7.7: The main stability analysis map for a change in eccentricity and right ascension of the ascending node.

fact that the two points in the third column have a lower 'minimum required ΔV' than the points in the fourth column (which again have a lower value than those in the fifth column), which could indicate that these two are more optimal points. With all this information that is immediately visible from this visualisation, it becomes clear that changing the eccentricity has a high potential of success, which is why further analysis will be performed on these results.

To analyse these interesting columns with their exact values and the behaviour of the distance between the two bodies and the minimum required ΔV, Figures 7.8a, 7.8b and 7.9 have been made. In the visualisation for column four (eccentricity difference 0.06, Figure 7.8a), the behaviour of the points with various differences for the right ascension of the ascending node can be observed, with the points further away from the Earth (in terms of right ascension of the ascending node) having larger extremes in minimum and maximum distance. This is to be expected from an astrodynamical point of view, when keeping in mind that both the eccentricity and the right ascension of the ascending node have been changed. The visualisation for column five (eccentricity difference 0.08, Figure 7.8b) shows very similar behaviour, but with slightly different values: both the minimum and maximum distance between the Earth and the asteroid are larger, which is a direct consequence of the larger eccentricity difference, also resulting in higher required ΔV values for a transfer between both bodies.

In the visualisation for column three (eccentricity difference 0.04, Figure 7.9), it is visible how the middle two points (with an Ω close to that of the Earth) exhibit the same behaviour as the simulation points in column four and five, while the other points show a drift-away. These two middle points also have a significantly lower required ΔV for the transfer, from which the following observation can be made: having a larger eccentricity difference gives more safety (and security in general) for the mission, by paying for it with a higher required ΔV, and thus in accessibility and efficiency. Next to this assessment in the 'eccentricity-dimension', it can also be observed that in the 'Ω-dimension' being further away from the Earth results in slightly less safety and stability (with lower minima and higher maxima for distance) but also a lower required ΔV and thus higher accesibility.

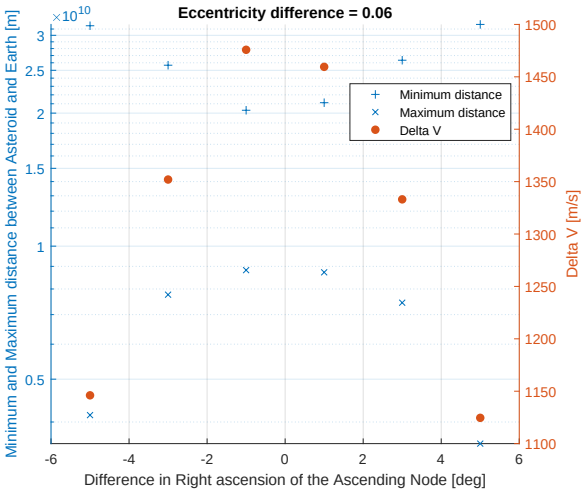

(a) The graph for column 4 (an eccentricity difference of 0.06).

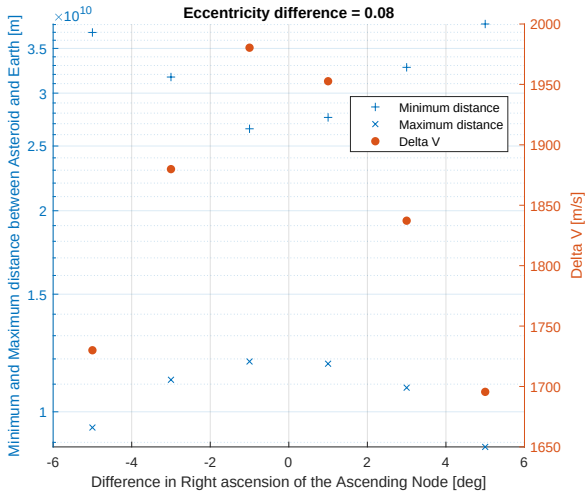

(b) The graph for column 5 (an eccentricity difference of 0.08).

Figure 7.8: The minimum and maximum distance between the asteroid and the Earth and a minimum required ΔV for two different eccentricity differences.

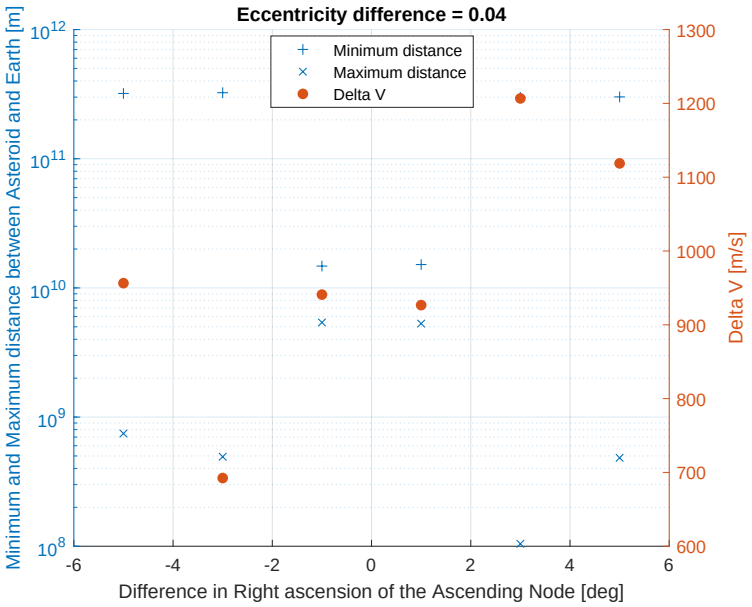

Figure 7.9: The minimum and maximum distance between the asteroid and the Earth and a minimum required ΔV for an initial difference in eccentricity of 0.04.

As a confirmation that the middle two simulations points of the third column are indeed suitable and according to the requirements as set up earlier, a visualisation is made of the distance between the asteroid and the Earth over the complete simulation period, similar to the visualisations in Figure 7.4. This is done for one of the two points in column three, to show its behaviour as one of the most optimal solutions in this first analysis. This can be seen in Figures 7.10a and 7.10b.
When compared to the simulation points that have an asteroid that drifts away from the Earth, like Figure 7.4, it becomes clear that this initial state provides a stable and safe orbit for the complete simulation period. The minimum distance is more than five million kilometres, while the maximum distance is not more than 15 million kilometres, both of which stay well inside the numerical boundaries mentioned in Section 7.1. For the measure of accessibility, the required ΔV's for each departure date can be plotted, as seen in Figure 7.11a, where it is visible that this criterion is also fulfilled throughout the complete simulation period.

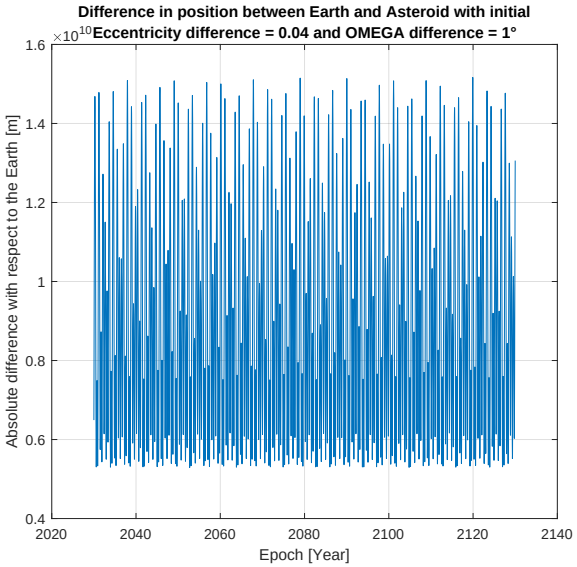

(a) The total distance between the asteroid and the Earth

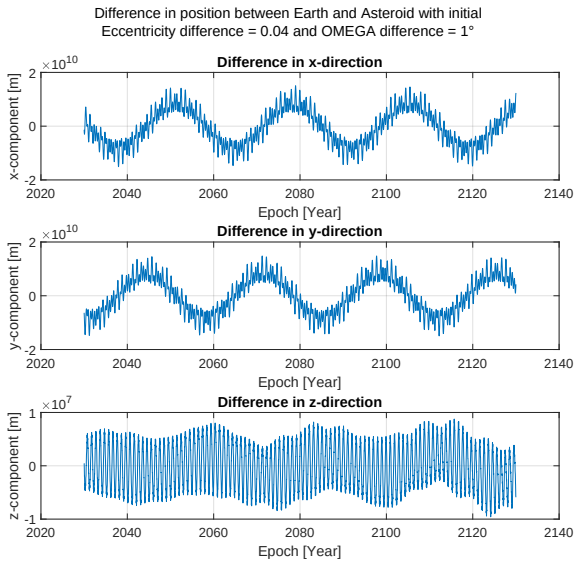

(b) The distance between the asteroid and the Earth in three directions.

Figure 7.10: The behaviour of the asteroid for one of the two middle points in column 3 (eccentricity difference = 0.04).

A final observation that can be made, is regarding the ΔV-percentages of column five, which are not very high, despite the fact that it could be seen that this column provides suitable initial conditions for the asteroid on the basis of the other indicators. These lower percentages are purely caused by the earlier established threshold value of $2000\,\mathrm{m/s}$. When looking at the required ΔV per starting date for a random point in this column, as is visualised in Figure 7.11b, it can be seen that the behaviour is quite similar to the behaviour in Figure 7.11a and not at all similar to the behaviour that could be seen in Figure 7.5, where the asteroid was drifting away from the Earth. The reason why the percentage is low, is because of the fact that most of the ΔV values simply are (slightly) above that threshold of $2000\,\mathrm{m/s}$, in line with the aforementioned observation that a larger eccentricity difference results in a larger required ΔV. The points in this column thus still provide suitable initial conditions for the asteroid.

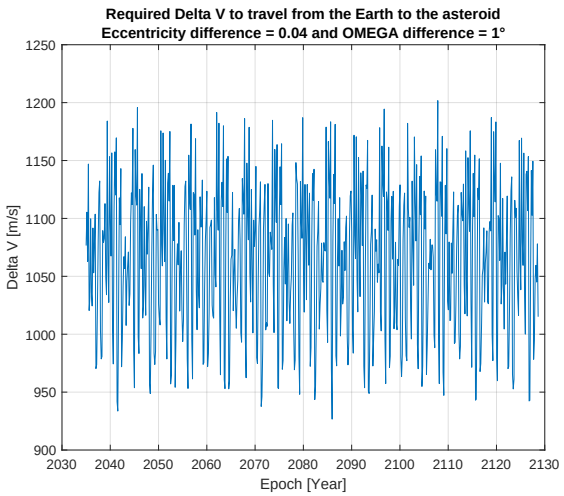

(a) The required ΔV's for a change in eccentricity of 0.04.

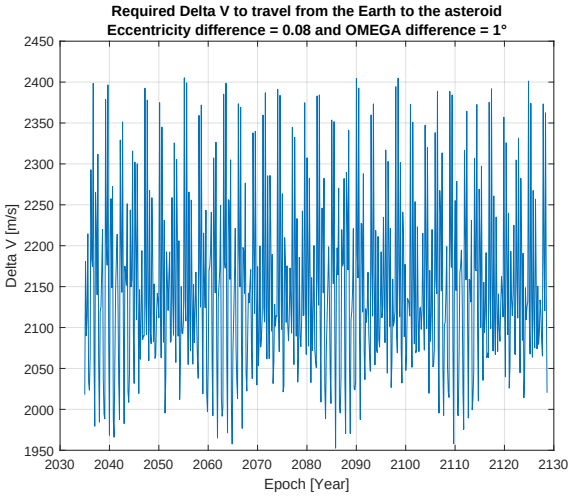

(b) The required ΔV's for a change in eccentricity of 0.08.

Figure 7.11: The required ΔV's for a transfer from the Earth to the asteroid using the Lamber Targeter at every starting date throughout the complete 100-year simulation for different changes in eccentricity and a change in Ω of 1°.

With the results from this first analysis, it can be concluded that changing the eccentricity provides suitable final orbits for the asteroid capture mission. Further analysis will thus be performed on this aspect, to find a range or an area of optimal solutions for this stability analysis.
This analysis is done by performing multiple simulations, in which the change in the Kepler elements is varied with each run. A summary of these multiple simulations and the analysed simulation points (and thus initial states for the asteroid) is visualised in Figure 7.12. To reach these sets of analysis points, many tests have been performed to see which areas are of interest at all, but also to see with which sort of spread the analysis will provide most information in the smallest number of simulations and thus computational time.
In the visualisation, it can be observed how the evolution of each analysis took place and how with every new analysis the area of interest is chosen to be smaller and more specific, in search for that area of optimal orbits and the boundary at which the simulation points start getting suitable.

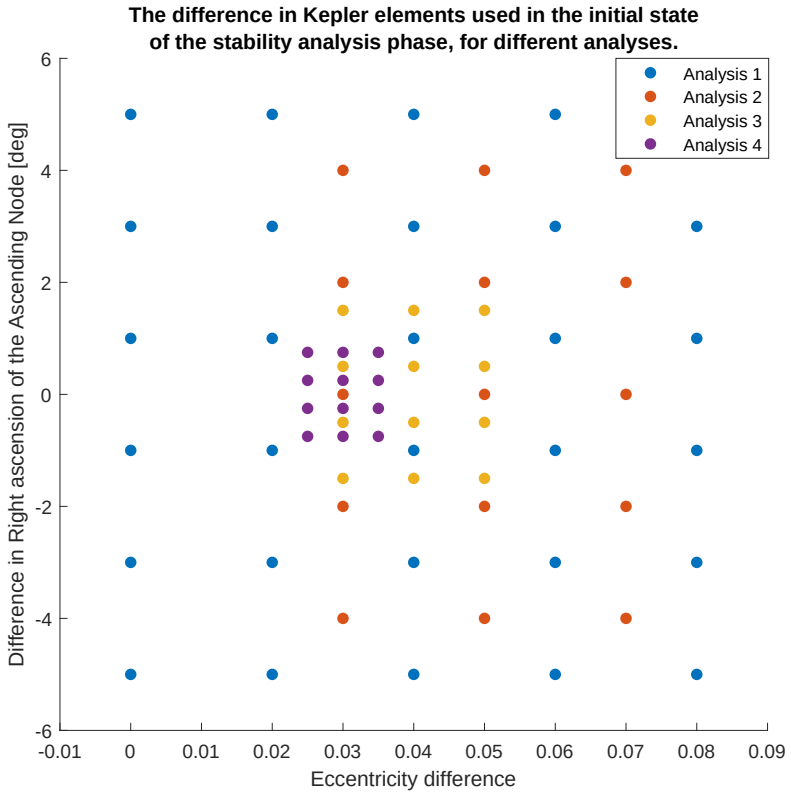

Figure 7.12: A map of the four performed simulations and the changes in the initial states for each of these simulations.

As can be seen, after the first analysis and the conclusions drawn from its results, it was decided to start increasing the eccentricity from a value of 0.03 and making three steps of 0.02. Furthermore, the difference in the right ascension of the ascending node was now made to be on the even numbers, including a difference of $0°$, which was now possible since the steps in eccentricity prevented the planets to start in exactly the same location. This second analysis resulted in the stability map that can be seen in Figure 7.13.
From this stability map it can be seen that the right column, with an eccentricity difference of 0.07, provides suitable initial conditions for all tested simulation points, as expected from the results of the first simulation. The middle column in this second simulation shows four simulation points that are suitable when looking at the different indicators, while the simulation point with an Ω of $4°$ shows a drift-away and is thus not suitable. Since this middle column is located between column three and four of the first simulation, it could be expected that not all simulation points would prove suitable, especially those with a higher difference in the right ascension of the ascending node. It is however interesting to observe that, although quite a high degree of symmetry exists between the upper points and the lower points in each map (with the same difference in degree, either ahead or behind the Earth), the simulation point for $4°$ is not suitable while the point for $-4°$ is suitable. This can be explained by a

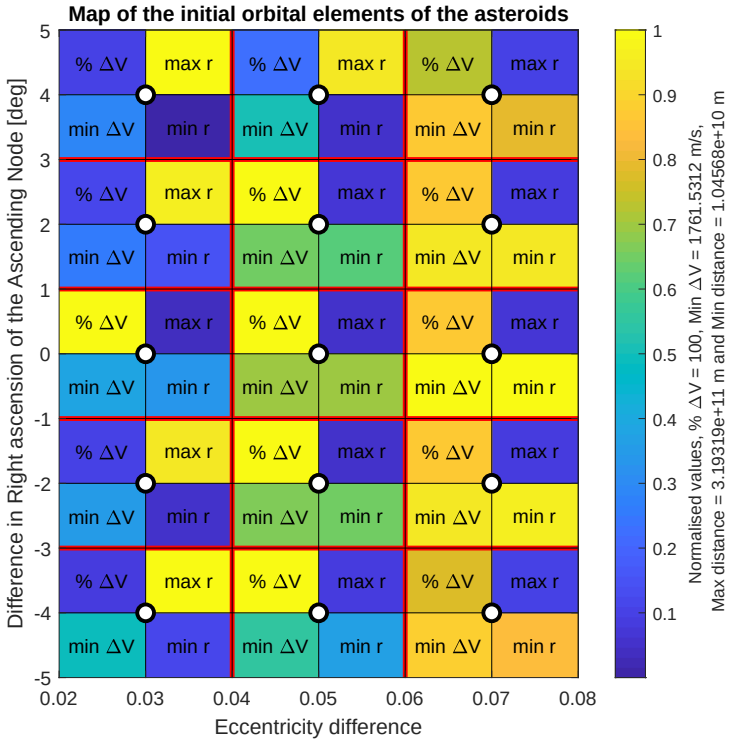

Figure 7.13: The second stability analysis map for a change in eccentricity and right ascension of the ascending node.

(slight) difference in perturbing forces working on the asteroid throughout these simulations, which in the former simulation slowly leads to a gravity assist with the Earth while in the latter simulation this situation does not occur.
Finally, in the left column, with an eccentricity difference of 0.03, the middle simulation point that corresponds to a difference in Ω of 0° appears to be suitable, while all other points are not. It can also be observed that this one point is more efficient than the points in the middle column, which again are more efficient than those in the right column. This follows the same line that was already seen in the first simulation. The minimum distance to the Earth in the left column is lower however, which again shows the lower level of safety with a smaller difference in eccentricity. Furthermore, the right column does not have yellow indicators for its continuous accessibility, which similarly to the right column in Figure 7.7 is purely caused by the threshold of 2000 m/s on the ΔV requirement. Overall these points still stay stable and accessible to the earth throughout the complete simulation period, with moments in which the required velocity change slightly exceeds the 2000 m/s, causing the percentage not to be 100 %.

With this second simulation, the boundary for suitable points has thus been detailed with respect to the first simulation, which is why the third and fourth simulations will continue on this same path. Both stability maps have been visualised and can be seen in Figure 7.14.
From these analyses, it can be concluded that the minimal addition to the eccentricity of the Earth, is 0.03. From there on, larger changes to the eccentricity increase the minimum required ΔV, but on the other hand are safer in terms of sensitivity when placing the asteroid in such a precise location. Furthermore, like discussed before, initial states with an Ω close to that of the Earth are more likely to be suitable, which especially can be seen in columns with a smaller change in eccentricity, such as the left column in Figure 7.14a.
To give an idea of how the actual orbits look over a simulation period of 100 years, Figure 7.15 has been made. In these 3D-plots, the orbits of the four simulations of the second column of Figure 7.14b have been plotted, together with the orbit of the Earth, all for the complete simulation period. These visualisations give an idea on how the orbits are really close to each other on the heliocentric scale. This also indicates the orbital stability, although whether or not a drift-away takes place can not be

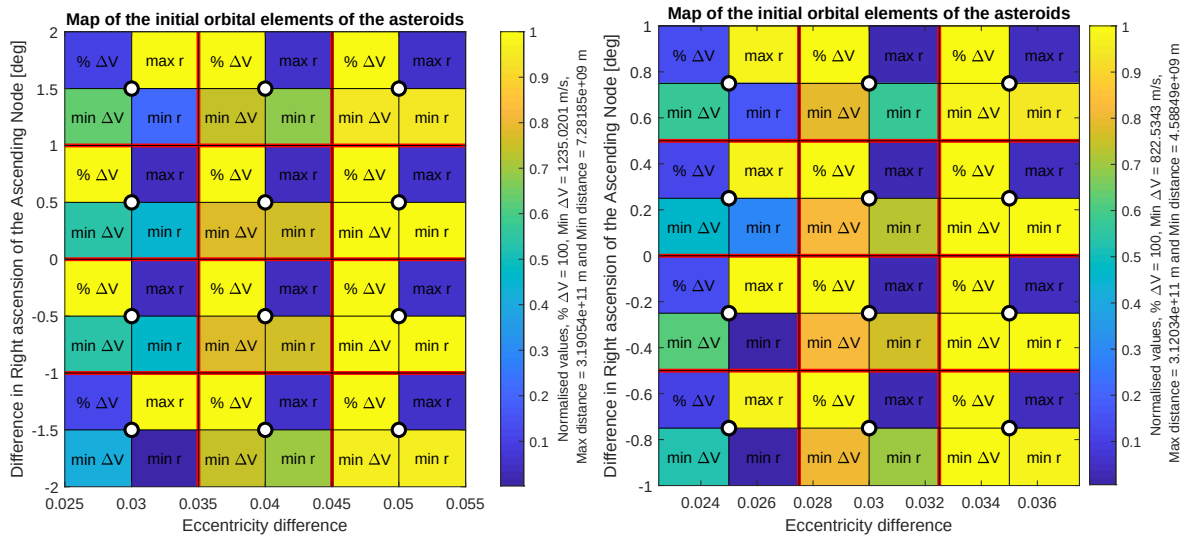

(a) The stability analysis map for the third analysis. (b) The stability analysis map for the fourth analysis.

Figure 7.14: The third and fourth stability analysis map for a change in eccentricity and right ascension of the ascending node.

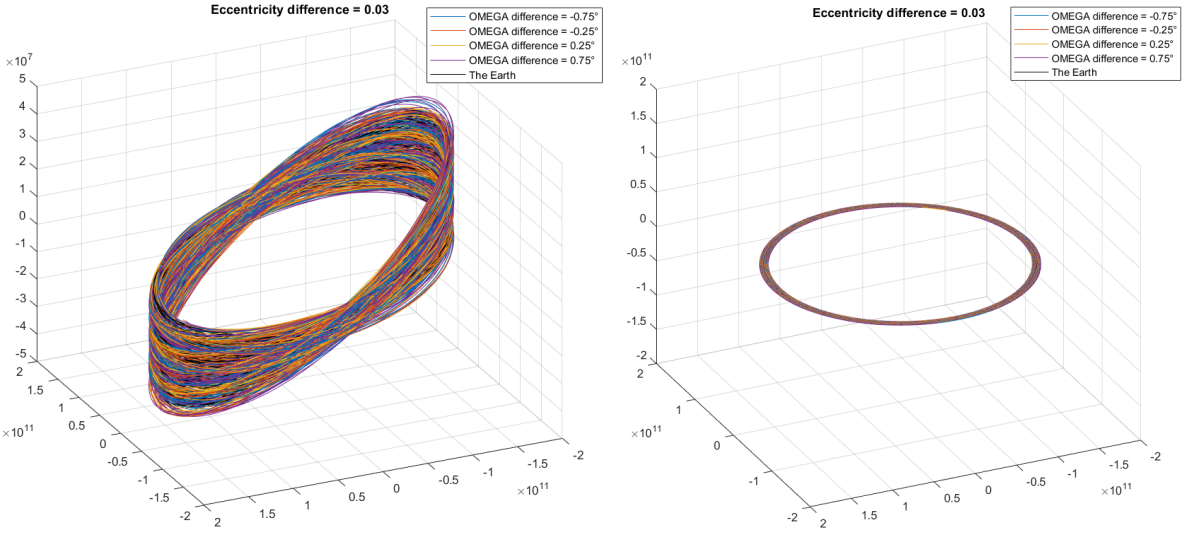

(a) The visualisation with a smaller range on the *z*-axis. (b) The visualisation with equal ranges on all axes.

Figure 7.15: 3D visualisations of the orbits' 100 year propagation for an eccentricity change of 0.03 and various changes in Ω.

seen from a plot like this. Also note that the range on the *z*-axis is different from the range on the *x*- and *y*-axes in Figure 7.15a, which gives the impression that the orbits have a large deviation in the *z*-direction. This is why Figure 7.15b is created, in which the range on all three axes is equal.

As a final analysis on the obtained data, it is decided to visualise the Kepler elements that the asteroid has after 100 years, for each suitable simulation point. These elements are also compared to the Kepler elements of the Earth after 100 years, to see the evolution of the elements with respect to each other. This is done for 'analysis 1' and 'analysis 3' from Figure 7.12, to give a good overview of a large portion of the suitable points in a broad range. First, for each analysis all suitable simulation points have been plotted for their initial Kepler elements, including the minimum required ΔV. This can be seen in Figures 7.16a and 7.16b, for analysis 1 and 3 respectively.

These same points have subsequently been plotted in a 3D visualisation, for three of their final Kepler elements, namely their semi-major axis, eccentricity and inclination. Since it can be tricky to see their exact location in the 3D space of a graph printed on a 2D surface, their location has also been marked on each of the three sides with a smaller cross in the same colour. In this way, it can be seen

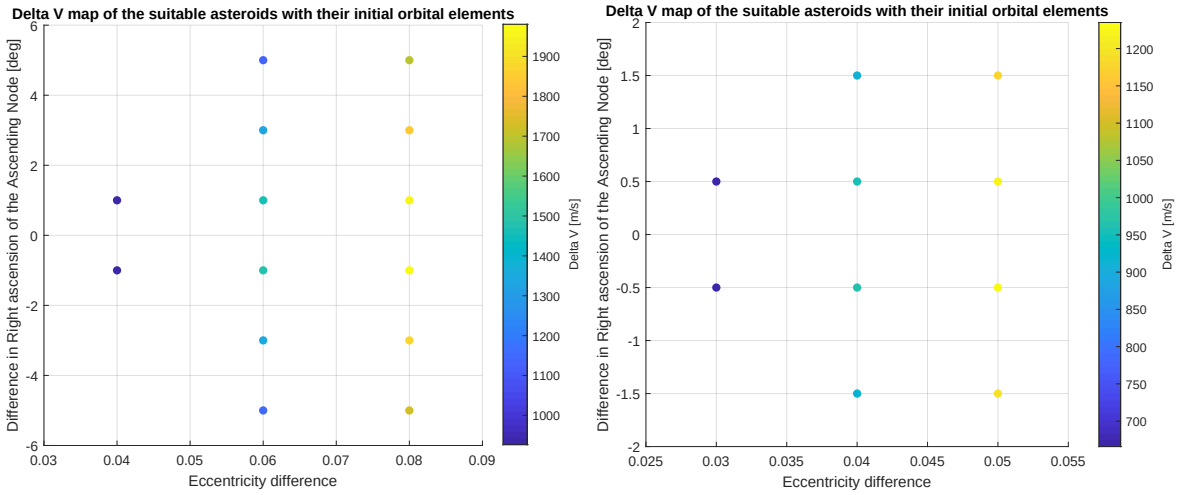

(a) The ΔV map for the suitable points from analysis 1. (b) The ΔV map for the suitable points from analysis 3.

Figure 7.16: The ΔV maps for the suitable points from two different analyses.

what the final Kepler elements are for all suitable simulation points, after 100 years of propagation. Next to this visualisation, in the same manner and for the same Kepler elements, the difference with respect to the Kepler elements of the Earth at the end of the propagation time has been visualised, in percentage. These two visualisations for analysis 1 (Figure 7.16a) can be seen in Figures 7.17a and 7.17b respectively.

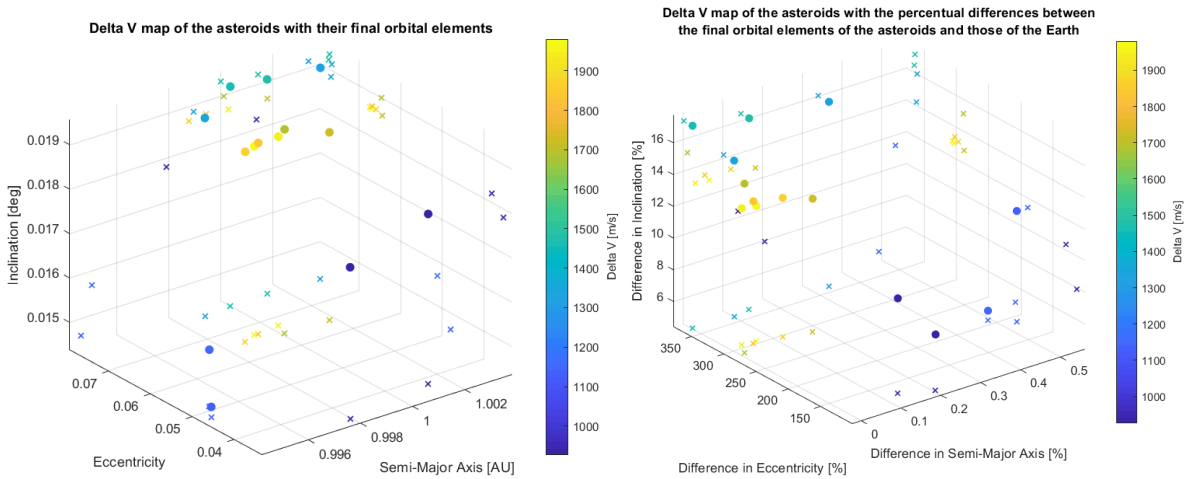

(a) A 3D visualisation of the first three Kepler elements of the final state for the asteroid.

(b) A 3D visualisation of the relative differences between the Earth's and asteroid's final elements.

Figure 7.17: 3D visualisations for the final state of the first three Kepler elements of the suitable points from Figure 7.16a.

Interestingly, it can be observed that the simulation points that started with a larger difference in eccentricity with respect to the Earth (the greenish, orange and yellow simulation points) have obtained a smaller difference in eccentricity, while some of the cyan simulation points have a larger eccentricity after the 100 year propagation. This does not affect their suitability however, since all of these points have already been identified as suitable. Furthermore, it can be observed that for most of the simulation points, the inclination has also increased slightly, due to the perturbations working on the asteroid during all those years. The difference in semi-major axis is also notable, as can be seen that quite some points have slightly drifted away from the 1 AU distance, again due to certain perturbations working on the asteroid. Overall, these small differences do not disturb the asteroid enough to cause it to be unstable or move too close or too far from the Earth.

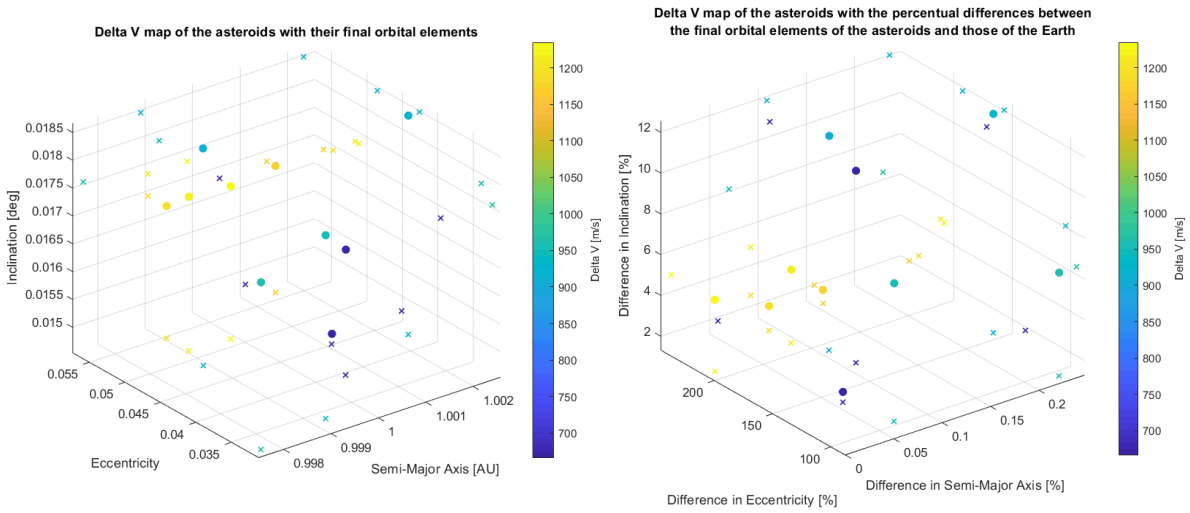

(a) A 3D visualisation of the first three Kepler elements of the final state for the asteroid.

(b) A 3D visualisation of the relative differences between the Earth's and asteroid's final elements.

Figure 7.18: 3D visualisations for the final state of the first three Kepler elements of the suitable points from Figure 7.16b.

The same has been done for analysis 3 (Figure 7.16b), for which both 3D visualisations can be seen in Figures 7.18a and 7.18b. Slightly similar to the 3D visualisations for analysis 1, it can be seen that the yellow and orange coloured simulation points (indicating the right column of Figure 7.16b) end up more closely together, while the cyan and blue simulation points are more spread out. This can indicate the higher level of perturbance when the initial conditions of the asteroid are closer to those of the Earth.

7.3.4. Sensitivity Analysis

After the previous three analyses have been performed, by varying the semi-major axis, inclination or eccentricity, it was decided to perform some small sensitivity analyses around the suitable points. These points have been identified to broadly lie in 'the area' of adding more than 0.03 to the eccentricity of the Earth. The idea for the first sensitivity analysis is to subsequently assess whether a variation in the other Kepler elements (semi-major axis and inclination) will have a large effect on the suitability of the simulation points, and thus assess how strict the target state of the transfer orbit has to be to ensure a successful mission.

To assess this, it is decided to perform a 'cloud analysis', with which is meant that instead of only looking at one or two elements at the same time (from which a line or plane of simulation points can be created), now three elements are changed at the same time to obtain a 'cloud' of simulation points. This is done by taking one (arbitrary) variation in eccentricity that proved to give suitable simulation points, and vary the other two elements for this eccentricity to see the effects.
The variation in eccentricity was chosen to be $+0.04$, since it gave suitable and thus safe and stable points (for not too high right ascensions of the ascending node) over the 100 years of propagation, but also is relatively close to the 'border' of 0.03 below which the simulation points are not suitable anymore. In this way, by adding (small) differences in the other Kepler elements it can properly be analysed whether a variation in eccentricity of that value has a very thin range of suitability in the other directions, or that the range is quite broad and thus indicates that the final state is not that sensitive for variations in other elements.

For the variation in semi-major axis, it is decided to make four steps of a million kilometres, starting from negative 1.5 million kilometres, resulting in -1.5×10^9 m, -0.5×10^9 m, 0.5×10^9 m and 1.5×10^9 m. This is done to analyse a slightly broader range of changes in semi-major axis, compared to the initial analysis of semi-major axis alone. The same is done for inclination, with five larger steps of $0.1°$, resulting in $0°$, $0.1°$, $0.2°$, $0.3°$ and $0.4°$. The results of this analysis are visualised in the same way as has been done previously, and can be seen in Figure 7.19.

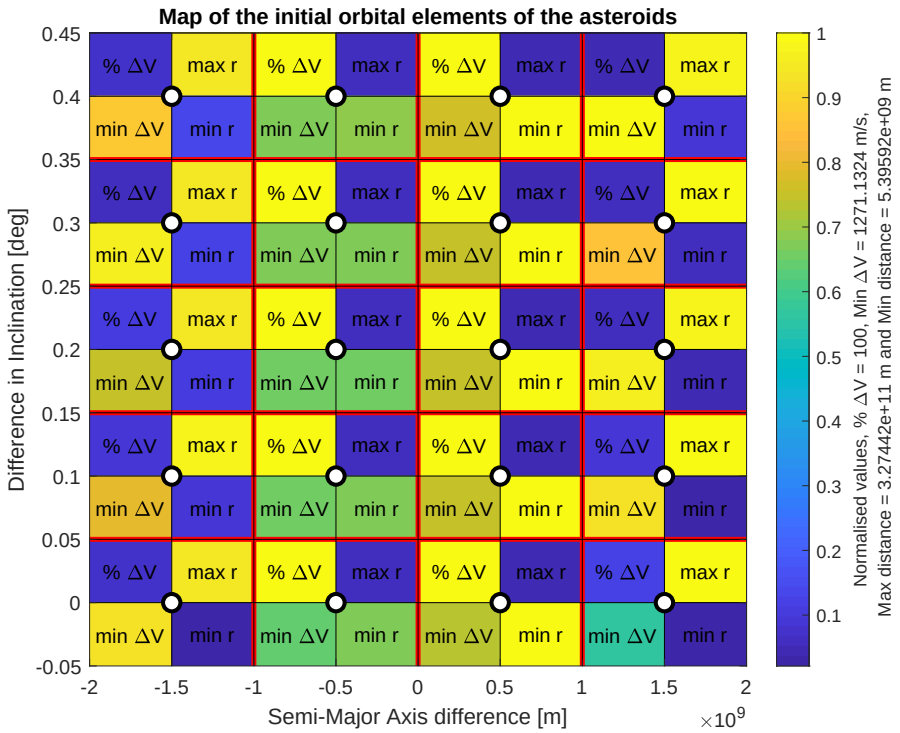

Figure 7.19: The stability analysis map for the cloud-simulation, as part of the sensitivity analysis. The eccentricity difference with respect to the Earth is 0.04.

From the stability analysis map, it can be seen that a larger variation in semi-major axis causes the simulation points to not be suitable anymore, since they drift away from the vicinity of the Earth. A smaller difference in semi-major axis (of half a million kilometres) does not affect the suitability of the simulation points, which thus roughly gives the error margin that the final state of the transfer orbit can have in terms of semi-major axis. For the inclination on the other hand, it can be seen that for all values, the difference is very minimal. This means that the change in inclination can be significant, without it affecting the suitability of the already suitable points. To find the boundary at which also the inclination causes a simulation point to not be suitable anymore, the same analysis has been performed with steps of 1°. This analysis resulted in an inclination difference of 1° that did not affect the suitability, while inclination differences of 2° and more did affect the suitability and caused those simulation points to not be suitable anymore. With this, the error margin for the final state of the transfer orbit in terms of the inclination can thus be placed at 1° with a certainty that the asteroid stays safe, stable and easily accessible for the next 100 years.

With this sensitivity analysis, a better understanding is thus obtained on how strict the margins are for the different Kepler elements, using the already suitable changes in eccentricity. With this cloud analysis, the final state and thus the boundary conditions for the transfer orbit can be better defined and tuned to achieve the most optimal result.

Next to the cloud analysis, another sensitivity analysis has been performed, in which the starting date of the 100 year propagation has been varied (and thus also the initial state of the Earth and the asteroid). The goal of this sensitivity analysis is to assess how the outcome changes if the simulation is started at a different epoch and what kind of implications this has for the changes that need to be set for the final state of the asteroid with respect to the Earth.
For this simulation, the eccentricity is set at a value for which it is known that it results in multiple suitable simulation points for the previously performed analysis with a starting epoch on the first of January, 2030. This value for the eccentricity is set at +0.05, to ensure the multiple suitable simulation points. Next, the two parameters that will be changed in this simulation will be the right ascension of the ascending node and the starting epoch of the simulation. The right ascension of the ascending

node will be changed in the same fashion as has been done in the first analyses for the three Kepler elements in Sections 7.3.1 to 7.3.3, as can be seen in Figures 7.1, 7.6 and 7.7, with 6 steps of 2° each. The simulation start epoch will make 13 steps of 30 days, starting from the first of January in 2030, which makes the last epoch to be approximately one year later. This is done to get a reasonable spread of the starting epochs and analyse the starting conditions for the 100 year propagation throughout one year, meaning one full rotation around the Earth.

This analysis resulted in the following stability map, as can be seen in Figure 7.20. A few notable observations can be made when looking at this visualisation. Firstly, it can be seen that for different starting epochs, different changes in the right ascension of the ascending node give suitable simulation points. This means that it is not always guaranteed to have a suitable point when the aim for the transfer orbit is a final state with the Earth's Kepler elements, but with an added 0.05 to the eccentricity and a difference close to zero in terms of the right ascension of the ascending node. It is thus very much dependent on the simulation start epoch, which can be expected when looking from an astrodynamical point of view, since the added eccentricity to the asteroid's orbit defines its shape in a certain orientation with respect to the Earth's orbit, due to the current argument of periapsis and the right ascension of the ascending node. If the two bodies subsequently move along their own orbits throughout that year (increasing their true anomaly), they can approach or distance each other quite significantly, dependent on the eccentricity change. Due to this fact, a certain periodical pattern should appear in the results, which leads to the second observation, namely of exactly this pattern. When looking at the visualisation, the line around which most of the suitable points are located, behaves somewhat similar to a sinusoid, going up in the first 'half year', reaching the centre point after around six months and subsequently making the same motion on the lower side of the graph, to come back to the centre after one year. After some tests, it was observed that for this specific increase in eccentricity (0.05), the 'width' of the range of suitable points in terms of right ascension of the ascending node was about four simulation points, meaning somewhere between 6° and 10°. For larger increases in eccentricity, this range becomes larger, while for smaller increases, close to 0.03, this range becomes smaller.
It can thus be concluded from this second sensitivity analysis, that it is very important to analyse which state for the asteroid with respect to the Earth will exactly give a suitable outcome of the mission, dependent on the epoch at which the transfer reaches its final state in the vicinity of the Earth. As can be seen from Figure 7.20, each epoch throughout the year has suitable points, but it is important to perform this analysis carefully for the expected epoch to assess what kind of difference needs to be applied to the right ascension of the ascending node.

7.3.5. Verification and Validation

A brief discussion on the verification and validation for the analyses in this chapter will be held in this paragraph. Very similar to the verification and validation of the asteroid selection analysis in Section 6.3.1, no significant modifications to the software have been made for the stability analysis. This is why, contrary to the verification and validation process that will be shown in Section 8.3.4, no large verification analyses will be performed here.

As mentioned before, during this stability analysis use has been made of already implemented functions in Tudat, in their original state without any modifications. It can be assumed that these all provide the correct results at all times, since they have been verified and validated extensively before they have been incorporated into the Tudat framework.
Similar to Section 6.3.1, intermediate checks of states have been performed regularly and with the amount of information that was outputted during each run, several aspects of each simulation could be checked. The visualisations that were created using all this information were also used as sanity checks, similar to what was explained before, to see whether the results make sense from an astrodynamical perspective (and physical and mathematical in general). The sensitivity analysis was also important to see how the results react to changes in certain components, where again, all the observed behaviour corresponded to what can be expected from an astrodynamical point of view.
With all of this combined with the first mentioned fact that everything already implemented in Tudat can be assumed to be correct, it can be concluded that the analyses in this chapter do what they do correctly and also do what they should do.

7.4. Conclusions

After all the performed analyses in this chapter, a clear conclusion can be drawn on what the final state of the asteroid should be for it to adhere to the posed requirements, namely those of safety, stability and accessibility.

First of all, and most importantly, it can be concluded that taking the current state of the Earth and adding at least 0.03 to the eccentricity will open the possibility for a suitable final state for the transfer orbit of the asteroid to a heliocentric orbit, in the neighbourhood of the Earth-Moon system. With an eccentricity increase of slightly above 0.03, the highest accessibility can be achieved, but at a price of more risk in terms of the asteroid's distance to the Earth. Increasing the eccentricity with a larger value will thus generally be safer for the Earth; the downside of this is that a larger velocity impulse will be required, but by not increasing the eccentricity too much (e.g. ≥ 0.1), the required ΔV's all stay withing the range of what is already feasible with the current technology.

Next to this, when looking at the sensitivity analyses that were performed, it can be concluded that it is very important to know what the expected epoch of arrival is for the transfer orbit, since the stability analysis should be performed with this information to assess which changes in right ascension of the ascending node are required for that state to be a suitable final state for the transfer orbit.
In terms of sensitivity of the other two Kepler elements that were analysed (semi-major axis and inclination), it can be concluded that the semi-major axis should not deviate too much from Earth's semi-major axis, generally not more than half a million kilometres, while the inclination is bounded by a maximum deviation of 1°.
These parameters can be summarised in a table, which can be seen in Table 7.1.

Table 7.1: The concluded requirements for the final state of the transfer orbit.

Primary parameter	Boundary values
Eccentricity	≥ 0.03
Secondary Parameters	
Semi-Major Axis	$\leq 500\,000\,000$ m
Inclination	$\leq 1°$
Right Ascension of the Ascending Node	Dependent on the starting epoch (in range of 6°)

In the end, after balancing the risk of being too close to those 0.03 extra in eccentricity or being too far with more required ΔV for a mission to the captured asteroid, it has been decided to use an eccentricity change of 0.05 for the analysis in Chapter 8.
With this information, the next phase of this mission design can be started, namely that of designing the transfer trajectory of the asteroid from its initial position to the found area of suitable states, which will be done in the next chapter.

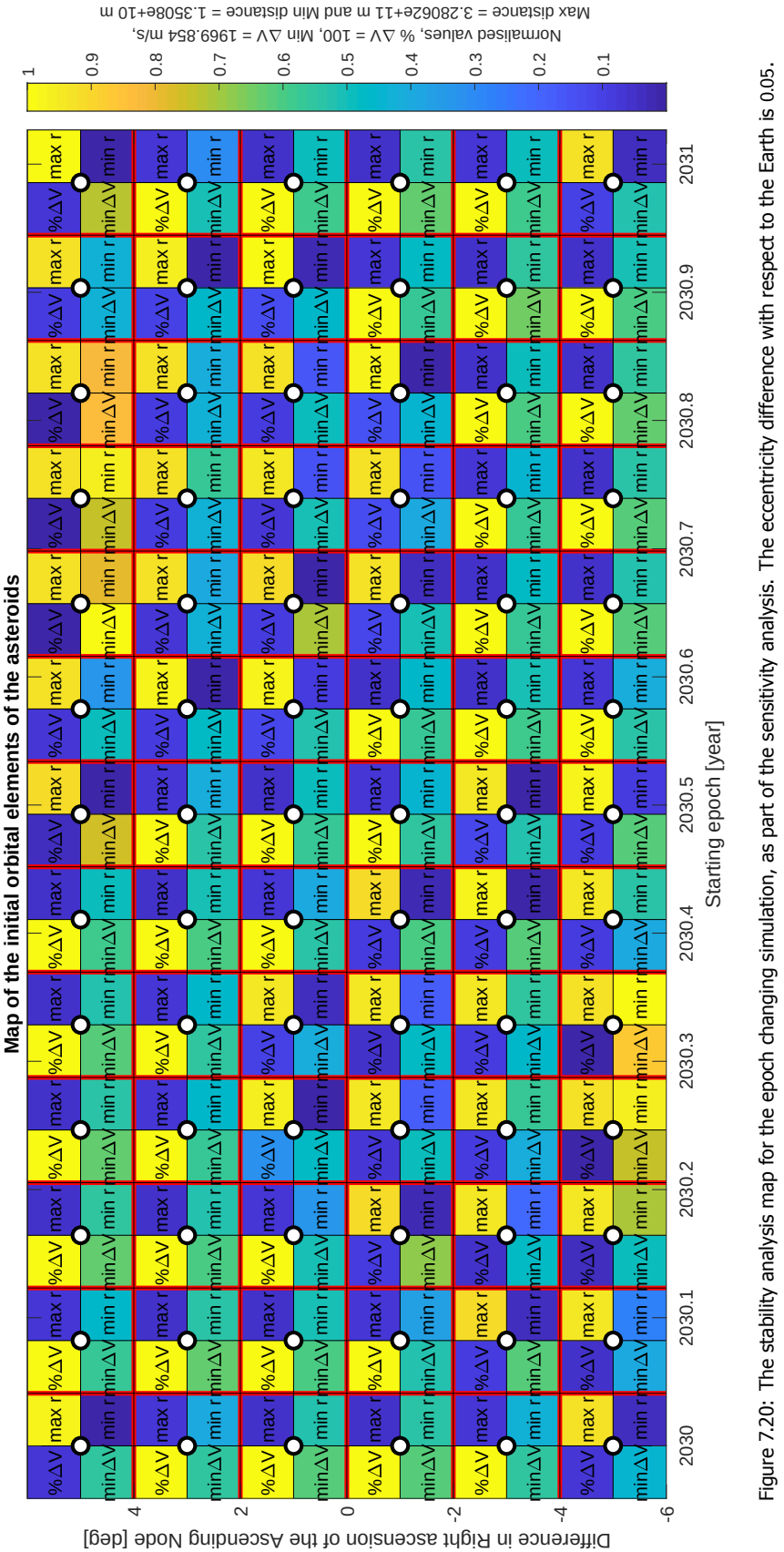

Figure 7.20: The stability analysis map for the epoch changing simulation, as part of the sensitivity analysis. The eccentricity difference with respect to the Earth is 0.05.

8

Transfer Trajectory

Following the identification of the most suitable asteroid for this asteroid capture mission (Chapter 6) and the assessment of which final orbit will adhere to the posed requirements (Chapter 7), it is now possible to design the actual transfer orbit that will place the asteroid in the desired final state. The design of this transfer trajectory to the heliocentric final orbit will be performed in this chapter, including all the necessary analysis that needs to be done prior to the design of the trajectory.

It is started by giving a description of the general approach in Section 8.1, while specifically focusing on the boundary conditions for this analysis and the division between an analytical and numerical analysis. Next, the chosen analytical method will be discussed in Section 8.2, after which the chosen numerical method is discussed in Section 8.3. In each of these sections, the theoretical background, software implementation and results are elaborated upon. Furthermore, an extensive verification and validation is performed on the software as used for the numerical method. Finally, the findings of both of these analyses are brought up in Section 8.4, after which the general conclusions for the complete thesis project are drawn in Chapter 9.

8.1. General approach

In this first section, the general approach that will be followed in this chapter will be described and elaborated upon. It is started by discussing the boundary conditions for the asteroid capture mission as they have already been defined, together with the boundary conditions that are expected to be added to the design after some analysis or are required for a follow-up analysis. This is followed by the reasoning for the division between the analytical and the numerical analysis, which together form the main content of this chapter.

8.1.1. Boundary conditions

To be able to design the transfer orbit and perform all required analyses, it should be clear which boundary conditions should be known and how they can be used to improve the process, in terms of computational time and accuracy of the outcome, but most importantly in terms of relevance of the outcome. This last element is emphasised, since various methods that can be used can provide different (sorts of) outcomes and (sets of) data, some of which may not be relevant to the problem at hand. These various methods also can require different (sets of) boundary conditions.

The clearest way of creating this inventory of boundary conditions, is to summarise what has already been achieved so far and assess which of these sets of data are useful for the coming analysis. Firstly, the asteroid that will be used for the asteroid capture mission has been chosen after a careful analysis in Chapter 6. Knowing which asteroid is to be transported, means that its state at any moment in time is also known, due to the possibility of propagating its state into the future, or by creating a (Kepler) ephemeris from its current state. This means that for every desired epoch in the future, the state of the asteroid (e.g. in Kepler elements or Cartesian coordinates) will be known and can be used for analysis. Another important piece of data for the chosen asteroid is its mass, since this will significantly

influence the amount of force that is required to achieve a certain acceleration for the asteroid. As has already been explained in Section 7.2.1, using the assumptions as mentioned there, the mass of the asteroid has been set at $20\,453\,\mathrm{kg}$.
Also not unimportant, is the estimated mass of the spacecraft at the beginning of the transfer trajectory from the asteroid's initial state to the final state. It should be noted that this mass will be the mass of the spacecraft after its transfer from the Earth to the asteroid and after physically attaching itself to the asteroid, both of which actions have not been part of the scope for this thesis project. For now, a rough estimate has been made of $2500\,\mathrm{kg}$, which seems in line with other interplanetary missions that have flown or are still in the design process. If this estimate appears to be unsuitable in later stages of this design (e.g. if the result for the required propellant mass exceeds $2000\,\mathrm{kg}$ and the resulting 'dry mass' is deemed too low for a realistic mission), this estimate will be updated and the corresponding analyses will be rerun. The initial mass for the asteroid-spacecraft system will thus be set at $22\,953\,\mathrm{kg}$.

Another important set of boundary conditions, or (initial) parameters for the analysis, is the engine settings that will be used for this analysis. As has already been discussed in Chapter 4, low-thrust engines can provide a fraction of the force of high-thrust engines, but in return can operate much more efficiently in terms of propellant. The used settings for this analysis, based on the previously discussed literature, will initially be as follows: a specific impulse (I_{sp}) of $3500\,\mathrm{s}$ and a thrust force that should not exceed $5\,\mathrm{N}$. If it is possible to obtain a smaller required thrust force, this will be used, since it will make for a more easily realisable mission.

Next to this, the final state for the asteroid in a heliocentric orbit in close proximity to the Earth has been identified in Chapter 7. The analysis was performed in such a way, that the resulting state is always defined with respect to the position of the Earth. It was concluded that placing the asteroid in an orbit with exactly the same Kepler elements as the Earth, with the eccentricity as an exception, could provide a suitable final state. The value of this change in eccentricity is set at $+0.05$. Next to this change in eccentricity, it was concluded that, dependent on the position of the Earth around the Sun and thus the time of the year, a change in right ascension of the ascending node could also be required to ensure a suitable result. This will thus be dependent on the epoch of arrival and the precise value of the required change in Ω will be defined when this epoch is known.

Finally, a brief discussion will follow on those boundary conditions that are not yet defined but will be crucial for the coming phases in the trajectory design. The departure date and the time of flight for the transfer orbit are such boundary conditions, which will improve the analysis significantly (especially in computational time and efficiency) once a general idea is obtained on what each of these boundary conditions should be to achieve a low required ΔV and a low overall maximum thrust. Once these two boundary conditions are known, the epoch of arrival will also automatically be known, since it is simply an addition of the time of flight to the departure date. In this way, the actual final state can be determined, including the analysis whether a change in Ω is required. Furthermore, dependent on the chosen methods in the next part of the analysis, other boundary conditions may present themselves, but naturally this will be discussed once it occurs.

8.1.2. Analytical and Numerical

Next, in terms of the approach, the design of the transfer orbit from the initial position of the asteroid to its final heliocentric orbit will be split up in two main parts, namely that of a (simplified) analytical analysis and a more detailed and accurate numerical propagation. With the analytical analysis, a good idea can be obtained on what the trajectory potentially will look like and what combination of departure date and time of flight will most likely provide the optimal solution. The numerical propagation will subsequently be used to generate a more realistic and accurate trajectory that adheres to the laws of physics in space and is not solely based on mathematical expressions.

The idea of the analytical analysis, is to analyse a certain search space in terms of departure date and time of flight in an efficient manner, due to the use of simple mathematical expressions and the exclusion of lengthy numerical propagations. The goal of the analytical analysis is thus to obtain an idea of which combination of the aforementioned two boundary conditions will provide the lowest required ΔV for the transfer orbit, as defined using the mathematical expressions of the chosen analytical method, such

that the numerical analysis afterwards can focus on these boundary conditions and find the optimal trajectory in a much more efficient way. Once the departure and arrival dates are known, the initial and final state can also be defined very precisely and subsequently, the final trajectory design can be performed in a well-defined way. With this information, the numerical part of the trajectory design phase can be commenced.

This numerical part will have as a goal to find the actual most optimal trajectory for the asteroid transfer, taking into account the real-life forces that can be expected to perturb the asteroid-spacecraft system during its transfer. The main source of acceleration will be the engine of the spacecraft, which is why the goal for this numerical part is to find the thrust profile for this engine corresponding to the most suitable trajectory, all while it is being perturbed by forces such as the gravitational force of various planets. The numerical part will therefore not analyse a multitude of combinations in terms of departure date and time of flight, but will focus on one 'best combination' of these (which flows out of the analytical analysis) and will try to find the optimal version of the trajectory for this 'best combination'.

8.2. Hodographic method

The first part of the design of the transfer trajectory will thus be done in an analytical way. In the field of astrodynamics, and specifically those applied to low-thrust engines, the concept of shape-based methods exists, as was already discussed in Section 5.5. As mentioned before, these shape-based methods entail the use of mathematical expressions and formulas to define the shape of the low-thrust trajectory. One of these shape-based methods is the so-called hodographic method. This method is based on using velocity hodographs for bodies in orbit and shaping the velocity components throughout the trajectory [38]. More elaboration on the theory of this method will follow in Section 8.2.1.
The hodographic method is chosen as the 'fast and initial' analytical method for this chapter due to its simplicity and efficiency when designing 3D heliocentric transfer orbits, while still retaining robustness. The boundary conditions that are required to perform the analysis with the hodographic method are all known and there is no need of specific additional parameters to make the analysis work (note that 'free parameters' can be added to try and make the solution better, as will be discussed in Section 8.2.1 and also will be done during the optimisation part of this analysis). All of the aforementioned, combined with the fact that the method has been implemented in Tudat, which is being used as the main software library throughout this thesis, has contributed to the reason why the hodographic method is chosen for this particular analysis.

8.2.1. Theoretical background

Before the analysis will be performed and the shaping method will be applied to the asteroid capture mission, a brief theoretical background will be provided here. In this way, it will be more clear what is actually being done and which steps are taken to reach the final result of the analytical analysis. Note that this is just a short summary to give the reader an idea of what this method is based on, which is why elaborate mathematical derivations will not be shown here. Only a few key expressions will be discussed in this section. The full theoretical background can be found in [38], which is also used as the main reference here.

As was briefly mentioned before, the hodogrpahic method is based on using velocity hodographs to shape the trajectory. It seeks to model the velocity behaviour of the low-thrust trajectory. By looking into the velocity domain of orbits, a transfer can be drawn from one orbit to another, the first being the initial orbit and the latter being the final orbit. To shape the velocity in the three different dimensions, use is made of the cylindrical coordinates r, θ and z. The equations of motion can then be formulated as can be seen in Equations (8.1) to (8.3), with $s = \sqrt{r^2 + z^2}$ and the forces on the right-hand side of each equation representing the accelerations in each direction.

$$\ddot{r} - r\dot{\theta}^2 + \frac{\mu}{s^3} r = f_r \tag{8.1}$$

$$r\ddot{\theta} + 2\dot{r}\dot{\theta} = f_\theta \tag{8.2}$$

$$\ddot{z} + \frac{\mu}{s^3} z = f_z \tag{8.3}$$

The total thrust acceleration can then be formulated as follows: $f = \sqrt{f_r^2 + f_\theta^2 + f_z^2}$. With this thrust acceleration, the required ΔV can be computed by numerically integrating it over time, as can be seen in Equation (8.4).

$$\Delta V = \int_0^{t_f} f \, dt \tag{8.4}$$

The velocity can be shaped as a function of time or as function of the polar angle, which are both discussed in [38]. Only the former has been implemented in Tudat however, which is why this will be used in this first analytical analysis.
The previously mentioned shaping of the path is performed using so-called velocity functions. These velocity functions are set up in a simple way, such that they can be integrated analytically. They are namely made up of various smaller base functions, such as trigonometric, polynomial and exponential functions. For each of the three different velocity functions (in the aforementioned cylindrical coordinates), three boundary conditions need to be satisfied (i.e. the initial and final velocity and the difference in position), making a total of nine boundary conditions. In the implementation in Tudat, a coefficient is added to these base functions to be able to weigh them. Next to the minimum of three base functions per velocity component, more base functions can be added along with their 'free coefficients' to introduce more degrees of freedom, which enables optimisation of the low-thrust trajectory. More on the application of these base functions will follow in Section 8.2.2.

8.2.2. Software setup

As mentioned before, the hodographic shaping method has been implemented into Tudat, but to be able to apply this to the asteroid capture problem the software has to be modified and new functionalities need to be added, using the already written hodographic functions. The way the software is set up will be described in this section, showing how each step is performed to obtain the final desired results.

Following some examples already implemented in Tudat, it has been decided to first do a broad analysis in a large search space to obtain a general idea on where the most optimal area is located. In this analysis, no additional free parameters will be added and therefore no optimisation will be performed. Instead, a grid search will be used to analyse the search space in a uniform manner.
Next, a different setup will be used, with the hodographic method still at its base, but now with added free coefficients (as has been described in Section 8.2.1). A multi-objective optimisation is applied on these coefficients, to obtain the most optimal combination of departure date, time of flight and various free coefficients for the velocity functions in terms of expected required ΔV and maximum thrust, all while still using a fast and efficient analytical method.

Preliminary analysis

The program starts by defining the celestial bodies that will be relevant throughout the analysis. In this analytical case without perturbations, only the Sun and the Earth are required to be loaded in. This is followed by the definition of the position of the asteroid. This is done in the same way as has already been done in Section 6.2, using the position of the asteroid at a certain epoch (in this case April 27th 2019, taken from the Minor Planet Center [39]) and generating ephemeris data for it based on a Kepler orbit. The useful feature of this function in Tudat, is that the ephemeris data is being generated with respect to the first of January in 2000, which gives a high versatility to the user in terms of analysis, since the position at any date after this initial epoch can be retrieved.

Following this initial part, the upper and lower bounds for the two dimensions in the upcoming grid search are defined. These two dimensions are the departure date and the time of flight, as discussed previously, which means that two epochs in seconds with respect to the baseline of the year 2000 will be defined for the former, and two periods of time (also in seconds) will be defined for the latter.
For the initial analysis, the departure date bounds have been placed from the first of January 2023, to the first of January 2035, to analyse a sufficiently broad starting period in the coming two decades.

The time of flight bounds are defined from 100 to 1000 days, to capture a broad-enough range of time of flights and make more than one revolution possible, if that provides a more suitable result.
Next to the outer bounds that have been defined, it is also of importance to properly define the steps between each grid point in the analysis. The goal is to get a grid that covers the complete search space in a proper way and find a balance between computational time and accuracy. Smaller steps and thus more grid points can come closer to the real optimum, but this can increase the computational time significantly. This is why this balance needs to be assessed carefully, by doing some initial small-scale tests. The eventual number of steps was then defined, keeping in mind that this is the first less detailed analysis, merely created to obtain a good idea of the behaviour of possible (analytical) transfer trajectories in the chosen search space and to see where the more optimal areas (in terms of required ΔV and maximum required thrust) in this search space are located. The step size in the time of flight dimension was set at five days, to obtain a good cover of the search space, while the complete range in departure days was split into 500 steps to get a step size of approximately 8.8 days.

The loop through all these grid points is subsequently started and inside, for each combination of departure date and time of flight, the recommended base functions for the three different velocity components in the hodographic method are obtained through the implemented functions in Tudat. Next to this, for each grid point the initial and final state for the transfer are defined, knowing the starting and ending epoch. With these epochs, the position and velocity of the asteroid at the departure date and the position and velocity that it has to have at the arrival date can be obtained, the latter of the two being linked to the position and velocity of the Earth at that moment in time, as has already been established in Section 8.1.1.
Finally, for each grid point multiple number of revolutions are analysed and the number of revolutions that provides the lowest ΔV is saved, along with this value for the required ΔV. Throughout the complete grid search, the grid point that provides the lowest required ΔV overall is also saved, along with its corresponding departure date, time of flight and number of revolutions.

Optimisation

This second analysis starts by defining the seed number, which is relevant for the optimisation part in the software. This seed number initialises a pseudo-random number generator used to generate the random spread in the search space. It is always important to note the used seed number, for reproducibility later. The seed numbers for each run will be stated along the corresponding results.
Next, in a way identical to the preliminary analysis, the bodies of interest are loaded and the relevant positions of the asteroid and the Earth are defined, such that they can be extracted for each desired epoch. Again, since the analysis does not take into account any perturbations (yet), only the Sun and the Earth are loaded. The boundaries for the departure date and time of flight are defined in pairs, similar to how it has been done in the preliminary analysis. Here however, due to the optimisation that is to be performed, the boundaries for the previously mentioned free coefficients are also added to the vector of pairs. This vector contains nine pairs in total, of which the first two define the departure date and the time of flight, the following two are free coefficients for the radial velocity function, the next two are free coefficients for the normal velocity function and the last three are free coefficients for the axial velocity function. With these nine pairs of boundaries, the optimisation can be commenced and executed in a meaningful manner. All of these parameters that are being optimised here, will be used in the numerical part of the design of the transfer trajectory, as will be discussed extensively in Section 8.3.

For the numerical values of these boundaries, the default values that existed in the already written example applications for this software tool have been adopted. This means a lower boundary of -5000 and an upper boundary of 5000, for each of the free coefficients that are being optimised. This has been done since analysing and pruning the actual search space for an optimisation like this is not part of the scope of this master thesis.
The boundaries for the departure date and time of flight have to be set up however, the latter of the two being done based on the choice of how many complete revolutions around the Sun are allowed. If this number is set to zero, most of the points that can be evaluated will lie below a time of flight of roughly 400 days. In the case this number is set to one, the time of flight zone in which most points will lie starts at around 300 and ends at approximately 800 days. Lastly, for at least two complete

revolutions, most points will require a time of flight of around 650 days and above. After a few initial low-detail test runs, it was established that zero complete revolutions provides the best results, both in terms of ΔV and required maximum thrust. This is why the boundaries for time of flight have been chosen to be between 100 and 500 days. The 100 day boundary on the lower end has been set up, since the observation could be made that points below this time of flight required very high thrust levels and therefore were not deemed suitable for this asteroid capture mission. The boundaries for the departure date are the same as for the preliminary analysis, namely spanning from the start of 2023 until the start of 2035.

Next, the actual hodographic shaping optimisation problem is set up, which is an existing function in Tudat. All of the required information for the objective function is passed through to this problem, such as the functions that define the state of the asteroid and Earth at each moment in time, the default shaping base functions and the above defined boundaries for all of the optimisation variables.
Inside this problem, the fitness function is set up and evaluated, such that it can be used later in the actual optimisation over multiple generations using many individuals. In this fitness function, first the free coefficients are added to their corresponding base functions. Next, the state of the Earth at arrival is extracted from the aforementioned state function, after which the required eccentricity is added to this state. With this final state properly defined, the actual hodographic function can be called and executed, after which the ΔV and maximum thrust are computed and added to the fitness vector, since both of these are optimised in this multi-objective optimisation.
With the already implemented functions in Tudat, there would be two ways to compute the maximum thrust, one of which was already implemented in Tudat and the other being written by the author. The former simply computes the required thrust acceleration at a set number of equidistant epochs and saves the largest value. This method does not take into account the lowering mass of the system (the asteroid + the attached spacecraft burning through its propellant) over time and therefore cannot output the actual thrust force required. The latter method does define a specific impulse and computes the mass profile of the system, so that it can calculate the actual thrust force. After some tests, it was found that this second method is roughly 100 times slower that the first. Also, due to the fact that the asteroid mass makes up the largest part of the total mass in the system by far, and a low-thrust engine with a high specific impulse will be used, the initial and final mass will not be significantly far apart from each other. With this in mind, a simple and slightly conservative assumption can be made (for the thrust calculation), namely that the mass stays constant over time. In this way, the output of the analysis will be a thrust acceleration, but in post-processing this value can simply be multiplied by the initial mass to get the final thrust force. It has been chosen to do exactly this, due to the much faster computing power and the fact that the assumption will not change the location of the most optimum solution, but merely will give a slightly conservative value for its thrust force level.

The fitness function has thus been defined and it can be passed through to the next process, in which the individuals are created and evaluated over a set number of generations. Due to its availability in the software and its solid and robust reputation, NSGA II has been chosen for the multi-objective optimisation algorithm [40]. To assess the problem in detail and to get an accurate and as optimal as possible final result, it has been decided to create a large set of 10 000 individuals. These individuals are then evaluated over 100 generations and the results for each 25th generation are saved.

8.2.3. Results

Now that an idea has been obtained on how the problem will be approached and how it has been set up in the software tool, the results of the analytical analysis can be presented.

Preliminary analysis

As described in Section 8.2.2, a grid search has been performed as the first broad analysis, which is why the results for this analysis have been plotted as a contour plot, as can be seen in Figure 8.1.
A few observations can be made from this figure, to get a better understanding of what exactly can be seen and what it means. First of all, it can be seen that the range for the ΔV value is rather large (up to almost 250 km/s), due to some areas in this search space that cause the required ΔV to be very high. This can be seen in the lower right corner for example, which indicates that the combinations of departure date and time of flight here do not provide suitable results at all. This is not particularly

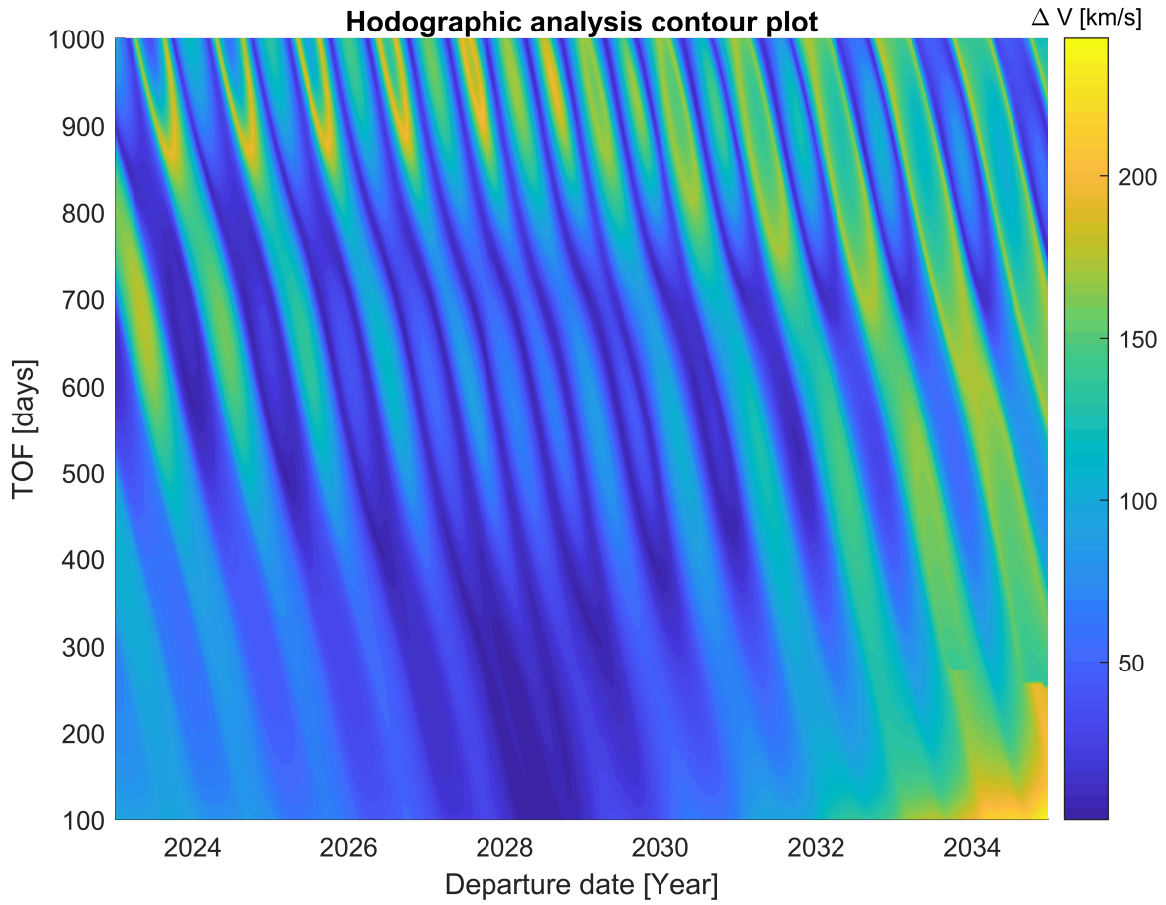

Figure 8.1: A contour plot following the grid search that has been performed on the selected search space, using the hodographic method without any extra free parameters and therefore without any optimisation.

problematic for the analysis, since the goal of this first visualisation is to obtain a general idea on how the suitability for different combinations of departure date and time of flight behaves and where the more interesting areas are located.

Another observation that can be made immediately is the repeating pattern of low required velocity impulses, which has a period of one year, exactly corresponding with the orbiting period of the Earth around the Sun. This adheres to the expectation from an astrodynamical point of view, since this means that every full orbiting period of one year, both bodies have time periods in which their states with respect to each other provide for more efficient transfers (in terms of required ΔV) and other time periods in which their states are in less optimal positions with respect to each other.

Furthermore, when looking at this pattern, it can be observed that there is a multi-year period in time for departure dates that requires lower velocity changes and thus provides more suitable results, while other multi-year periods (such as the previously discussed period towards the bottom right corner, roughly after 2033) require significantly higher ΔV's. This suitable period is centred around a moment in time somewhere in 2028 for low time of flights and moves back in terms of departure date for longer time of flights. This makes sense from an astrodynamical point of view, since the required ΔV is closely related to the difference between the final state and the initial state. Since the final state is dependent on the position of the Earth at that moment, this can also be viewed as the difference between the position and velocity of the asteroid at the departure date and the position and velocity of the Earth at the arrival date. From this first broad analysis, it can thus already be concluded that these two states are most optimal with respect to each other for a transfer between both around the year 2028. By departing earlier, but having a longer time of flight, the arrival date essentially stays equal, which is why the dark blue areas (of more suitable combinations) have a pattern upwards and to the left.

Next to this full visualisation of all of the assessed points in the first hodographic analysis, a visualisation has been made in which only those grid points (and thus combinations of departure date and time of flight) that result in a required ΔV of $15\,\mathrm{km/s}$ and lower and a required maximum thrust throughout the complete transfer trajectory of less than $15\,\mathrm{kN}$ are being shown. This required maximum thrust has been computed by numerically propagating the orbit that comes out of the analytic hodographic method, in such a way that the resulting thrust force profile steers the propagated object to follow the analytic orbit that was the result of the hodographic method. Since this part of the analysis takes a huge amount of computational effort (due to the departure from the purely analytical method and actually propagating the full trajectory numerically), it has been decided to only do this for grid points that adhere to the previously mentioned boundary conditions of a maximum required velocity impulse of $15\,\mathrm{km/s}$ and thrust force of $15\,\mathrm{kN}$. In this way, the usefulness of analysing the broad grid in an analytical way still exists, while further analysis (and in this case numerical integration) can still be performed on the more suitable and therefore interesting points.

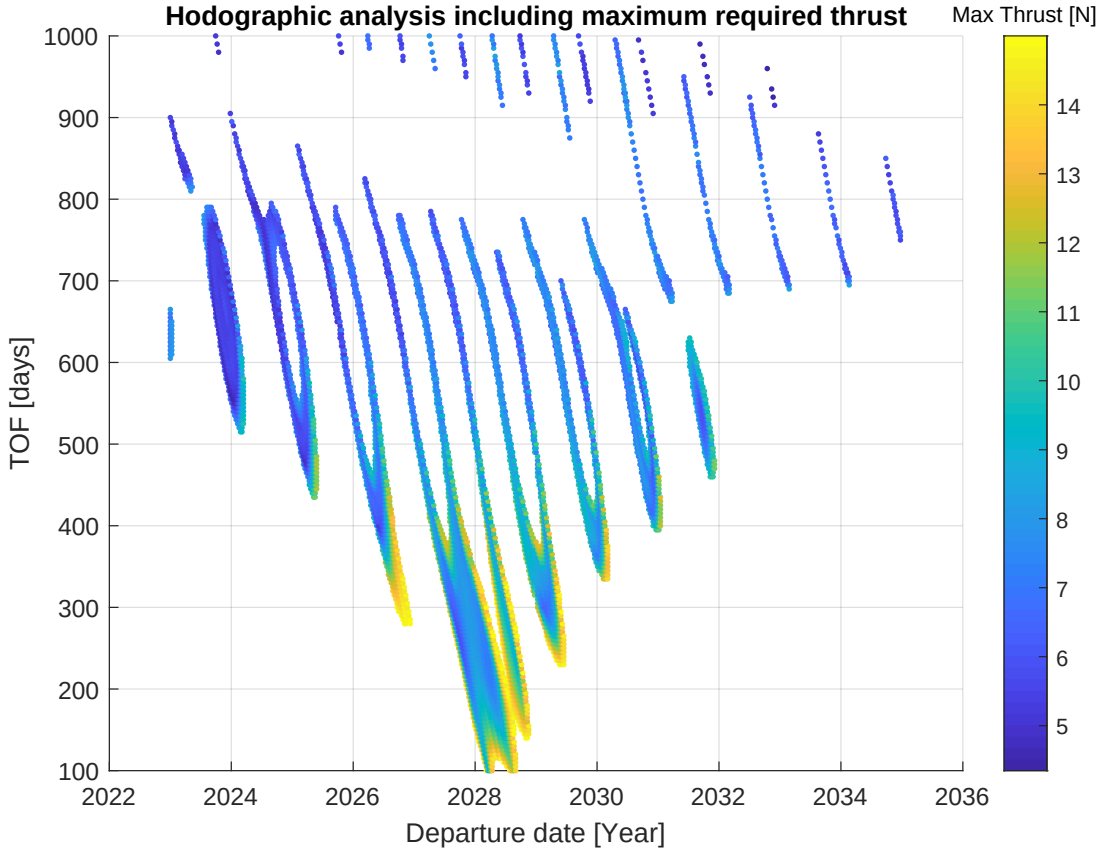

Figure 8.2: A visualisation of the more suitable points, showing their required maximum thrust following the transfer trajectory resulting from the hodographic analysis.

This second visualisation can be seen in Figure 8.2. The required ΔV has not been visualised in this figure, but the required maximum thrust as it results from the preliminary analysis of numerical integration is shown with a colour scheme. Again, since this is still part of the preliminary analysis, the goal is not to already find the 'best' point from this graph, but merely to give the reader an idea of where the more suitable areas are located. Next to that, this visualisation illustrates what approximately the expected maximum thrust can be inside these more suitable areas. Note however that this maximum thrust is obtained without any added free coefficients and the optimisation thereof. Inside each (yearly) area, it can be seen that the lower boundary (in terms of time of flight) requires a higher thrust than elsewhere in that same area. This is indicated by the greenish and yellow zones in each of these areas. The darker blue zones in each area, which are located more towards the centres of these areas, are the places to which more careful attention should be payed and in which the most suitable points can be expected in the following more detailed analysis.

Optimisation

Next, the results of the optimisation analysis will be presented. As was elaborately explained in Section 8.2.2, the results of this multi-objective analysis will be some points that are most optimal in terms of required ΔV and maximum thrust throughout the trajectory. These points contain information on which departure date and time of flight are required for this optimal (hodographic) trajectory, but also which value the free coefficients for the velocity functions in the three different dimensions need to have.
Since this analysis is a multi-objective optimisation in two dimensions, namely with respect to the required ΔV and the maximum thrust force, the results are expected to form a Pareto front. This front represents a curve in the objective-space on which points lie with approximately the same fitness. The difference between these points is in which dimension their fitness is expressed in a stronger manner. This means that some points will have a lower value with respect to one of the two objectives, while its value with respect to the other objective will be higher. This always results in a decision for the designer and to which part of the Pareto front more priority should be given, dependent on what is desired by the designer.

Due to the fact that this analysis contains a major optimisation part, which is initiated by means of a random number generator, it is very wise to repeat the same analysis multiple times with different seed numbers for the random number generator. In this way, unintentional local convergence can be prevented (if this were to occur in the first run and no further runs are performed), but it also generally can help improving the final result and makes it easier to draw a sound conclusion based on the results. This is why it has been decided to perform the exact same analysis three times, with three different seeds. It does not matter what the actual seed numbers are, so these can be chosen randomly, as long as they are documented well for reproducibility.
In this section, the results for the three different runs will be presented. As mentioned in Section 8.2.2, the optimisation ran for 100 generations and each 25th generation has been outputted. It is chosen to show the full progression of both the fitness and the population (two elements thereof, namely the departure date and time of flight) throughout the generations of one run, while for the other two runs only the last generation is shown. The seed number for the first run is 125, while the second and the third run have a seed number of 341 and 67 respectively.

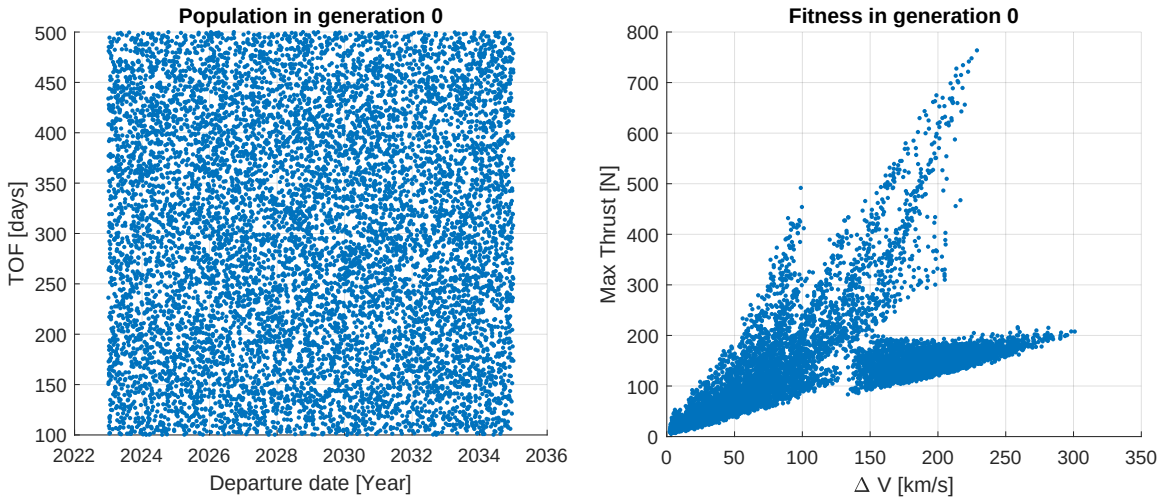

(a) The distribution of individuals at generation 0.

(b) The fitness of the population at generation 0.

Figure 8.3: The results for generation 0, with a seed number of 125.

In Figure 8.3a, it can be seen how the population is well distributed over the complete search space in terms of departure date and time of flight, as can be expected in the generation before any evolution has taken place. The corresponding fitness for this distribution (including the distribution of the values for the free coefficients that have not been visualised here) can be seen in Figure 8.3b.
In the following three pairs of figures, from Figures 8.4 to 8.6, the evolution throughout the generations can be seen and how the population and the corresponding fitness behaves over the generations. The

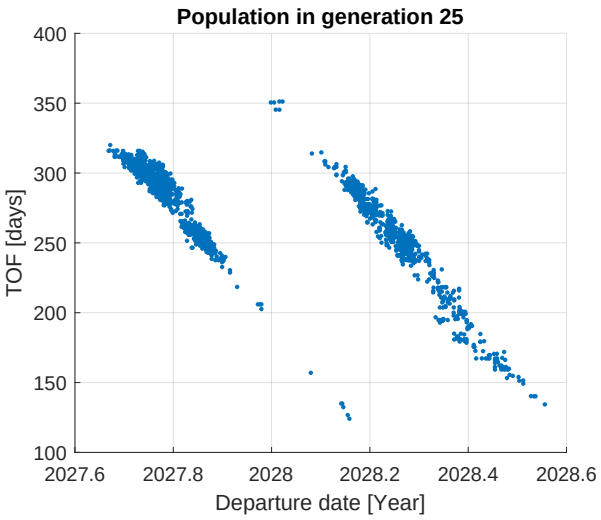

(a) The distribution of individuals at generation 25.

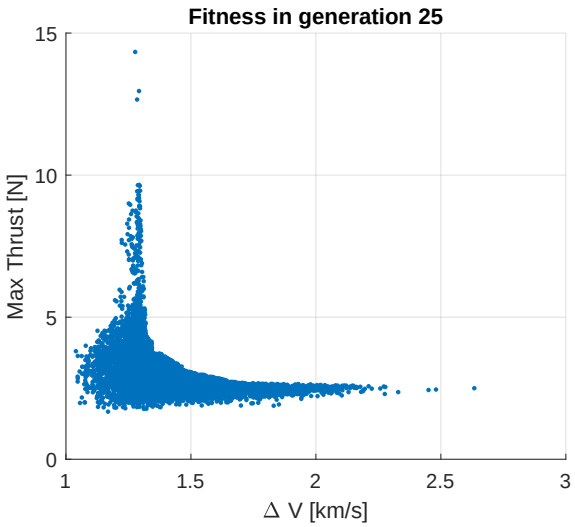

(b) The fitness of the population at generation 25.

Figure 8.4: The results for generation 25, with a seed number of 125.

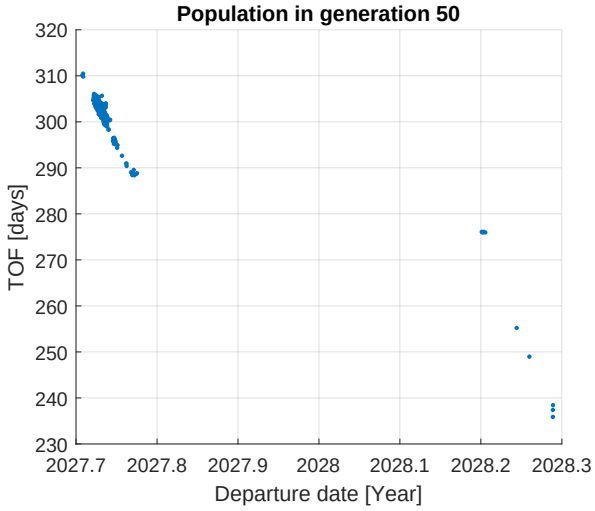

(a) The distribution of individuals at generation 50.

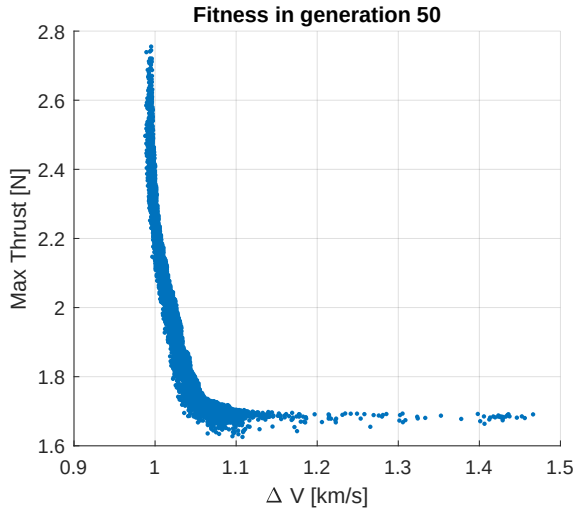

(b) The fitness of the population at generation 50.

Figure 8.5: The results for generation 50, with a seed number of 125.

start of a Pareto front can already be seen in the fitness in generation 25, becoming much clearer after 50 generations and really taking its form in generation 75. On the population side, it is visible how the individuals start to group at certain locations in this two-dimensional search space, from large areas after 25 generations to very small and precisely defined areas in the later generations.
In the last generation of the analysis, number 100, the final Pareto front can be seen, well defined and without any large 'disturbances' along its front (as could be seen in the previous generations). This is illustrated in Figure 8.7b. It should be noted that the range of both axes in Figure 8.7b has been manually set, taking into account the results from this run, but also from the other two runs that will be discussed later and can be seen in Figures A.1 and A.2. This has been done so that the fitness of the three runs can be compared easier to each other, without any shifting axis-values. Furthermore, it can be observed that all individuals in Figure 8.7a have clustered in a few well defined and small areas, spanning a rather small area of the complete search space. This could indicate that there is a clear combination of departure date and time of flight from which the most suitable trajectories can be formed (using mathematical expressions). The previously mentioned second and third run, with a seed number of 341 and 67 respectively, can be seen in Appendix A, in Figure A.1 and Figure A.2 specifically.

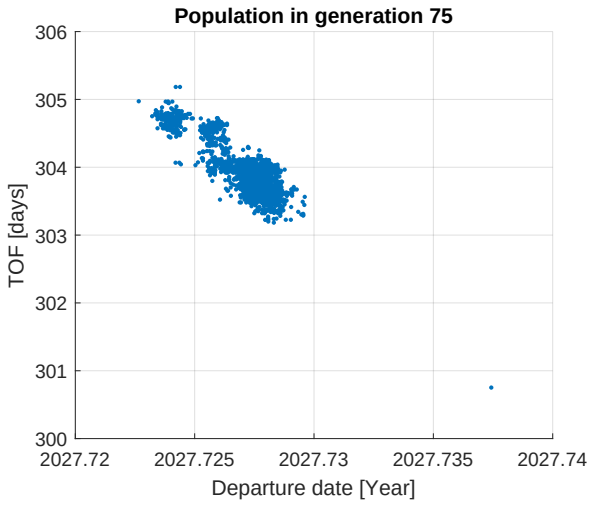

(a) The distribution of individuals at generation 75.

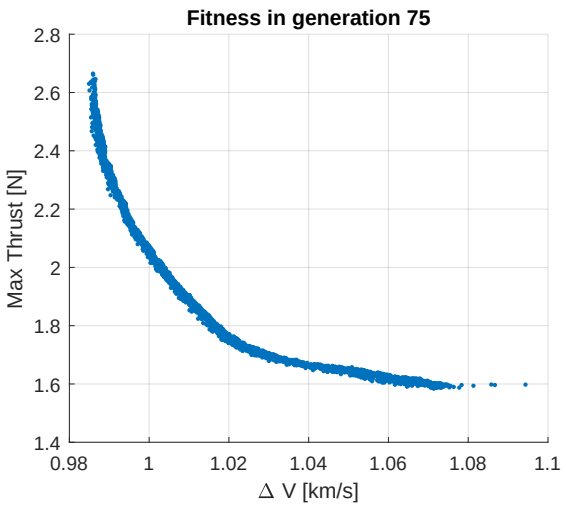

(b) The fitness of the population at generation 75.

Figure 8.6: The results for generation 75, with a seed number of 125.

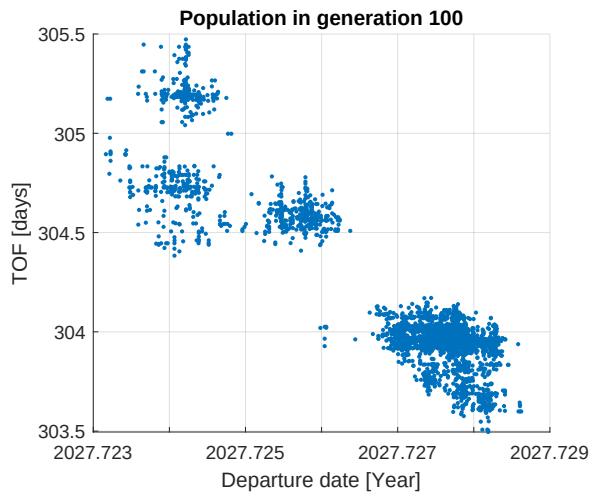

(a) The distribution of individuals at generation 100.

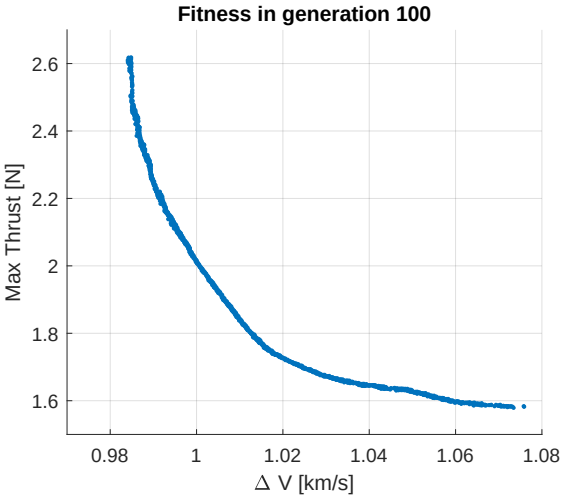

(b) The fitness of the population at generation 100.

Figure 8.7: The results for generation 100, with a seed number of 125.

When comparing the three runs (identical but with the seed number as an exception) to each other, the observation can be made that there is a difference in the fitness between the three separate runs, as well as a variation in the spread of the individuals. Due to this small spread that is still present between separate runs after 100 generations, but also to generally try and obtain an even more suitable point, it has been decided to run the analysis a final time. This time however, a much smaller search space in terms of two of the variables for which is being optimised, namely the departure date and time of flight, has been selected. The boundaries for the other seven variables, which are all free coefficients for the velocity functions, are kept at -5000 and 5000. The range for the departure date however, has been reduced to be between 2027.5 and 2027.9, while the range for the time of flight has been chosen to lie between 290 and 360 days. With these new boundaries, the final analysis has been performed, of which the hundredth generation can be seen in Figure 8.8, plotted with black dots in the same figure together with the results of the previous three runs. The seed number used for this analysis is 49.
The first conclusion that can be drawn, is that rerunning a certain analysis multiple times with different seed numbers shows its usefulness. In both the regular reruns, 67 even more than 341, the Pareto front visible in Figure 8.8b has shifted down and to the left, meaning the optimisation process has found better parameters for its population, such that the fitness of the individuals can be improved.

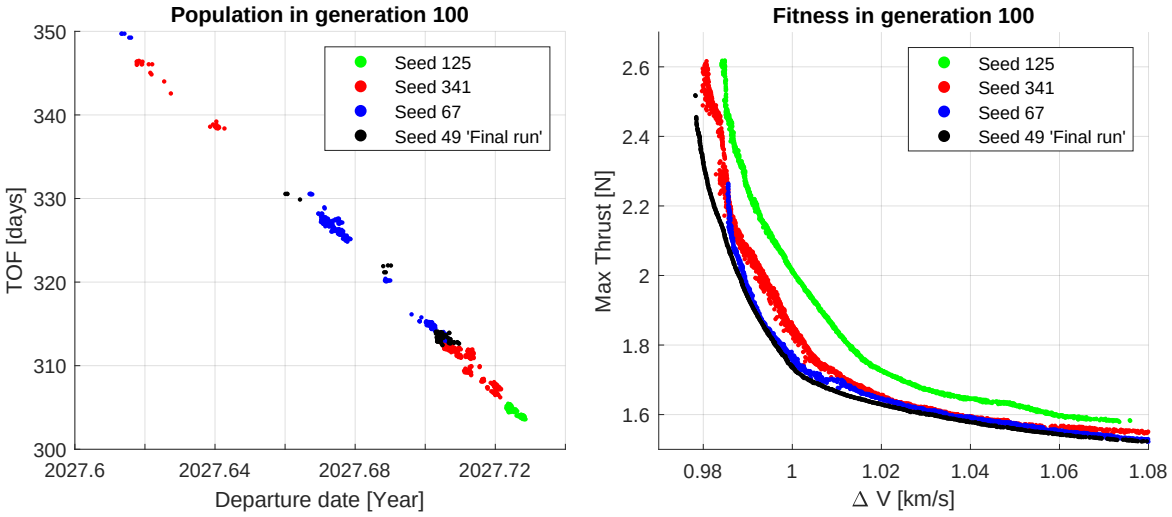

(a) The distribution of individuals at generation 100.

(b) The fitness of the population at generation 100.

Figure 8.8: The results for generation 100, for the four different runs.

The locations of the clusters of individuals in the population as seen in Figure 8.8a have also slightly shifted, although the general area in which the most optimal points lie, which is with a departure date roughly between 2027.6 and 2027.75 and a time of flight between 300 and 350 days, has remained the same.

When closer examining the fitness curve of this last analysis, which can be seen in black in Figure 8.8b, a slight shift in the Pareto front can be observed. The front is also more well defined than the previous three analyses, without many disturbances being present. This gives a higher confidence that the real optimum has been achieved. The disturbances in the fitness of the previous three runs can be caused by the fact that seven other variables are being optimised (that are not plotted in these figures), which means they simply have not achieved their most optimal value after 100 generations and still some improvements can be made. This could explain the variation in the individuals in the Pareto fronts and them not being located on a 'smooth' line. In the population, which can be viewed in more detail in Figure A.3a, it can be seen that almost all individuals have clustered themselves around a departure date of approximately 2027.705 (which for 2027 is around the 14th of September) and a time of flight of around 313 days. With these two pieces of information, the arrival date can be calculated and the stability check with respect to a change in the Ω can be performed.

The arrival date as obtained by addition of the previous two values, gives an epoch of 2 461 977.7 Julian days, or in date form the 25th of July in 2028. Rerunning the sensitivity analysis with respect to time from Section 7.3.4 with this value, gives the results as can be seen in Figure 8.9. In this stability analysis map that has been created, in an identical manner as was done in Chapter 7, five moments in time have been taken to analyse the stability at, with increments of five days around the date as established above: ten days before, five days before, the date itself, five days after and ten days after. This has been done to analyse the (small) time frame around this date and to see whether the change in Ω that potentially is required changes significantly over this time frame, since in case a different point is chosen, the epoch can shift slightly ahead or behind.

The map will be analysed in exactly the same way as has been done in Chapter 7. From the stability map, it can be seen that at the epoch of interest, all points that have an Ω smaller than $+1°$ up until at least $-5°$ will give a suitable result (which is best observed by looking at the yellow $\%\Delta V$ rectangles). This is convenient news, since it means that no change in Ω is required and therefore the optimisation analyses do not need to be rerun.

With all the results of the optimisation produced, a small selection of points can be made with which the numerical analysis will continue. As was mentioned before, the fitness of the individuals on the Pareto front are approximately equal, the difference being in which dimension more focus is laid on achieving a lower value. The decision on which point is being selected is completely up to the designer.

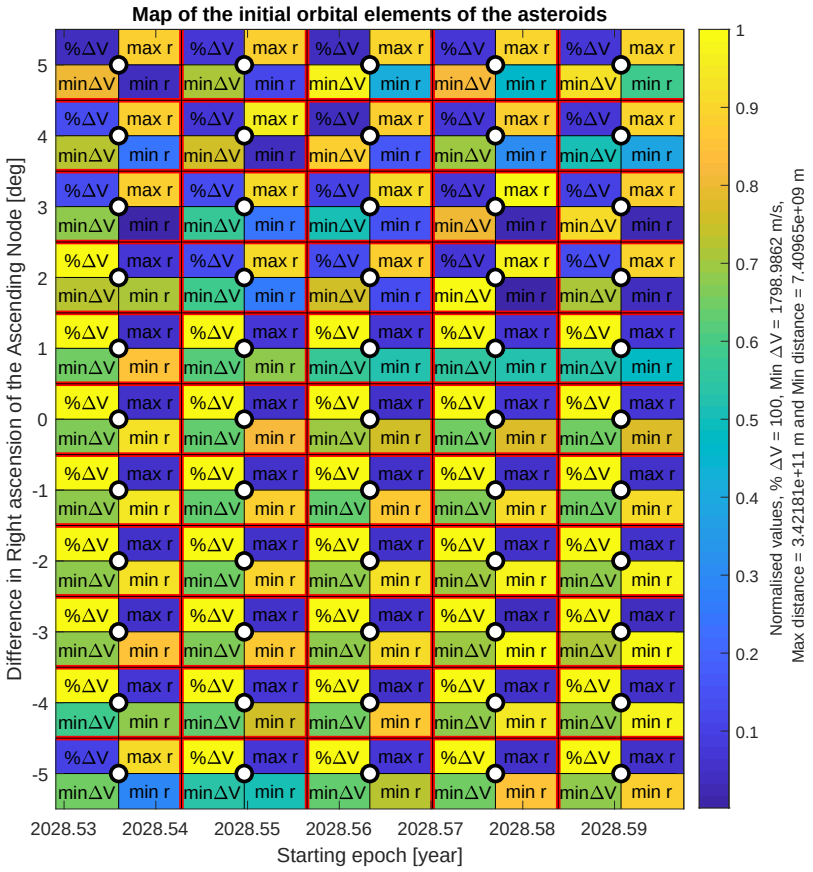

Figure 8.9: The stability analysis map, as created to check whether a change in the right ascension of the ascending node is required.

This means that some individuals should be chosen, based on their location in the Pareto front. As a starting point, it is decided to take a (random) point from the part of the Pareto front where the largest deflection occurs, which can also be seen as the most lower-left point of the Pareto front if a 45° tangent would be drawn. This would be one of the individuals that have a fitness resulting in a required ΔV of around $1\,\mathrm{km/s}$ and a maximum thrust of approximately $1.7\,\mathrm{N}$, when looking at the black Pareto front in Figure 8.8. All variables for which is being optimised are saved for each individual, which means these variables can easily be accessed during the post-processing phase of the analysis. The variables for this first point have been tabulated in the red column in Table 8.1. Two more points have been handpicked, for which the variables have been tabulated in the yellow and green column. These points are picked to create an approximately even spread along the Pareto front of three points with which the analysis can be continued.

Table 8.1: The rounded values for each optimised variable for a set of handpicked individuals.

Individual #	1	2	3
Departure date	08:39 15/09/2027	19:42 15/09/2027	08:32 15/09/2027
Time of flight [days]	313.84	313.59	313.12
Radial free coefficient 1	2433.2	2367.2	2278.8
Radial free coefficient 2	595.93	455.23	468.98
Normal free coefficient 1	-436.28	-638.49	-529.08
Normal free coefficient 2	3011.9	3004.3	2568.9
Axial free coefficient 1	3633.9	-482.54	3624.1
Axial free coefficient 2	-4228.3	-477.45	-4893.3
Axial free coefficient 3	-559.21	522.93	89.700

In this table, the values are rounded off to one decimal digit. The full accuracy (as it will be given as input in the numerical analysis) has been displayed in Table B.1.
The location of these three points in both the search pace and the objective space have been visualised in Figures 8.10a and 8.10b respectively, to make it clear where they are exactly located in both of these two-dimensional spaces.

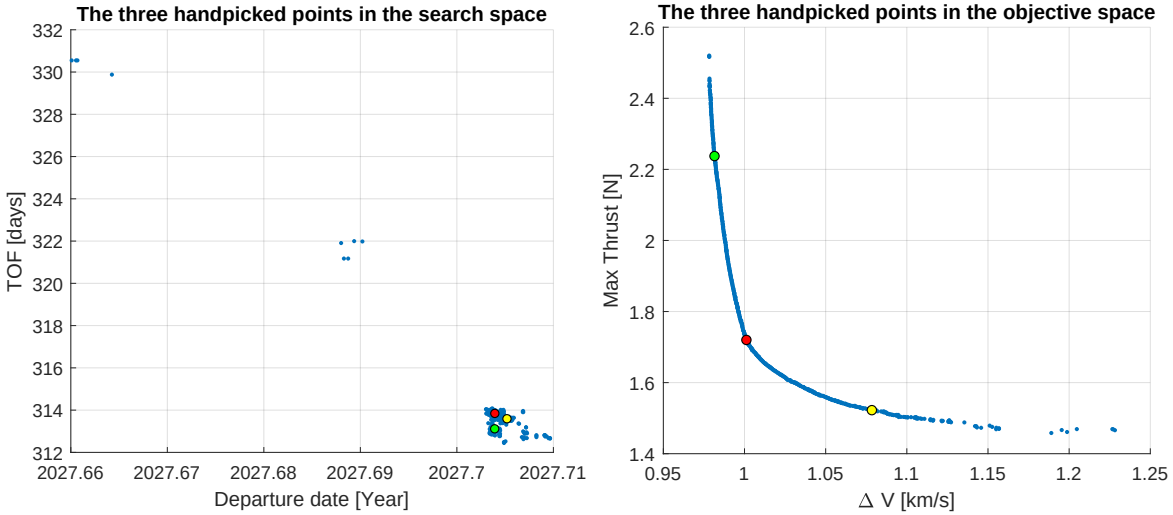

(a) The three handpicked points shown on top of the population distribution in the search space.

(b) The three handpicked points shown on top of the Pareto front in the objective space.

Figure 8.10: The results for generation 100, for the fourth run, with the handpicked points on top.

8.3. Sims-Flanagan's method

After the extensive analytical analysis has been performed, the focus can be moved to numerically propagating a single trajectory and finding the best way to transfer the asteroid from its initial state to the safe, stable and easily accessible final state that has been determined. As was mentioned earlier in this chapter, the goal of this part of the analysis is to obtain the best possible transfer trajectory in an accurate and realistic way, taking into account the major perturbing forces that will work on the asteroid-spacecraft system during the transfer. The required thrust profile for the spacecraft engine to achieve such a trajectory will therefore be the final result of this analysis.

Firstly, a decision needs to be made on which method will be used to perform the numerical analysis. For this decision, various elements should be taken into account, similarly to when the decision was made on which method will be used for the analytical part. One of these is relevance, since the way the trajectory is computed and the result of the chosen method should be relevant for the goal that is to be achieved, namely that aforementioned thrust profile including perturbing forces. Other elements that need to be taken into account, are its efficiency and accuracy, but also its robustness. The chosen method should calculate the required computations in a (relatively) fast yet accurate way, while also working in a multitude of scenarios. Finally, the method should be available to use, since it is outside of the scope of this thesis project to develop a new or fully implement an existing method into software.

Taking all of the aforementioned into consideration, it has been decided to use Sims-Flanagan's method of direct optimisation for the asteroid capture problem [41]. When looking at relevance, the framework that this method uses is closely in line with the already available information, data and boundary conditions, but also with what is to be achieved. Sims-Flanagan's method can produce exactly what is desired for this mission design in an efficient way, as will be elaborated upon in Section 8.3.1. Also, the fact that Sims-Flanagan's method has been implemented in some form in the software toolbox that has been used so far throughout this thesis project (Tudat), gives a greater incentive to use this method for the low-thrust trajectory design.

As will be discussed in Section 8.3.2, some modifications have been applied to the software as it was implemented in Tudat, in order for the analysis to be more valuable and relevant for the current problem. These modifications have also been verified and validated extensively, as will be shown in Section 8.3.4.

8.3.1. Theoretical background

It is started by briefly discussing the theoretical background of Sims-Flanagan's method, such that a better understanding is obtained on the principle of this method of analysis. Similar to the provided theoretical background for the hodographic method in Section 8.2.1, in this section merely a short summary will be given, without any elaborate mathematical derivations. The method as created by J. Sims and S. Flanagan is explained in [41], which will serve as the main source for this section. Furthermore, some underlying theoretical concepts that have not been mentioned in their original paper will also be discussed briefly here, to help and give the reader a comprehensive understanding of the used method in this part of the thesis project.

The basis of Sims-Flanagan's method, is to divide the trajectory into two separate parts that will be propagated. One of these is the forward propagation leg, going from the departure date to the moment halfway between the departure date and arrival date, or at half of the time of flight. The other part is the backward propagation leg, going from the arrival date backwards to the same point, halfway between the departure and arrival date. The idea is thus to propagate these two legs towards each other and to end up at the same point halfway between the departure and the arrival date, called the match point. In this way, faster convergence can be achieved compared to simply trying to propagate from the departure date all the way to the arrival date.

Next to this division in a forward and backward propagating leg, both of the legs have been divided further into separate segments. The trajectories in both legs are then modelled using impulsive shots (ΔV) for the spacecraft engine, located in the centre of each segment. Therefore, for n number of segments, n impulsive shots are modelled. The magnitude of each velocity impulse that is given in the centre of the segment is limited by the total change in velocity that can be provided by the engine, accumulated over the entire duration of the segment. This limit is dependent on the thrust force that can be provided by the engine, since this is directly related to the resulting thrust acceleration (through Newton's second law, knowing the mass of the system) which can be integrated over the duration of the segment to obtain the velocity impulse. This thus means that a limit can be placed on the magnitude of the thrust force as provided by the engine.

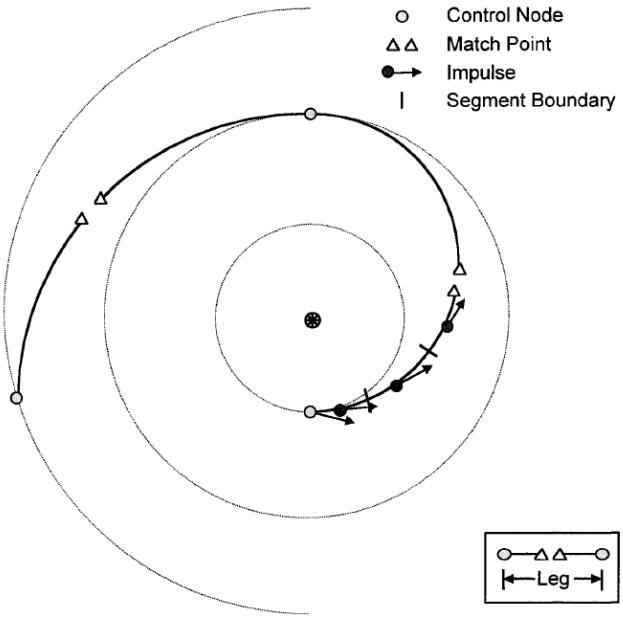

Figure 8.11: Sims-Flanagan's method of direct optimisation for a preliminary low-thrust trajectory design [41].

Furthermore, constraints are placed on the mismatch between the forward and backward leg at the match point halfway along the trajectory. This mismatch is to be minimised to achieve a feasible trajectory. In the original paper, this method has been visualised as can be seen in Figure 8.11. In this illustration, they have shown an example trajectory including a flyby around a planet, which is denoted by a control node. The two parts of the complete trajectory around this control node have been modelled exactly as described in this section, with a match point halfway and the division in segments with an impulse at the centre of each segment.

With Sims-Flanagan's method, the goal is thus to obtain this sequence of impulses that need to be applied at the centre of each segment, which provide for the lowest overall required ΔV and at the same time minimise the mismatch between the forward and the backward propagation leg. If this design method should simply start from scratch (or thus with a completely random initial guess), convergence could take a very long time and could perhaps not even be achieved. This is why it is important to start with a good initial guess, such that the direct optimisation method can continue from there on and find the most optimal solution. The optimisation that is being performed here thus 'looks around' the thrust vectors of the initial guess and tries to find the sequence of impulses that minimise the aforementioned objectives. An elaboration upon how this initial guess is obtained will follow in Section 8.3.2.

Finally, the propagation inside the actual segments around the velocity impulses, can be performed in various ways. In the original paper, a two-body model around the Sun was proposed, which is a fast method to propagate the body around the Sun, without any additional complications such as third-body accelerations. Since it was designed as a preliminary design tool, this is enough to achieve a satisfactory accuracy for the desired goal. Over the years, other methods have been proposed as improvements over the original method, such as replacing the impulses by continuous thrust segments, which are propagated numerically, instead of using simple (analytical) Kepler orbit propagation [42]. This adds the possibility to include perturbations into the analysis, but also requires more computational effort. Similar to the initial guess, this element of the analysis is also important and can be approached in different ways. How it was implemented in Tudat and what kind of modifications have been performed to achieve a different result will be discussed extensively in Section 8.3.2 and especially in its subsection on the modifications.

8.3.2. Software Setup

In this section, the software setup for the current analysis using Sims-Flanagan's method will be elaborated upon. As was established before, Tudat will also be used for this analysis, including various of the already implemented functionalities, the main one being Sims-Flanagan's method. Some modifications to the method of computing certain elements have been made, which will be discussed in the modifications subsection.

For this final analysis of the thesis project, it is started by defining all bodies of interest, which in this case are the Sun, the Earth, the Moon, Venus, Mars and Jupiter, since perturbing forces from some of these bodies will be added in this analysis. Next to that, in the same fashion as was described in Section 8.2.2, the orbit of the asteroid was defined, again using [39].
Next, the initial guess for the Sims-Flanagan method is defined. This is an important step for the complete process, since the forthcoming trajectory design is largely based on this initial guess. The way in which this initial guess is implemented in Tudat, gives an important role to the hodographic analysis, which is why the analytical analysis as it was done in Section 8.2 has been performed. The result from the hodographic analysis is namely used as an initial guess for Sims-Flanagan's method. The point that was identified as the most suitable point in Section 8.2.3 will be analysed again through the hodographic method. Using the combination of departure date and time of flight, together with the identified free coefficients for the velocity functions, a trajectory is created using the hodographic method. This means that in the software for this Sims-Flanagan trajectory design, all those values from a certain column in Table 8.1 are loaded in and using them the initial guess for the Sims-Flanagan trajectory is created, based on the hodographic method.

Similar to the software for the hodographic method, next the initial mass of the system is defined, which is $22\,953\,\mathrm{kg}$ as was established in Section 8.1.1. The I_{sp} is set at $3500\,\mathrm{s}$, also as established before. This

specific impulse will be important for the propagation of the mass and therefore also linking the thrust force to the acceleration.
As was discussed in Section 8.1.1, once the departure date and time of flight are defined for the final analysis, the actual states at these moments in time are also known, due to the previous analyses that were performed in Chapters 6 and 7. The next part of the software thus defines exactly these two states. For completeness, both these states corresponding to the first (red) column in Table 8.1 have been displayed in Table 8.2.

Table 8.2: The initial and final state for the transfer trajectory, corresponding to the red column in Table 8.1.

Coordinate	Initial State	Final State
x [m]	1.508061E+11	8.508484E+10
y [m]	2.080385E+10	-1.341860E+11
z [m]	-1.084514E+9	1.413609E+7
V_x [m/s]	-4634.019	23241.14
V_y [m/s]	29381.92	15765.08
V_z [m/s]	228.7217	-0.5361564

Identical to the optimisation part of the hodographic analysis, the required base functions are then defined, to which the established free coefficients will be linked. With everything as defined up until this point, the actual hodographic shaping can take place, using the same function as was used during the analytical part in Section 8.2.
Next, the integrator settings are defined, which dictate what kind of numerical integrator will be used, what the initial time of integration is and other integrator-dependent information. It is chosen to use the Runge-Kutta 4 (RK4) integrator scheme, for its simplicity and robustness. Since it is a fixed time step integrator, the step size should be defined as well, such that the numerical integrator knows in how many steps it should divide the total time of flight. With this time divided in a certain number of steps, the epochs at each step can be saved for use in the following computations. Subsequently, the trajectory and the mass, thrust and acceleration profile at each of these epochs can be extracted.

Using this generated hodographic trajectory and its corresponding mass and thrust profiles, the initial guess can be made. First, it is required to setup the desired number of segments for Sims-Flanagan's method, together with the maximum thrust as it is defined by the designer. With these parameters, the initial guess for the thrust profile for Sims-Flanagan's method can be made, with an impulse in each segment's centre, as was described in Section 8.3.1. The function for this creation of the initial guess already exists in Tudat, and briefly summarised does the following: it takes the thrust profile as extracted from the hodographic method and makes an average of this thrust vector for each segment, after which it replaces this with one instantaneous impulse in the centre of that segment.
With this initial guess, the actual design and optimisation part of Sims-Flanagan's method can be commenced. For the optimisation settings, the number of individuals and generations is defined, just as which optimisation algorithm will be used and the tolerance that it can have with respect to the constraints. Finally, the degree to which the final thrust impulse as found by the optimisation process can differ from the initial guess is defined as well.

All the necessary variables are passed through the implemented Sims-Flanagan function, which then initiates the optimisation process. Inside this optimisation, the fitness is defined so that the optimisation can start and minimise for this fitness. To be able to compute this fitness, the actual trajectories and all the corresponding variables of interest need to be propagated and calculated. For this, the Sims-Flanagan Model function is created, in which all the actual computations take place.
From here on, a brief description will follow of how the Sims-Flanagan method is implemented originally into Tudat. Following that, in the 'modifications to the software' subsection, all changes to this original implementation will be discussed, with which the final analyses have been performed and therefore also the results have been produced.

Inside the Sims-Flanagan Model function, the setup of performing the computations is structured in a top-down approach. First, the call is given to propagate the complete leg, whether it is forward or

backward, from the beginning (respectively the departure or arrival date) to the end (at half of the time of flight). In the second function, which is one layer below the first, the leg is divided into the predefined segments and by means of a loop a call is given to the next function, to propagate inside each segment.
Reaching this third and lowest level function, the actual propagation inside each segment is performed. In the implementation in Tudat this propagation is done using analytical Kepler propagation, which is a very fast method, but cannot include any real-life physical perturbing forces. Since the impulse is located exactly in the middle of each segment, the first half up until this impulse and the second half right after this impulse therefore are sections in which no force at all is acting upon the propagated body. In these two sections the Kepler elements of the body are thus propagated in a straightforward manner. Since the states are generally expressed in Cartesian coordinates, this means that a quick conversion back and forth to Kepler elements is required for the actual propagation. Halfway each segment, where the impulse is applied, this vector (with its three velocity components in x, y and z direction) is simply added to the velocity components of the state of the propagated body in Cartesian coordinates.

In this way, each segment for both the forward and backward leg is propagated and the total propagated trajectory corresponding to a certain set of velocity impulses is returned to the optimisation function, where the fitness can be calculated and the optimisation algorithm can decide whether to continue with this 'individual' or not. After the predefined number of generations with the predefined number of individuals, the individual with the best fitness and thus the sequence of velocity impulses that requires the lowest ΔV and has minimised the mismatch in the best way is selected as winner. Using this best sequence of velocity impulses, the trajectory is computed once more and this trajectory with its corresponding mass, thrust and acceleration profile is extracted and saved into various files.

Modifications to the Software

Since for this thesis project a higher accuracy and more realistic analysis is desired, where real-life forces work on the dynamics of the propagated body, it has been decided to modify this already existing implementation of Sims-Flanagan's method in Tudat. A summary of these modifications will be given in this section, including a brief discussion on the various challenges that arose during implementation of these modifications.
The framework that existed around the implementation of the Sims-Flanagan method in Tudat was already very solid, with many functionalities for various computations or other analyses. To maintain this existing framework as much as possible, it was decided to apply the changes in the lowest levels of the functions, such that specific variables to which some functions were linked could still work. Some functions were even dependent on a certain value for those variables to properly compute everything that was required. An example of this is the initial time as defined in the integrator settings. Since the Sims-Flanagan method is originally implemented in Tudat using Kepler propagation and no numerical integration including perturbing forces from other bodies, as described before in Section 8.3.2, no 'real' epochs (in Julian days since the first of January 2000, or better known as J2000) were required. This is due to the fact that no ephemeris information for perturbing bodies at certain epochs was required to be extracted. With this in mind and for simplicity, the initial times in the Sims-Flanagan framework were defined as 0, independent of when the actual departure date is, since this is irrelevant for a simple Kepler propagation without perturbing forces.

Therefore, it was necessary to pass certain predefined variables and parameters through all of the aforementioned layers of functions all the way to the lowest layer, in which these variables then could be used. A few examples of these pieces of information that were needed to be passed through all functions, are the departure date, a list of the central bodies and bodies to propagate, a map of all the other relevant bodies containing necessary information (such as their states at each epoch) and an accelerations map including all the perturbing accelerations working on the body that is to be propagated. Using the departure date as it is passed through the different functions for example, gives the possibility to accurately extract the epoch at which a certain segment is being propagated, along with the location of all the perturbing bodies at that epoch and therefore to obtain the accurate perturbing accelerations both in terms of magnitude and direction.
Once the lowest layer of functions is reached, the actual way of computing the states can be changed. As was mentioned before, initially this was done using simple Kepler propagation. In the modified

version however, this has been replaced by numerically propagating the first and second half of each segment. The velocity impulse that was added to the velocity components of the Cartesian state of the body halfway the segment was left unchanged. The state in the first and second half however was thus propagated using numerical integration (with Runge-Kutta 4 as the integration method, as discussed before). For this, inside each segment some of the integrator settings needed to be updated, such as the initial time of integration, which now accurately was defined with respect to J2000. Similar to that, the propagation settings also need to be defined in a proper way, meaning that the termination conditions need to be defined, also accurately with respect to J2000. Finally, the perturbing accelerations that are being included are added and the actual propagation can take place.

To make this all work properly and output the correct results, various elements should be taken into account. In this paragraph, a brief summary will be given of some of the challenges that arose during the modification process. Since a large number of changes were needed to properly implement all of the desired extra functionalities, many opportunities existed in which a mistake could occur. This is why an extensive verification was performed on everything that was modified, which will be discussed elaborately in Section 8.3.4.

A challenge that arose quite early in the process of modifications, is the correct definition of all the epochs and durations that come to play in the process of propagation. Kepler propagation is set up in a very elementary way in Tudat, in which only the initial state, the propagation duration and the central gravitational coefficient is required. For numerical integration on the other hand, both the initial and final time need to be defined, which therefore need to be updated each time correctly taking into account the departure date that is defined with respect to J2000.

An extra layer of complexity comes from the way in which this Sims-Flanagan method is programmed into Tudat. During the optimisation part, the segments are propagated completely, as can be expected. Once the most optimal individual is chosen after all generations have been evolved, a final propagation is taking place to output the results for this individual. The results however are desired at each of the integration steps (which are smaller than the segments), which means that in this final integration, the largest part of the integration steps will lie inside a segment and will not include a velocity impulse inside of them. In the way it was programmed in Tudat, this was not a problem when Kepler propagation was used. However, with the added complexity of numerical integration and the need to define the accurate epoch at all times for each integration step, this required to slightly rewrite the lowest layer of functions in such a way that it could handle these two different cases of propagating the complete trajectory. Especially due to the forward and backward propagation that takes place, a mistake can easily be made with this and therefore it is a sensitive modification that is tested extensively, as will be seen in Section 8.3.4.

8.3.3. Results

In this section, the results of the analysis using Sims-Flanagan's method will be presented and discussed. The points with which this analysis will be performed have already been established in Section 8.2.3 and are tabulated in Table 8.1.

As explained in Section 8.3.2, all of the parameters as obtained from the optimisation part of the hodographic analysis are loaded into the Sims-Flanagan part, such that the final trajectory design can be performed. Before the results can be obtained, a process of tuning the software is required, such that the most optimal trajectory can be obtained. This tuning will be discussed elaborately in this section, after which the obtained trajectory along with its corresponding thrust profile will be presented.

A few things should be noted before the process of tuning is discussed. Due to the complexity of the problem and the used Sims-Flanagan method, it was found that a perfect mismatch of zero halfway the trajectory could not be obtained with the amount of tuning that was performed during the time frame of this thesis project. This is why the tuning is generally focused on getting this mismatch as low as possible and not so much to get the absolute lowest possible value for the required overall ΔV.

Next to that, the values that will be mentioned as examples during the discussion of the tuning parameters below will apply for the combination of hodographic parameters as can be seen in the red column in Table 8.1. The values for the combinations in the other columns will be mentioned briefly once the results for their respective Sims-Flanagan analysis is shown, later in this section.

Tuning

There are many parameters in this software tool that can be tuned, to change the outcome of the results. Most of these have already been mentioned in Section 8.3.2, but all of them will be discussed here in no particular order, including the impact each of them has on the final result. Many of these values have been chosen after a large amount of testing in combination with other parameters, meaning that it is not a simple process of just tuning one parameter at a time and then moving on to the next one. This is also why it may very well be possible that with the given time of the thesis project, not the absolute best set of tuning parameters is obtained. This will be discussed more in Section 9.2.

The first parameter to discuss here is the number of steps used in the integration process, which can be set since a fixed-step integrator has been used for the analysis. After testing various options for this parameter, a value of 8000 was chosen to be used during this thesis project, since it displayed a good balance between accuracy and computational effort. As can be expected, with a larger number of steps the accuracy of the integration can be increased, but the computations will take much longer. As will be seen in Section 8.3.4, this value can be increased for certain use-cases, such as during the verification process.
Next, the factor of freedom with respect to the initial guess around which the individuals can search for the most optimal solution can be tuned as well. This number can take any value between zero and one, where zero means that the individuals will only lie exactly on the initial guess, while a value of one means a freedom as large as the value of the thrust force of the initial guess at that moment. It was found that a rather low value for this parameter gave the best solution with respect to the mismatch halfway the trajectory. The final value that has been chosen for this analysis is 0.075. With this value, the individuals still had quite some freedom around the initial guess to search for a better solution, but were also constrained enough to focus on the locations where the most suitable solutions are expected to be found.

Another set of parameters that needs to be tuned is the pair that is responsible for the optimisation process, namely the number of individuals and the number of generations. The values that are chosen for these parameters scale linearly with the required computational time, meaning that twice the number of individuals means a doubling in computational time and half the number of generations means a halving in the computational time. This is why it is very important to test the impact these parameters have on the solution and on the computational time. Especially with the perturbations added to the numerical integration, the computational time for one individual in one generation grows significantly. It was found that after a certain number of generations, the results did not continue to improve significantly, which is why not too many generations have been chosen. In terms of individuals, ideally a large variety in options around the initial guess is desired such that the optimisation process can really try many possibilities and with that continue the optimisation process. This is why it has been chosen to evolve 2000 individuals for 30 generations. With these values, a good balance between accuracy and required computational time has been found.
Also relevant for the optimisation process, are the weights that have been placed for the calculation of the fitness function on either the required ΔV or the mismatch halfway the trajectory. In the way this was implemented in Tudat, it was simply a choice of which ratio was to be used between these two weights, with them being 1:10 (in favour of more weight on minimising the mismatch) by default. This has been changed to 1:15, so more weight on minimising the mismatch. Next to this, a modification has been made in which not only a general weight on the total mismatch is placed, but also extra weights can be placed on the three components of the mismatch, namely in x, y or z direction. For this tuning, a few different values have been tried and tested, but due to time constraints no extensive tuning could take place. During testing, it was noticed that the difference in z direction was much more significant compared to the other directions, which is why much more weight is placed on minimising the mismatch in z direction, both in position and velocity. The final values that have been used are an extra weight of 2.5 for both the x and y component, while for the position in z direction a value of 75 is chosen and for the velocity in the same direction a value of 45.

The last and arguably most important parameter that can be tuned to obtain better results, is the number of segments. Throughout the whole testing and tuning process, various values for this parameter have been used to see which values give the most suitable results. With less segments, the thrust

profile becomes more 'rough' and has less room to apply small changes to the trajectory. With a large number of segments on the other hand, less variation in the thrust profile can be investigated by the same number of individuals, meaning a potentially not so optimal trajectory will be the result. This is why it is important to tune this parameter well.
It was decided to tune the number of segments by looping through the complete Sims-Flanagan optimisation process, while changing the number of segments each time. The range of this loop went from 2 segments to 99 segments. Most of the other tuning parameters were set as they have been described above, with the exception of the number of individuals and generations. During this tuning of the segments, the original implementation of Sims-Flanagan's method in Tudat using Kepler propagation has been used, to speed up the process significantly and because the perturbations are not that relevant during tuning. This is why it was possible to opt for many more individuals, which is why during this tuning it was decided to use 10 000 individuals for 25 generations.
It should also be mentioned how the mismatch was calculated exactly. This is done by taking the two states right before the middle of the trajectory (in the forward propagated leg), calculating the derivative for both the position and velocity in all three components and propagating these one time step further. This newly obtained state is then compared to the state as was obtained from Sims-Flanagan's method, which comes from the backward propagated leg. The distance in each component between these two is calculated and the norm or Euclidean distance is then considered as the mismatch between the forward and backward propagated leg.

This tuning was performed, for which the results can be seen in Figure 8.12. It was decided to continue with the number of segments being 27, since it gave a small mismatch and could give the individuals a lot of different options to investigate by not being too large. With this final parameter defined, the actual final trajectory design can take place. The results for the different points from the Pareto front in Section 8.2.3 will be discussed in the next few sections.

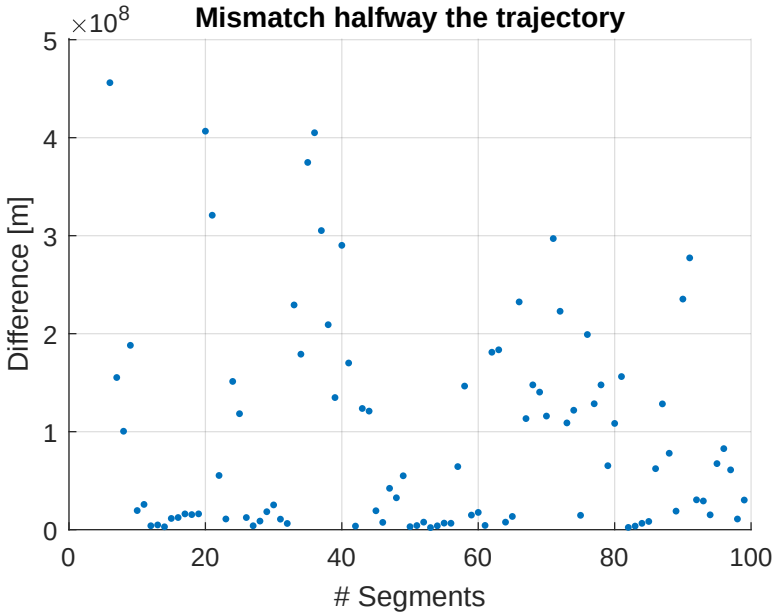

Figure 8.12: The mismatch halfway the trajectory for various numbers of segments (Note that the y-axis is constrained at 5×10^8 m to increase the visibility of the points with a lower value. This means that the first few numbers of segments (2-5) cannot be seen in this graph).

Red column

The first results that will be presented here are those created using the initial guess based on the hodographic method with the free parameters as obtained in Section 8.2.3 and shown in Table 8.1 in the red column.
The used parameters, as they have already been discussed in the tuning section above, are summarised in Table 8.3.

Table 8.3: The settings and parameters used to design the final trajectory corresponding to the red column from Table 8.1.

Setting	Values
Integration steps	8000
# Segments	27
Generations	30
Individuals	2000
Factor of freedom	0.075
Main seed	5
Optimisation seed	28

The 3D motion of the transfer trajectory as obtained by using Sims-Flangan's method has been visualised in red in Figure 8.13, with the applied thrust force vectors shown with red arrows. The blue dashed line represents the orbit of the Earth, while the grey dashed line represents the original orbit of the asteroid, if it would not be moved. The point of departure is illustrated with a green dot, while the point of arrival is illustrated with a black dot.

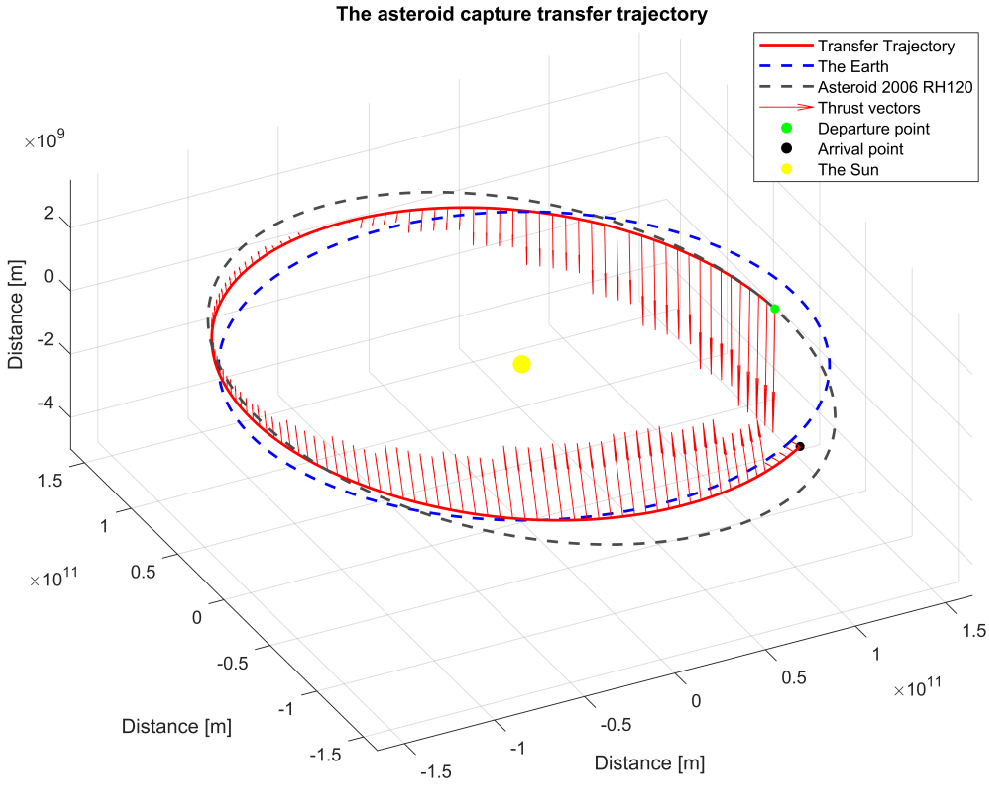

Figure 8.13: A 3D visualisation of the final transfer trajectory for the asteroid to its safe, stable and easily accessible location in close proximity to the Earth, together with the required thrust profile to perform the transfer.

A few notes should be made with respect to this 3D illustration. The first being the difference between the scale of the *z*-axis and the scale of the *x*- and *y*-axes. Since the scale on the *z*-axis is much smaller, the forces and motion in this direction look slightly exaggerated, which should be taken into account when observing the figure. Furthermore, it can be observed how the transfer departs from exactly the orbit of the asteroid, but does not arrive exactly on the orbit of the Earth. This is due to the previously obtained difference of 0.05 in eccentricity, which the final state should have with respect to the orbit of the Earth, for it to stay in a safe, stable and easily accessible orbit.
To get a better view of the forces in the *xy*-plane, a 2D visualisation has been created, which can be seen in Figure 8.14. This visualisation has the same indicators as the 3D version and the red arrows clearly show in which direction the asteroid should be pushed for it to reach its final state.

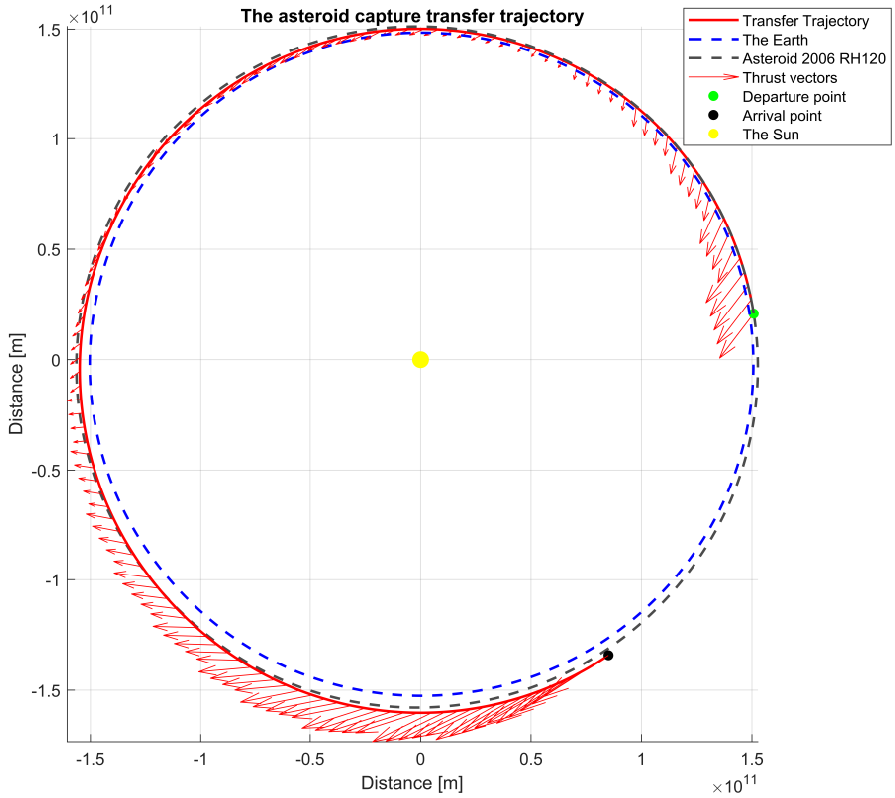

Figure 8.14: A 2D visualisation of the final transfer trajectory for the asteroid to its safe, stable and easily accessible location in close proximity to the Earth, together with the required thrust profile to perform the transfer.

When looking at the values of the states halfway the trajectory, a small mismatch can be observed, as expected. The calculated total mismatch in position is $64\,215\,\mathrm{km}$ and in velocity $8.5\,\mathrm{m/s}$. Next to that, the required total ΔV is $994.53\,\mathrm{m/s}$. These results and those of the other runs can be seen summarised in Table 8.5.

It was decided to perform an extra final analysis on top of this, using the same method as was used in the third method of the verification and validation process for this software, which can be read in Section 8.3.4. Briefly summarised here, using other general propagation functions in Tudat (so no Sims-Flanagan anymore), the thrust profile as obtained by Sims-Flanagan is loaded into those propagation functions and with them, a new trajectory is created. This trajectory can be seen as a higher fidelity variant compared to the trajectory obtained by Sims-Flanagan's method (in case a mismatch exists, which does exist in this study), due to the fact that the propagation is continuous from departure to arrival without a backward leg and therefore no mismatch halfway the trajectory. This does however mean, that there will be a mismatch all the way at the end of the trajectory, or at the arrival date. This is exactly what is sought out, namely: where will the asteroid actually end up if the obtained thrust profile is used to transfer it? It should be noted that exactly the same conditions have been applied to the new straightforward propagation method, meaning the same perturbations are acting on the asteroid and the same integrator and propagator settings have been used.
The distance between the trajectory as obtained by Sims-Flanagan's method and the trajectory as obtained by the straightforward propagation can be seen in Figure 8.15.
The mismatch that exists halfway the Sims-Flanagan trajectory can immediately be observed in the figure. Furthermore, as will be elaborated upon in Section 8.3.4, after the mismatch halfway the time of flight, the distance between both trajectories starts to accumulate much faster, due to the fact that in the different analyses, the asteroid is now at a different location and therefore the forces working on it will be different, causing the larger deviation between both trajectories. Generally however, it can be seen that the overall mismatch at the end, which thus means how far the asteroid will end up from the state it is supposed to end up in, is not too large on a heliocentric scale, at around $100\,000\,\mathrm{km}$.

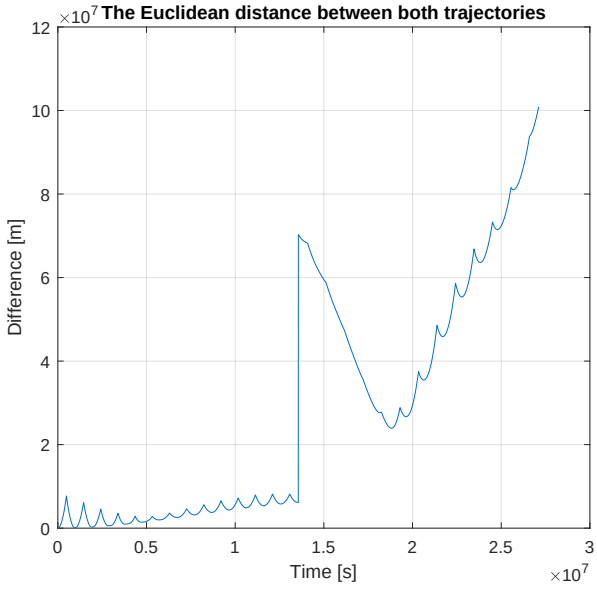

Figure 8.15: The distance between the trajectory as obtained by Sims-Flanagan's method and the trajectory as obtained by the simple forward propagation method.

The newly obtained trajectory is drawn in the same way as has been done in Figure 8.13, and can be seen in Figure 8.16. From this visualisation, it can be seen that indeed, the trajectory as seen on a heliocentric scale is very close to the one obtained from Sims-Flanagan's method. This can also serve as a form of validation, since the objective of obtaining a thrust profile that will bring the asteroid to its desired location is achieved, but more on that will follow in Section 8.3.4.

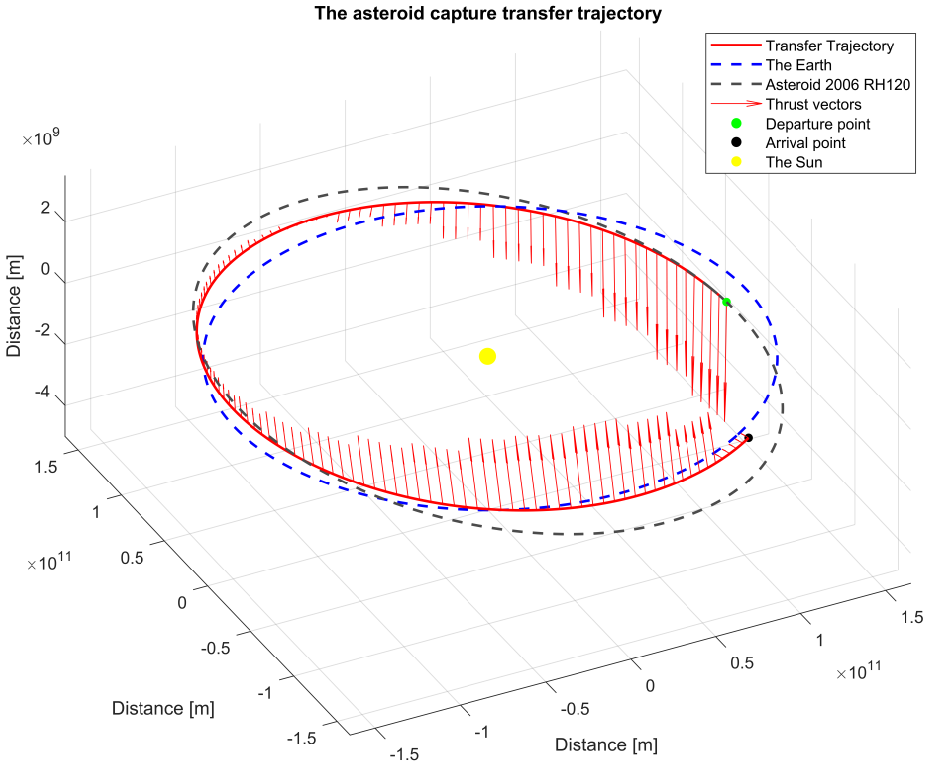

Figure 8.16: A 3D visualisation of the final transfer trajectory for the asteroid using the straightforward propagation, together with the required thrust profile to perform the transfer.

Yellow and green column

Next, the results as obtained by using the free parameters from the second (yellow) and third (green) column in Table 8.1 are presented. Similar to how it was done for the red column, first a summary will be given of the parameters as obtained from the tuning process for both points, in Table 8.4.

Table 8.4: The settings and parameters used to design the final trajectory corresponding to the yellow and green column from Table 8.1.

Setting	Yellow	Green
Integration steps	8000	8000
# Segments	26	23
Generations	30	30
Individuals	2000	2000
Factor of freedom	0.055	0.075
Main seed	126	71
Optimisation seed	88	98

The same visualisations as for the 'red column' results have been produced and they can be seen in Figures A.4 and A.5 for the yellow column and in Figures A.6 and A.7 for the green column. As can be expected, due to the fact that the combination of departure date and time of flight are very similar to each other, the orbits look similar to each other from first observation. The only difference that can be seen from these angles is the difference in the thrust vectors.

Table 8.5: The results for the three different runs, summarised in one table.

Result	Red	Yellow	Green
Hodograph ΔV [m/s]	1001.16	1078.45	981.52
Sims-Flanagan ΔV [m/s]	994.54	1069.64	973.03
Hodograph max thrust [N]	1.7201	1.5225	2.2374
Sims-Flanagan max thrust [N]	1.7363	1.4902	2.0514
Mismatch Position [km]	64215	61951	51171
Mismatch Velocity [m/s]	8.54	12.46	11.95

The results for all three analyses have been summarised in Table 8.5. It can be seen that for all three analyses using Sims-Flanagan's method, an improvement of the required ΔV compared to the hodographic method has been realised. The improvement in terms of both the required ΔV and maximum thrust force has also been visualised, by plotting the new values in the Pareto front as it was already shown in Figure 8.10b. This can be seen in Figure 8.17.
Next, similar to as was done for the red column, the thrust force profiles as obtained through Sims-Flanagan's method have been loaded into the straightforward propagation software and the difference between the trajectories has been plotted. The results for this can be seen in Figure A.8a for the yellow column and in Figure A.8b for the green column. A very similar behaviour of the difference between trajectories can be observed, with the same cause at its origin, namely the non-zero mismatch halfway the trajectory and the subsequent accumulation in difference. The new trajectories visualised in the heliocentric reference frame can be seen in Figure A.9 for the yellow column and Figure A.10 for the green column.

8.3.4. Verification and Validation

In this section, an in-depth analysis is performed to check whether all the applied modifications do what they do correctly and whether they do what they should do. In other words, an extensive verification and validation is performed to make sure that the results as they are presented in Section 8.3.3 are accurate and relevant.
In this verification and validation, it is assumed that the functions that are present in Tudat are fully verified and validated. This means that everything that is already implemented into Tudat is correct and does not need to be checked. This assumption can be made since there are strict guidelines as to

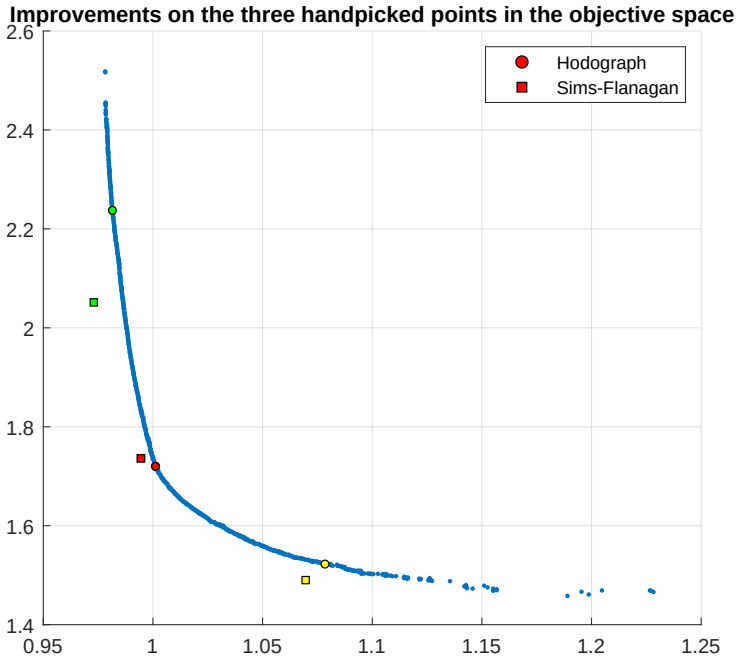

Figure 8.17: The newly obtained values for the trajectories using Sims-Flanagan's method

what is allowed to be approved inside the Tudat toolbox, to which everyone that adds something onto Tudat is deemed to adhere. New functionalities in Tudat are tested extensively by others and proof of verification and validation needs to be shown before it is implemented into the toolbox.

This is kept in mind, together with the fact that as far as the author of this thesis is aware no ready-to-use mission analyses or example projects in this specific field exist, that can be used directly as material to verify with. Therefore it is decided to find several other methods of verification and validation, by comparing the obtained results internally with already existing and implemented (and therefore verified) functions inside Tudat. These various methods will be discussed in this section.
It should be noted that the combination of departure date, time of flight and all the free parameters that is used in this verification is the same as the one used for the final results of this analysis as was shown in Section 8.3.3. All of the verification methods and runs have also been performed with other combinations and have shown similar results.

First method

The first method of verification is to compare the results of an analysis using the already implemented analytical Kepler propagation with an analysis using the modified numerical propagation without any perturbations. These two different analyses should provide almost identical results, since the numerical analysis does not have any additional perturbations or other external forces compared to the analytical analysis and therefore the variation between these two will only be due to numerical inaccuracies and very small differences in the found thrust profile.
This results in running each analysis twice with exactly the same settings and parameters, the only difference being the lowest layer of functions in which the actual propagation happens. The two versions - the original and the modified - are simply swapped between both analyses and the results are compared. This is repeated several times with different settings and parameters, such as the number of segments and the number of individuals and generations. In this way, it is checked whether the modifications are robust and will produce the same results as the original in a wide variety of situations.

The results for two of these verification cases have been presented in Figure 8.18. The used settings and parameters have been displayed in Table 8.6. In here, the main seed is defined in the main software file, while the optimisation seed is specified in one of the layers of functions and is only used during the optimisation performance in that layer.

Table 8.6: The settings and parameters for two of the verification runs using the first method.

Setting	Run 1	Run 2
Integration steps	8000	8000
# Segments	10	15
Generations	25	15
Individuals	100	50
Factor of freedom	0.3	0.2
Main seed	10	12
Optimisation seed	28	18

As can be seen from both figures, the differences in all three directions stay very small throughout the complete simulation time and thus during the complete trajectory. The largest difference between the analytical and numerical method for both runs is around five metres, which is insignificant with respect to the order of magnitude of the orbits. In this way, it can be concluded that this first aspect of the modification is verified and validated, since it does exactly what is expected to do and does it with a high accuracy.

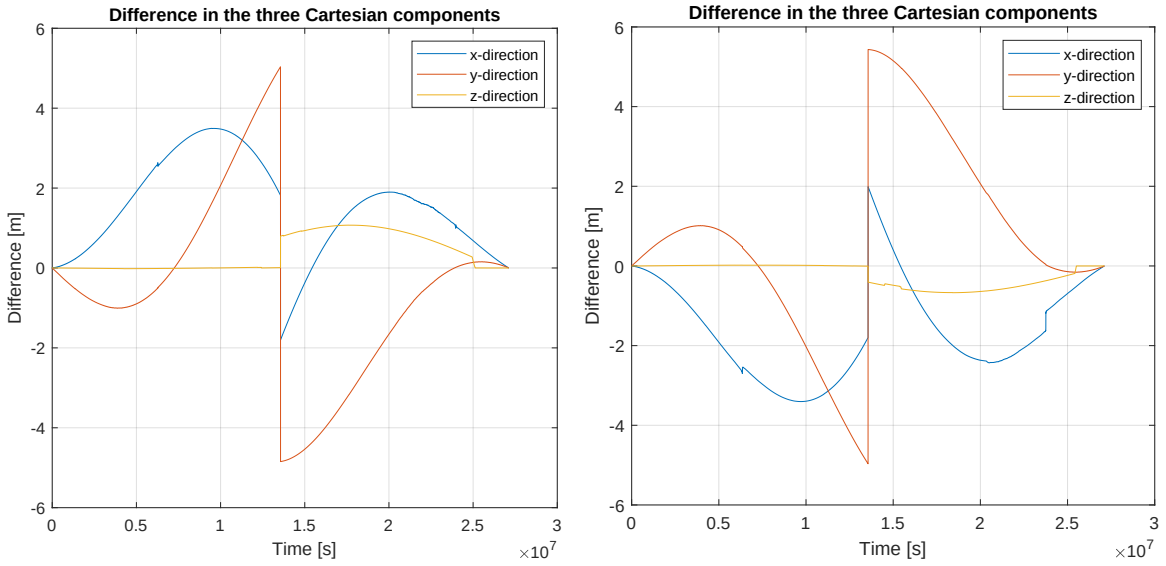

(a) Difference in metres in the three different directions, for the first verification run.

(b) Difference in metres in the three different directions, for the second verification run.

Figure 8.18: The results for two runs using the first verification method.

Second method

The next method of verification is to compare the modified software with a certain functionality that has been implemented in the original version of Sims-Flanagan's method in Tudat. This functionality provided the possibility to perform a numerical propagation from the states as obtained from Sims-Flanagan's method at half of the time of flight using forward and backward propagation, back to the departure time and forward to the arrival time. This numerical propagation uses the exact thrust profile as is obtained from Sims-Flanagan's method. This means that if the same perturbations have been added to the modified version of Sims-Flanagan's method and this numerical propagation, the resulting trajectory should be similar.

It should be noted that there will be an inherent difference between the results of this extra 'numerical check' and the modified software, which also numerically propagates the states. This is due to the fact that the numerical check takes the thrust profile as it is obtained through Sims-Flanagan's method and uses that thrust profile directly. This means that no velocity impulses halfway each segment will

be used, like in Sims-Flanagan's method, but the actual continuous thrust profile. This has as a result that there will be a distinction between the two obtained trajectories, where one will be smooth (using the numerical check) and the other will have step-like features in its orbit (using the modified Sims-Flanagan software). Also, an accumulative difference can build up between the two. When investigating the software and its results, this small difference was discovered to be caused by a very slight deviation in the mass of the system at each point in time. Due to this deviation, the acceleration as computed by the software to work on the spacecraft-asteroid system is also slightly different, causing the small accumulation of difference. Since this difference was observed in all the simulation runs, it did not affect the verification process.
The first of these effects can be minimised by using a large number of segments, such that the segments are small and the difference between the smooth trajectory and the 'step-wise' trajectory is also small. Next to that, increasing the number of integration steps also helps decrease the difference between both trajectories.

The idea of this verification is thus not to obtain two exactly identical trajectories, but more to see whether both results are approximately similar and show that indeed, with the obtained thrust profile and with or without perturbations, the trajectory from and to the states of interest can be recreated.
It is thus decided to do this verification both with and without added perturbations, to see the behaviour of the trajectories. Next to that, a verification run is done in which one of these does have perturbations included, while the other does not have these perturbations, to show how the difference between those two trajectories is orders of magnitude larger. The expectation is thus to obtain two illustrations with similar deviations in all three directions, while the last illustration should display much larger deviations.

The first verification run, without any perturbations can be seen in Figure 8.19a. The settings for the run have been displayed in Table 8.7. It should be noted that these settings are kept the same for the following two runs, the first with perturbations on both trajectories and the second with perturbations only applied to the numerical check. Also, since this verification is more focused on the actual propagation and the inclusion of perturbations, the fitness of the result is not that important and therefore the number of individuals and generations is kept low, to increase efficiency.
As can be seen in the figure, the difference in the three different directions starts at zero at half of the time of flight, due to the fact that the numerical check starts its propagation from that point, as mentioned before. The difference then propagates outwards, towards the departure and arrival date. The disturbance that can be seen in each of the three directions is due to the previously mentioned difference between the smooth trajectory of the numerical check and the step-like trajectory of the modified Sims-Flanagan software. Because the number of segments is large, this is not visible as large steps but rather the disturbance as is visualised now.
Furthermore, it can be seen that the total accumulation in difference between both is not larger than 3×10^4 m, meaning not larger than 30 km.

Table 8.7: The settings and parameters for all of the verification runs using the second method.

Setting	Values
Integration steps	64000
# Segments	2000
Generations	5
Individuals	30
Factor of freedom	0.45
Main seed	16
Optimisation seed	48

In the second verification run, which can be seen in Figure 8.19b, perturbations have been added to both trajectory propagations. The added perturbations are the same as have been used so far, both in Chapter 7 and Section 8.3.3, namely the Earth, the Moon, Venus, Mars and Jupiter. It can be seen that the pattern of differences is very similar to the pattern that occurred in the non-perturbed analysis, as was expected before. This strengthens the verification, since it means that the perturbations are

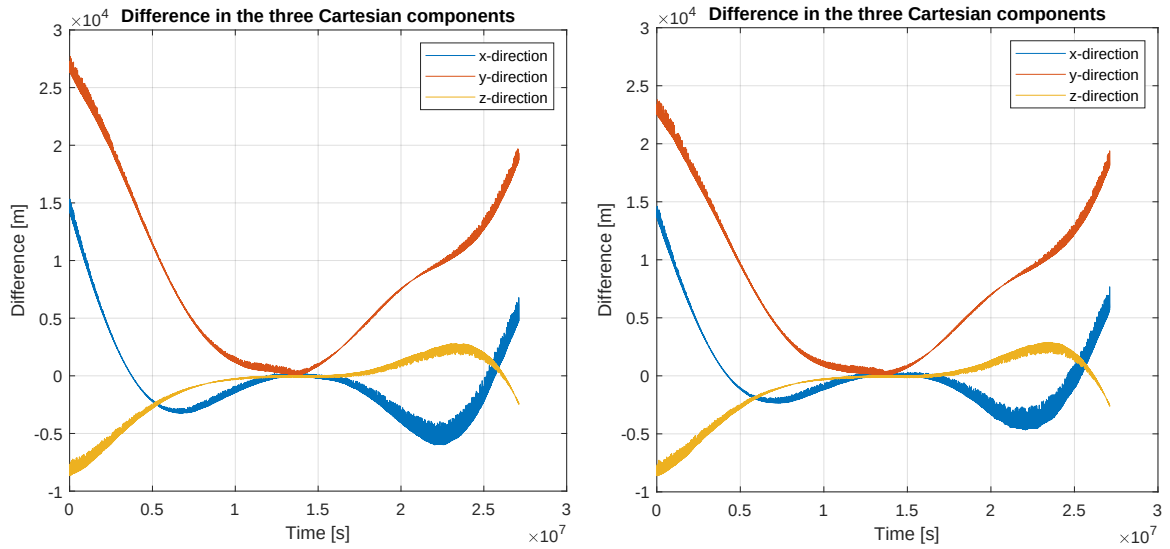

(a) Difference in metres in the three different directions, without any perturbations.

(b) Difference in metres in the three different directions, with added perturbations.

Figure 8.19: The results for the first two runs of the second verification method.

correctly implemented and the shown accumulation in difference is due to the way of propagating the states.

The third and last verification run for this method is performed by generating a trajectory using the modified Sims-Flanagan method without any perturbations and using the same thrust profile generating a trajectory including perturbations with the numerical check. The difference between these two trajectories can be seen in Figure 8.20. A few observations can immediately be made, starting with the range on the axes and therefore the difference between both trajectories. It can be seen that the difference between both trajectories can go up to 13×10^7 m, which is at least three orders of magnitude larger than the previous two runs during this verification. Due to this larger difference, the disturbances in the lines (caused by the segments) have also become invisible in this scale, even though they are still present.
The conclusion can therefore be drawn, that the functionality of adding perturbations inside the propagation process, used to optimise the trajectory with Sims-Flanagan's method, has been implemented correctly.

Third method

Finally, the third method for verification and validation of the applied modifications is based on the resulting thrust profile that flows out of the analysis as it is being performed. By using this thrust profile and simply performing a separate numerical propagation using another piece of software in Tudat, it can again be verified that the resulting trajectory from the modified software will be correctly computed when using the obtained thrust profile. Also, as a validation, if this third method is successful it shows that the goal of this whole analysis, which is to design a suitable transfer trajectory along with its corresponding thrust profile, is achieved and that with said thrust profile the correct transfer trajectory will be created.

Before the results of this verification and validation method are presented, a few notes should be made. Similar to what could be seen in the second verification method, a difference between the trajectory is accumulating, again due to a small deviation in the mass profile as it is being outputted by the software. This (ever so slight) deviation in mass translates to a small deviation in acceleration and due to this, an accumulation of the difference between the trajectories occurs. As said before, this occurs in all simulations and it has been decided to still perform this verification, despite this accumulating deviation, because the verification overall still proves its value in showing that the trajectory will be followed closely when using the corresponding thrust profile.

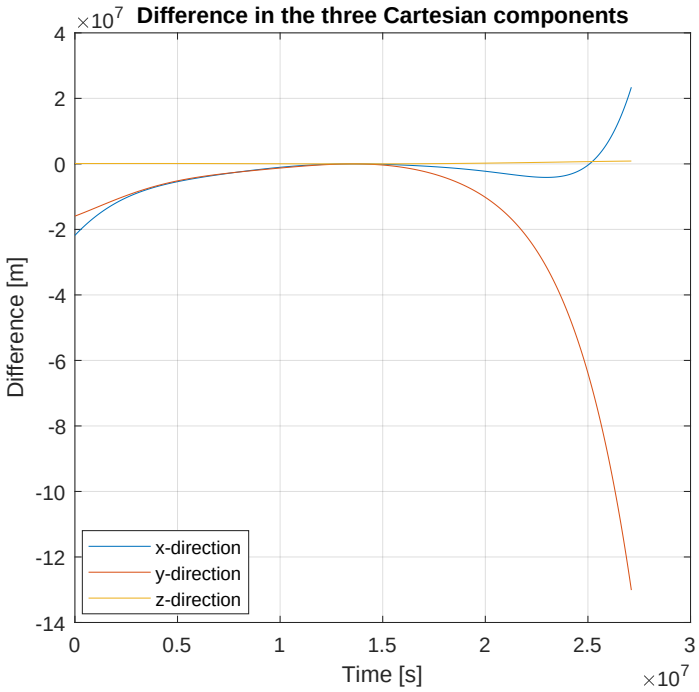

Figure 8.20: The difference between a trajectory created using the modified Sims-Flanagan software without perturbations and the numerical check with perturbations.

Next to this, due to the fact that by using this specific implementation of Sims-Flanagan's method in Tudat no perfect convergence of the mismatch halfway the trajectory has been achieved, a jump will be present halfway the difference graphs in this verification method. The numerical propagation that is used to compare it with, performs its propagation namely in a smooth manner from departure to arrival, while the trajectory resulting from the modified Sims-Flanagan has the unconverged mismatch at its centre.

With these two important notes in mind, the results for one of the few runs that have been performed with this verification method will be discussed next. This verification method can both analyse unperturbed and perturbed trajectories, which is why both will be shown and discussed here.
The first analysis is performed by running the modified software without added perturbations, using the set of parameters as can be seen in Table 8.8. The resulting thrust profile is saved and loaded into a different program in Tudat, which is specifically modified for this verification. In this program, a 'simple' numerical propagation is performed using the same integrator settings and with the loaded thrust profile. This propagation is performed twice, once forward from departure to arrival and once backward from arrival to departure. The resulting trajectories for both of these analyses have been compared to the trajectory as it was obtained through the modified Sims-Flanagan software and the results can be seen in Figure 8.21.

Table 8.8: The settings and parameters for all of the verification runs using the third method.

Setting	Values
Integration steps	64000
# Segments	2000
Generations	12
Individuals	120
Factor of freedom	0.045
Main seed	26
Optimisation seed	58

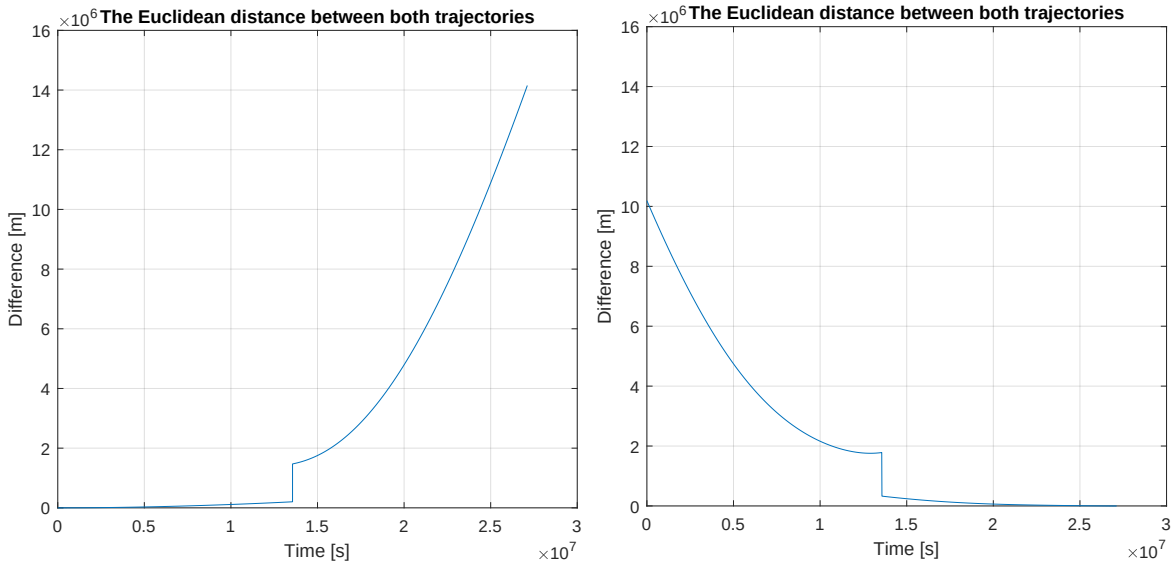

(a) Modified Sims-Flanagan compared to a forward numerical propagation.

(b) Modified Sims-Flanagan compared to a backward numerical propagation.

Figure 8.21: The results for the unperturbed run of the third verification method.

It can be observed that for both analyses, performed either forward or backward, the first half of the trajectory stays very close to the trajectory obtained using the modified Sims-Flanagan method. The small difference that is accumulating is due to the already mentioned slight deviation in mass profile and therefore acceleration. Halfway a jump can be seen, caused by the fact that the mismatch has not fully converged, after which the Euclidean distance (or norm) between both trajectories starts increasing significantly. This makes sense from an astrodynamical perspective, since the body that is propagated will be in a slightly different location and therefore the force that works on the body and causes the acceleration (in this unperturbed case just the gravitational acceleration from the Sun) on that body will be slightly different in both direction and magnitude.

Next to this, for the same trajectory (and corresponding thrust profile) two other numerical propagations have been performed with this third verification method, only now the usual set of perturbations has been added. With these extra perturbations, it is expected that the Euclidean distance between the unperturbed modified Sims-Flanagan trajectory and the perturbed new trajectories will increase much faster and more significantly.
The results are shown in Figure 8.22. Immediately the larger difference can be observed, when a closer look is taken to the *y*-axes. With a difference of two orders of magnitude, it is clear that once the perturbing forces are added, the Euclidean distance really becomes significant. Due to this change in scale, the mismatch halfway the trajectory also cannot be seen anymore.

Finally, the analysis using the modified Sims-Flanagan method is repeated with exactly the same parameters, only now with the usual perturbations added to it and different seed numbers (main seed: 126, optimisation seed 88). The newly generated thrust profile was again saved and loaded into the verification software, with which two new runs have been performed, one forward and one backward. The results can be seen in Figure 8.23.
A few observations can be made from these two figures, which are all relevant for both Figures 8.23a and 8.23b. The first is that the distance between both trajectories stays small during the first half of the propagation (just like in Figure 8.21). The mismatch in this run with perturbations is much larger than in the unperturbed simulation and after this large jump, the distance between both trajectories continues to deviate largely. Again, this can be explained by the large change in state and therefore the change in how the forces work on the body. This time however, this is not only the gravitational force from the central body, but also the perturbing forces that can also work in a slightly different way (in terms of magnitude and direction) on the body after the jump.

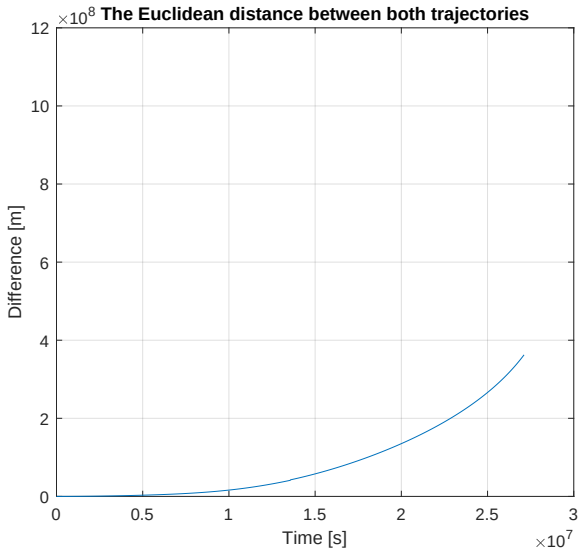

(a) Unperturbed modified Sims-Flanagan compared to a perturbed forward numerical propagation.

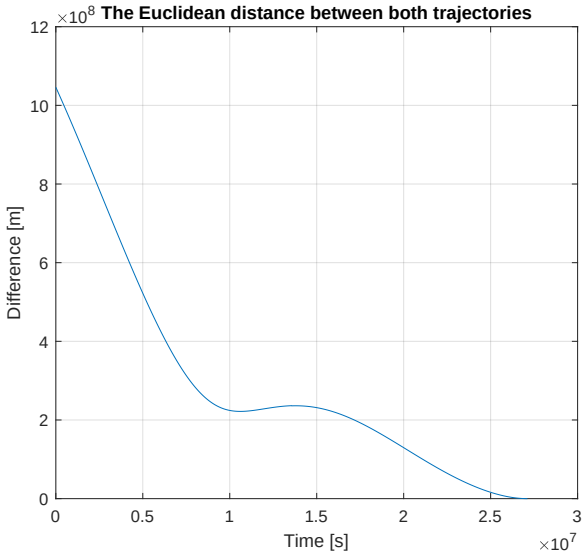

(b) Unperturbed modified Sims-Flanagan compared to a perturbed backward numerical propagation.

Figure 8.22: The results for the unperturbed/perturbed run of the third verification method.

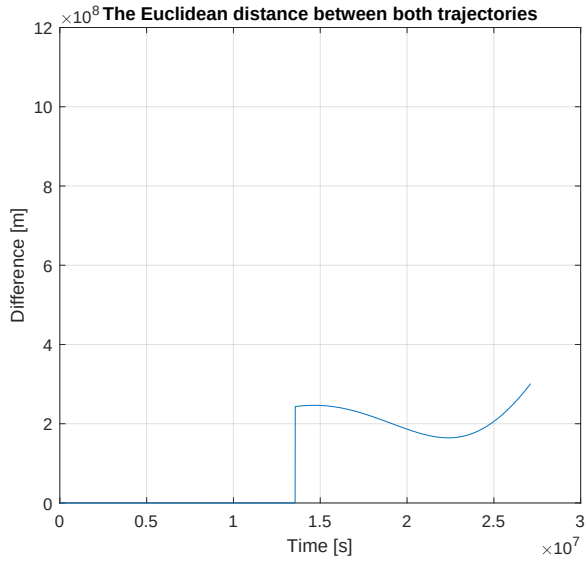

(a) Modified Sims-Flanagan compared to a forward numerical propagation.

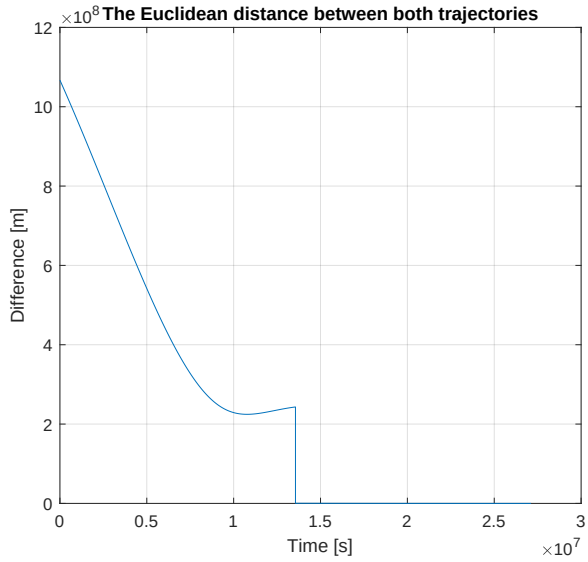

(b) Modified Sims-Flanagan compared to a backward numerical propagation.

Figure 8.23: The results for the perturbed run of the third verification method.

After these various analyses, it can thus be concluded that apart from some small numerical inaccuracies, the modified software correctly computes what is expected for it to compute. Despite the fact that the mismatch halfway the trajectory has not converged yet and therefore even in the verification some deviations existed, as was discussed elaborately, the modified software still performs well and its results are valuable for the analysis. The results of the modified software are relevant to the problem at hand and do what is desired from the viewpoint of the designer. In this way, it can be concluded that the software is both verified and validated.

8.4. Conclusions

Concluding this chapter, in which multiple different analyses have been performed to reach the final goal of designing a transfer trajectory for an asteroid capture mission, a brief recap will be given on the obtained results.

First, by means of a design process using the hodographic method, a good idea was obtained of what combination of departure date and time of flight is the most suitable for the mission at hand. In the final optimisation phase, a Pareto front was generated, in which the fittest individuals could be seen. Each of these individuals directly translated (by means of their variables) to a certain transfer trajectory that could serve as an initial guess for the subsequent analysis which made use of Sims-Flanagan's method for the design of low-thrust trajectories.
A modified version of this Sims-Flanagan method, extensively verified and validated, was used to perform the optimisation process and to find the best thrust force profile, with which the asteroid could be transferred to its final state. The final thrust profiles and the corresponding trajectories were visualised to give a good idea of how the transfer will look like on a heliocentric scale. A mismatch still existed halfway in these final trajectories, which is due to the complexity of the problem, combined with the use of Sims-Flanagan's method and the limited time available to tune and run the simulation. Finally, each obtained thrust force profile was used in a straightforward propagation from departure to arrival, to see how far off this final state will be compared to the one as obtained from Sims-Flanagan's method.

9

Conclusions and Recommendations

In this last chapter, all findings throughout this thesis project will be briefly discussed and a general conclusion will be drawn based on these findings. Next to that, several recommendations will be given for further research and analysis on this subject.

9.1. Conclusions

This section will discuss the various findings in chronological order, meaning it will start with the background in the first few chapters of this thesis report, followed by the analysis that decided which asteroid will be used for this asteroid capture study. Then, the findings on the stability analysis will be discussed, after which the chapter on the transfer trajectory will be concluded. Finally, some general conclusions on the complete study will be drawn.

9.1.1. Background

After analysing various research studies that have already been performed, a conclusion could be drawn on what the target orbit for this thesis project will be. Considering the studies that have been performed and proposals that have been made, in which often a geocentric or selenocentric target orbit was chosen, or otherwise a target orbit around some Lagrange libration point was proposed, it was decided to investigate the possibility of placing the asteroid in a heliocentric target orbit in close proximity to the Earth-Moon system. The potential benefits of this proposed target orbit include a higher safety and stability compared to placing an asteroid inside the Earth-Moon system.
Next, some research on the types of asteroids was performed, from which certain constraints were formulated in terms of the suitability of the asteroid to be captured. Generally this encompassed its initial orbit, which should be similar to that of the Earth (meaning a NEA would be captured), and its size and therefore also mass, which should not be too large for the mission to be feasible with current technology levels.

The different propulsion methods have been discussed, with the advantages and disadvantages of each method. It has been decided to use a low-thrust engine, also based on various research studies that have been performed on the topic of asteroid capture. The constraints for the low-thrust engine were subsequently defined, such that these constraints can be used during the actual design of the transfer trajectory.
Finally, some of the basic concepts of astrodynamics have briefly been discussed, along with the relevant theories for the upcoming analysis phase, such as the dynamics of low-thrust trajectories, the expected perturbing forces in the Solar System and the basics on stability in space.

9.1.2. Analysis

Starting in the next part, an extensive analysis was performed on a constrained set of NEA's, in which the transferability from their original orbit to the position of the Earth was assessed by means of a Lambert targeter. In this way, by using the mathematical framework of the Lambert targeter without any added complexities such as perturbations, a useful and fast preliminary analysis could be performed

to determine the most suitable asteroid for the capture mission. This resulted in the asteroid '2006 RH120' to be used in this design study.

Subsequently, a broad investigation on the suitability of final states in the vicinity of the Earth was performed. The setup of this analysis was to take the state of the Earth at a certain moment in time and change some of its Kepler elements slightly. An object would then be placed in this newly created state and be propagated for the next 100 years, to investigate whether an object placed in that state will stay stable, at a safe distance from the Earth and other bodies and will be easily accessible throughout the complete simulation period. In this way the elements that were mentioned in the research question would be satisfied.
It was concluded that by taking the Earth's state and adding at least 0.03 to its eccentricity, a final state that adheres to all these elements from the research question could be found. By adding more than this 0.03, the required ΔV for missions from the Earth to the asteroid in that state would be higher, but with the benefit of a safer orbit. This is why it was decided to use the state of the Earth and add 0.05 to the eccentricity for the final state of the transfer trajectory.

Finally, in terms of the design of the transfer trajectory from the asteroid's initial orbit to its final state, several remarks can be made. From the first broad analysis using the analytical hodographic method, it became clear that transferring the 2006 RH120 asteroid towards the final state that was decided upon, can best be done around the year 2027. This is due to the position that the initial state and final state have with respect to each other during this time frame. From the optimisation analysis that followed, a few precise departure dates and time of flights could be extracted, along with the free coefficients that could be used to shape the trajectory using the hodographic method. These precise departure dates were all on the 15th of September, 2027, while the time of flights were all slightly higher than 313 days.
The results from Sims-Flanagan's method were generated using the hodographically shaped trajectory as an initial guess. All three points that were analysed proved to give a better result in terms of the combined objective function, consisting of the required ΔV and the maximum thrust. The combinations for all three points consisted of a required ΔV of around 1000 m/s and a maximum thrust force between 1.5 N and 2 N, which is well within the margins of what modern-day low-thrust engines can provide. This means that such a transfer trajectory to a heliocentric orbit is feasible.
Using the resulting thrust force profile indeed brought the asteroid very close to its desired final state. There was a difference however, which is mainly caused by the existing mismatch halfway the trajectory from using Sims-Flanagan's method. This is why some recommendations for further research will be given in the next section.

9.2. Recommendations

In this section, a brief overview will be given on findings of the author of this thesis, which were considered interesting research material for future studies.

First of all, as already mentioned before, it will be very interesting to investigate how the now existing mismatch halfway the trajectory when using Sims-Flanagan's method can be reduced to zero. Whether this is done by tuning the algorithm in a better way, simply letting it run with more individuals and for more generations, or actively modifying something in the existing functions such that they are being computed in a (slightly) different way, obtaining a mismatch of effectively zero will be a great benefit and it will mean that the trajectory will reach the previously identified suitable final state where it will stay for the complete 100 years in its safe, stable and easily accessible orbit.

Next, another area in which further research can be done, is on obtaining higher-fidelity positional information, especially for the asteroid. With the available functions in Tudat, it was decided to take the state of the asteroid at a certain epoch and create an ephemeris for this asteroid using simple Kepler orbits. If a higher-fidelity tool existed that could provide a much more accurate ephemeris for each body for a certain time frame, the whole analysis would be even more realistic.
This is especially relevant in case the orbit of the asteroid is not very stable and undergoes various different perturbing forces in its already unstable orbit.

Finally, another recommendation for future studies that will be given, is on the use of gravity assists. Due to time constraints this has not been treated in this thesis project, but making use of gravity assists around either the Earth or the Moon, could potentially give a much more efficient (in terms of required ΔV) and therefore feasible result.

A

Additional figures

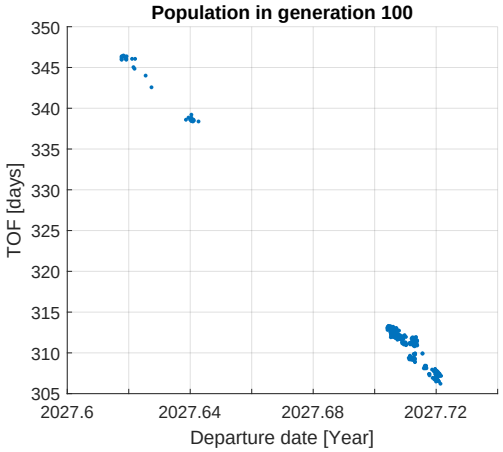

(a) The distribution of individuals at generation 100.

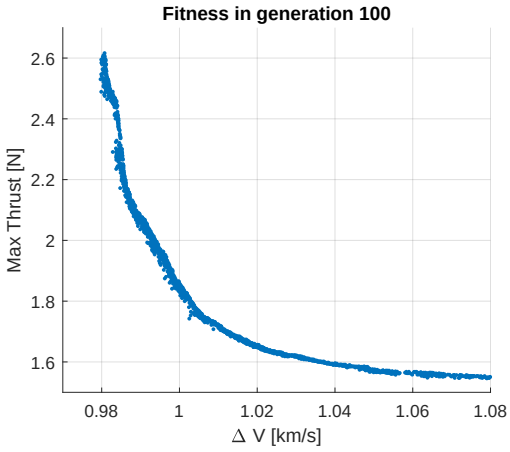

(b) The fitness of the population at generation 100.

Figure A.1: The results for generation 100, with a seed number of 341.

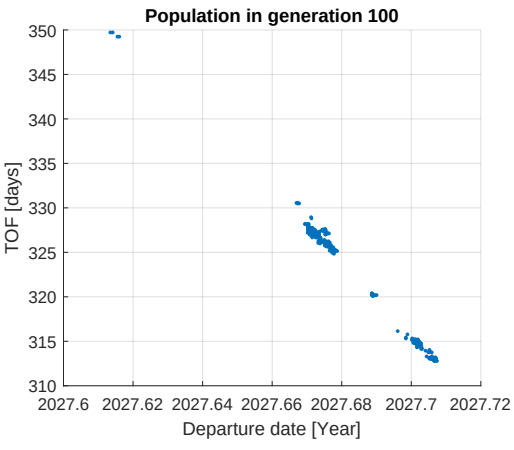

(a) The distribution of individuals at generation 100.

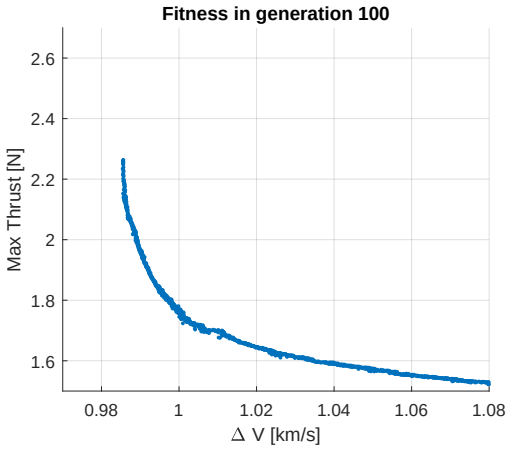

(b) The fitness of the population at generation 100.

Figure A.2: The results for generation 100, with a seed number of 67.

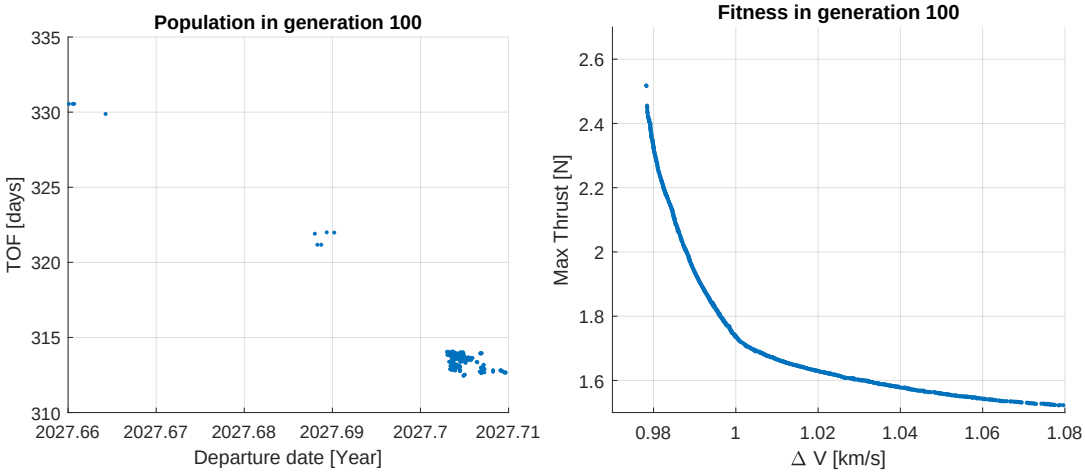

(a) The distribution of individuals at generation 100.

(b) The fitness of the population at generation 100.

Figure A.3: The results for generation 100, with a seed number of 49.

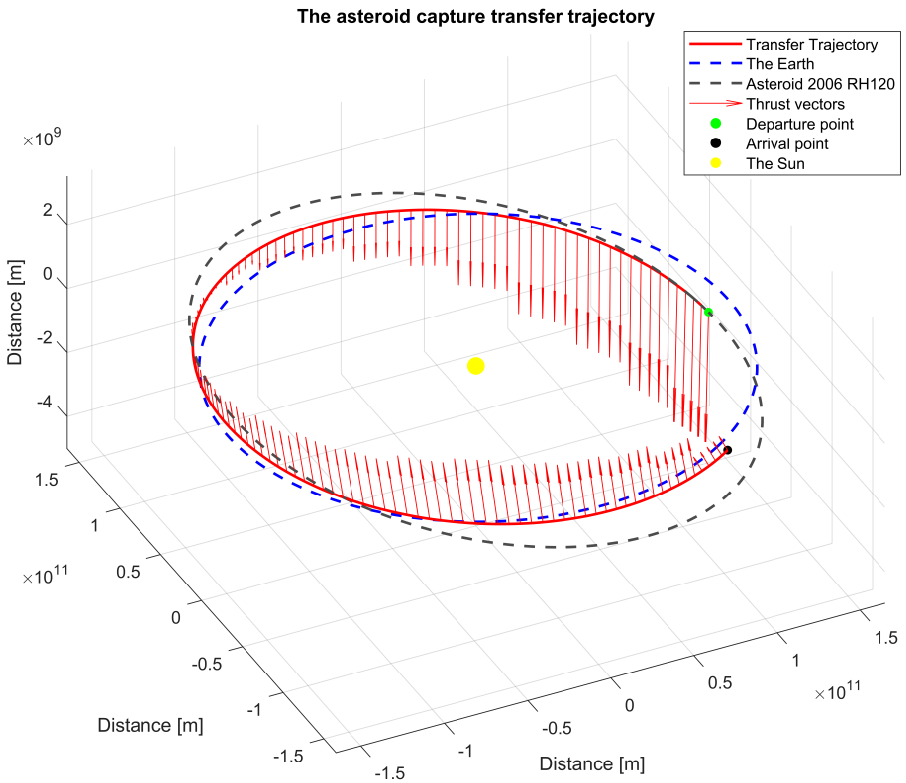

Figure A.4: A 3D visualisation of the final transfer trajectory for the asteroid to its safe, stable and easily accessible location in close proximity to the Earth, together with the required thrust profile to perform the transfer, using the parameters from the yellow column.

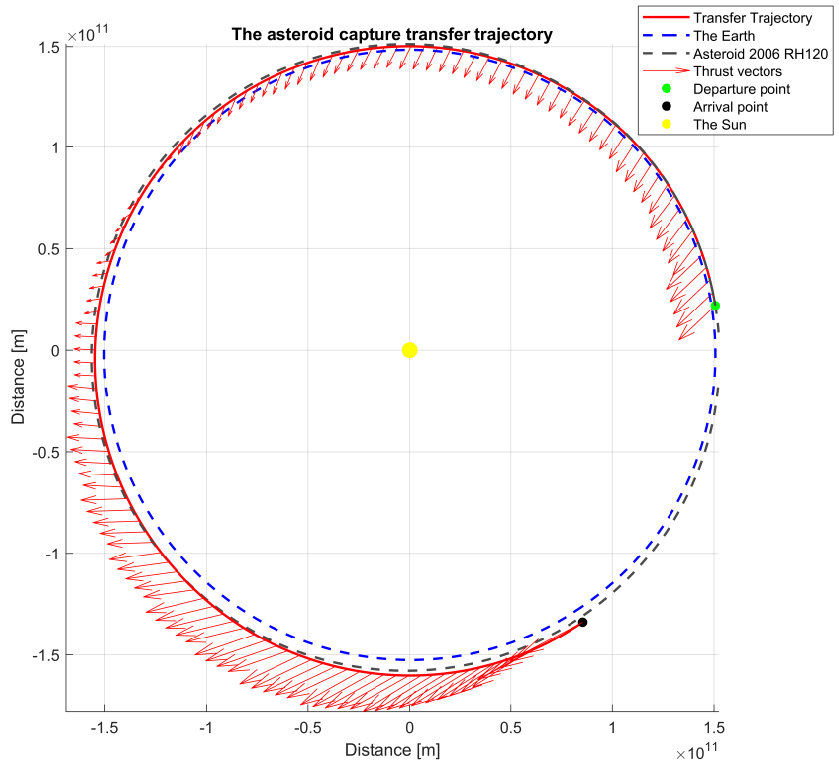

Figure A.5: A 2D visualisation of the final transfer trajectory for the asteroid to its safe, stable and easily accessible location in close proximity to the Earth, together with the required thrust profile to perform the transfer, using the parameters from the yellow column.

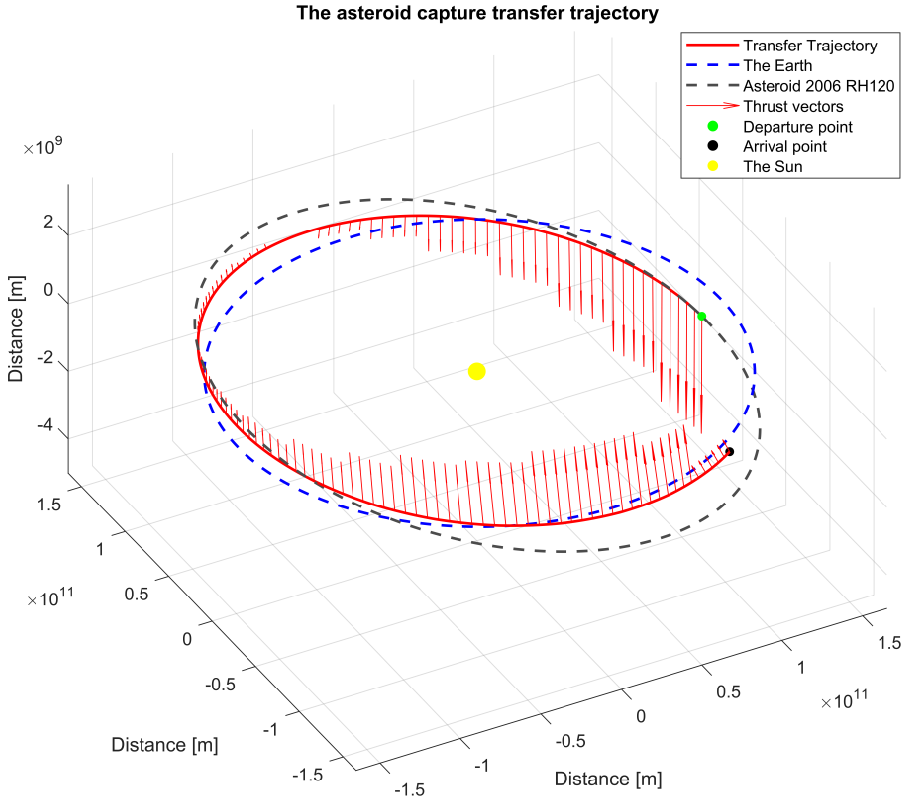

Figure A.6: A 3D visualisation of the final transfer trajectory for the asteroid to its safe, stable and easily accessible location in close proximity to the Earth, together with the required thrust profile to perform the transfer, using the parameters from the green column.

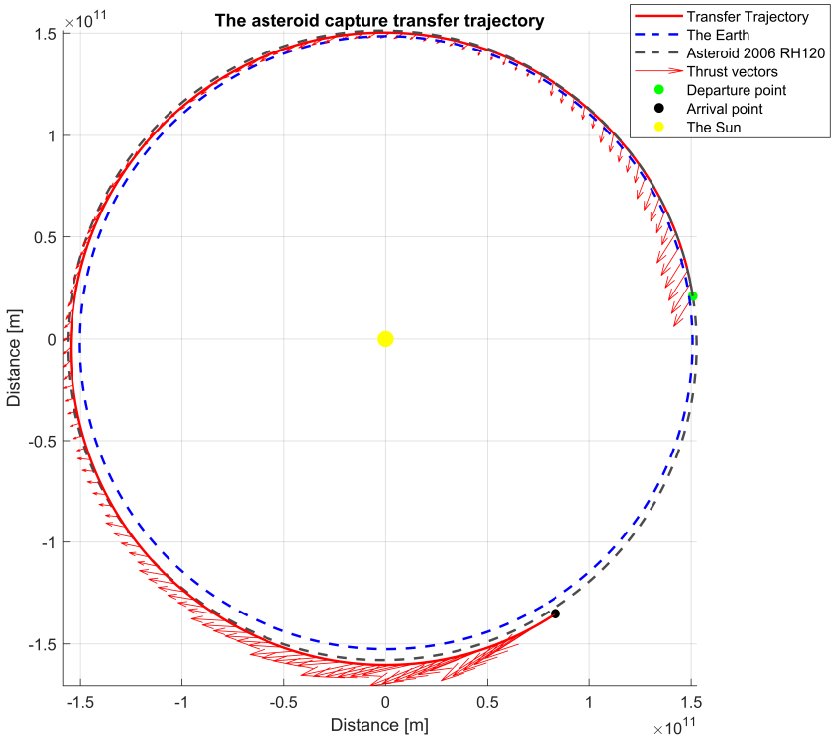

Figure A.7: A 2D visualisation of the final transfer trajectory for the asteroid to its safe, stable and easily accessible location in close proximity to the Earth, together with the required thrust profile to perform the transfer, using the parameters from the green column.

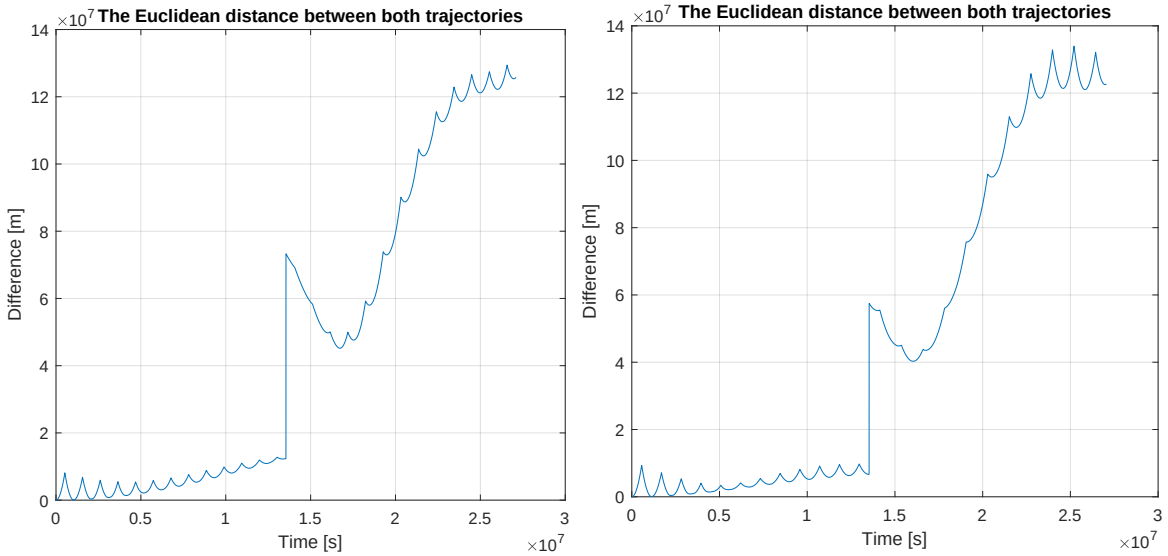

(a) The results for the yellow column.

(b) The results for the green column.

Figure A.8: The distance between the trajectory as obtained by Sims-Flanagan's method and the trajectory as obtained by the simple forward propagation method.

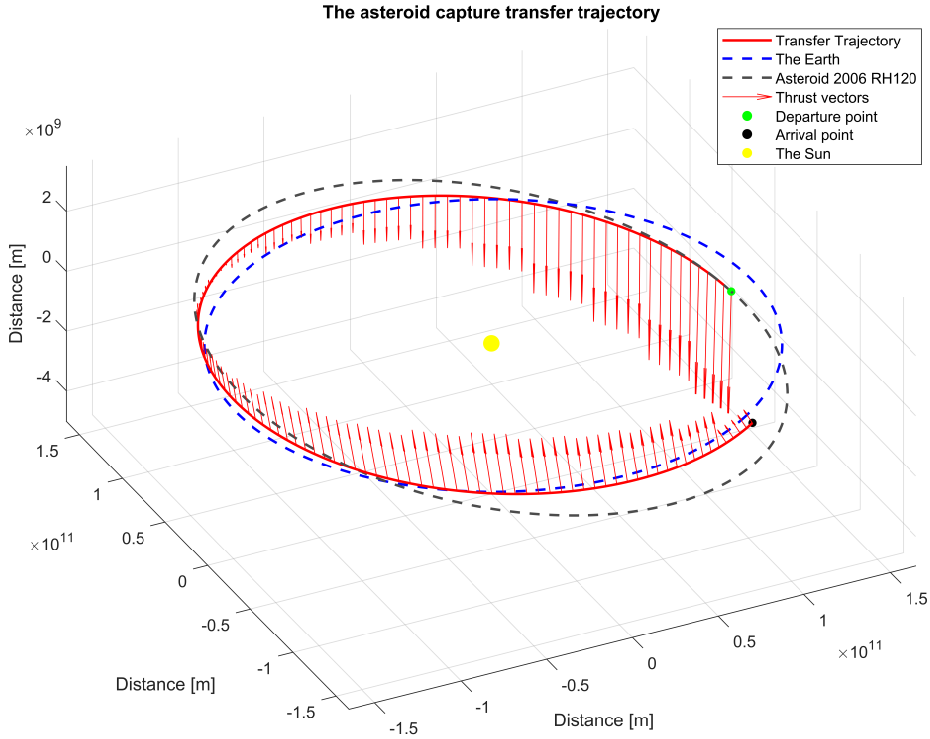

Figure A.9: A 3D visualisation of the final transfer trajectory for the asteroid using the straightforward propagation, together with the required thrust profile to perform the transfer, using the parameters from the yellow column.

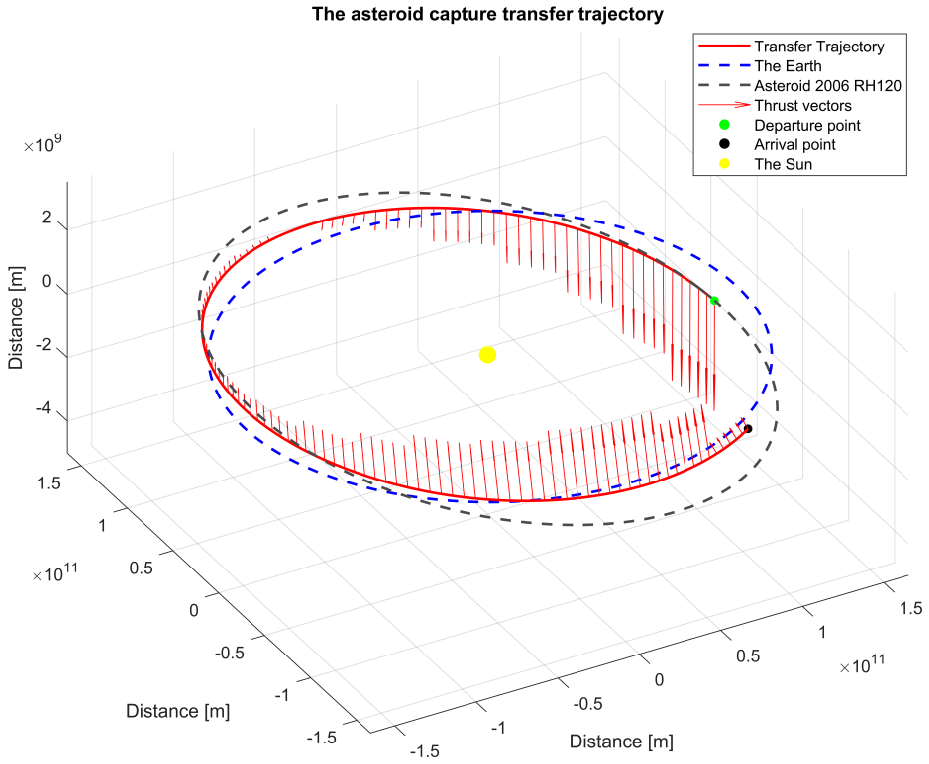

Figure A.10: A 3D visualisation of the final transfer trajectory for the asteroid using the straightforward propagation, together with the required thrust profile to perform the transfer, using the parameters from the green column.

B

Additional tables

Table B.1: The precise values for each optimised variable for a set of handpicked individuals.

Individual #	1	2	3
Departure date [s since J2000]	874269575.097348	874309361.242898	874269138.471113
Time of flight [s]	27116154.1925664	27094333.7504767	27053194.6945929
Radial free coefficient 1	2433.21543280342	2367.18229960735	2278.83708695106
Radial free coefficient 2	595.932419279622	455.228433623061	468.982220202219
Normal free coefficient 1	-436.284017739686	-638.491648197568	-529.078557742931
Normal free coefficient 2	3011.89842121722	3004.32890496669	2568.86196482335
Axial free coefficient 1	3633.90667014190	-482.540423962400	3624.14925060475
Axial free coefficient 2	-4228.30102548890	-477.451500334463	-4893.27747790835
Axial free coefficient 3	-559.211505833810	522.925629146254	89.7002942085618

Bibliography

[1] V. Badescu, *Asteroids: Prospective Energy and Material Recources* (Springer, Berlin, Heidelberg, 2013).

[2] W. L. Nicholson, *Ancient micronauts: interplanetary transport of microbes by cosmic impacts,* Trends in Microbiology **17**, 243 (2009).

[3] A. A. Ledkov, N. A. Eismont, R. R. Nazirov, and M. N. Boyarsky, *A method for capturing asteroids into earth satellite orbits,* Astronomy Letters **41**, 442 (2015).

[4] J. R. Brophy, L. Friedman, and F. Culick, *Asteroid retrieval feasibility,* in *2012 IEEE Aerospace Conference* (2012) pp. 1–16.

[5] M. Tan, C. McInnes, and M. Ceriotti, *Direct and indirect capture of near-earth asteroids in the earth–moon system,* Celestial Mechanics and Dynamical Astronomy **129**, 57 (2017).

[6] M. Tan, C. McInnes, and M. Ceriotti, *Low-energy capture of asteroids for the logistic support of future mars missions,* (2018) pp. 3425–3442.

[7] J. Souchay and R. Dvorak, *Dynamics of Small Solar System Bodies and Exoplanets*, Lecture Notes in Physics (Springer Berlin Heidelberg, 2010).

[8] S. B. Nicholson, *The Trojan asteroids,* Leaflet of the Astronomical Society of the Pacific **8**, 239 (1961).

[9] J. Horner, N. W. Evans, and M. E. Bailey, *Simulations of the population of Centaurs – I. The bulk statistics,* Monthly Notices of the Royal Astronomical Society **354**, 798 (2004).

[10] M. J. Duncan, H. F. Levison, and S. M. Budd, *The Dynamical Structure of the Kuiper Belt,* The Astronomical Journal **110**, 3073 (1995).

[11] https://cneos.jpl.nasa.gov/about/neo_groups.html, accessed on 13-05-2020.

[12] https://minorplanetcenter.net/mpc/summary, accessed on 17-11-2020.

[13] W. P. R. and L. S. C., *Structure and density of cometary nuclei,* Meteoritics & Planetary Science **43**, 1033 (2010).

[14] B. Carry, *Density of asteroids,* Planetary and Space Science **73**, 98 (2012), Solar System science before and after Gaia.

[15] A. Taylor, J. C. McDowell, and M. Elvis, *A delta-v map of the known main belt asteroids,* Acta Astronautica **146**, 73 (2018).

[16] *JPL Small-Body Database Search Engine,* https://ssd.jpl.nasa.gov/sbdb_query.cgi (2020), accessed on 19-04-2020.

[17] https://www.minorplanetcenter.net/iau/mpc.html, accessed on 21-06-2020.

[18] B. Zandbergen, *Thermal Rocket Propulsion* (Delft University of Technology, Delft, The Netherlands, 2017).

[19] A. Cervone, *AE 4S10, Microsat Engineering lecture slides,* TU Delft (2017-2018).

[20] M. Martinez-Sanchez and J. E. Pollard, *Spacecraft electric propulsion-an overview,* Journal of Propulsion and Power **14**, 688 (1998).

[21] J. P. Sánchez and D. García Yárnoz, *Asteroid retrieval missions enabled by invariant manifold dynamics,* Acta Astronautica **127**, 667 (2016).

[22] S. Kitamura, Y. Ohkawa, Y. Hayakawa, H. Yoshida, and K. Miyazaki, *Overview and research status of the jaxa 150-mn ion engine,* Acta Astronautica **61**, 360 (2007), bringing Space Closer to People, Selected Proceedings of the 57th IAF Congress, Valencia, Spain, 2-6 October, 2006.

[23] J. Brophy, R. Gershman, N. Strange, D. Landau, R. Merrill, and T. Kerslake, *300-kw solar electric propulsion system configuration for human exploration of near-earth asteroids,* 47th AIAA/ASME/SAE/ASEE Joint Propulsion Conference & Exhibit (2011).

[24] K. F. Wakker, *Fundamentals of Astrodynamics* (Institutional Repository, Library Delft University of Technology, Delft, The Netherlands, 2015) Faculty of Aerospace Engineering.

[25] https://en.wikipedia.org/wiki/File:Orbit1.svg, wikimedia, user:Lasunncty, accessed on 19-06-2020.

[26] R. Noomen, *AE 2104, Flight and Orbital Mechanics lecture slides,* TU Delft (2012-2013).

[27] A. E. Petropoulos and J. M. Longuski, *Shape-based algorithm for the automated design of low-thrust, gravity assist trajectories,* Journal of Spacecraft and Rockets **41**, 787 (2004).

[28] B. J. Wall and B. A. Conway, *Shape-based approach to low-thrust rendezvous trajectory design,* Journal of Guidance, Control, and Dynamics **32**, 95 (2009).

[29] R. H. Gooding, *A procedure for the solution of lambert's orbital boundary-value problem,* Celestial Mechanics and Dynamical Astronomy **48**, 145 (1990).

[30] D. d. l. Torre Sangrà and E. Fantino, *Review of lambert's problem,* in *ISSFD 2015: 25th International Symposium on Space Flight Dynamics, 19-23 October, Munich, Germany* (2015) pp. 1–15.

[31] D. Izzo, *Lambert's problem for exponential sinusoids,* JOURNAL OF GUIDANCE CONTROL AND DYNAMICS **29**, 1242 (2006).

[32] D. Izzo, *Revisiting lambert's problem,* Celestial Mechanics and Dynamical Astronomy **121**, 1 (2015).

[33] B. W. Barbee and P. W. Chodas, *Near-Earth Asteroids 2006 RH120 AND 2009 BD: Proxies for Maximally Accessible Objects?* (2015).

[34] B. D. Anderson and M. W. Lo, *Dynamics of asteroid 2006 RH120: pre-capture and escape phases,* (2016).

[35] D. Farnocchia, M. Mommert, J. L. Hora, S. R. Chesley, D. Vokrouhlický, D. E. Trilling, M. Mueller, A. W. Harris, H. A. Smith, G. G. Fazio, and et al., *Trajectory and physical properties of near-Earth asteroid 2009 BD,* Proceedings of the International Astronomical Union **9**, 142–145 (2014).

[36] C. F. Yoder, *Astrometric and geodetic properties of Earth and the Solar System*, Vol. 1 (Wiley Online Library, 1995).

[37] *Navigation and ancillary information facility,* https://naif.jpl.nasa.gov/naif/ (2019), accessed on 12-06-2019.

[38] D. J. Gondelach and R. Noomen, *Hodographic-shaping method for low-thrust interplanetary trajectory design,* Journal of Spacecraft and Rockets **52**, 728 (2015).

[39] *Minor Planet Center,* https://minorplanetcenter.net/db_search/show_object?utf8=&object_id=2006+RH120 (2019), accessed on 11-05-2019.

[40] K. Deb, A. Pratap, S. Agarwal, and T. Meyarivan, *A fast and elitist multiobjective genetic algorithm: NSGA-II,* IEEE Transactions on Evolutionary Computation **6**, 182 (2002).

[41] J. Sims and S. Flanagan, *Preliminary design of low-thrust interplanetary missions,* **103** (2000).

[42] C. H. Yam, D. Izzo, and F. Biscani, *Towards a high fidelity direct transcription method for optimisation of low-thrust trajectories,* (2010).